Development, Implementation and Testing of an Expert System for Detection of Defects in Gas Turbine Engines

Choucri-Gabriel Taraboulsi

A Thesis

in

The Department

of

Mechanical and Industrial Engineering

Presented in Partial Fulfillment of the Requirements

For the Degree of Doctor of Philosophy at

Concordia University

Montreal, Quebec, Canada

February 2008

Your file Votre référence
ISBN: 978-0-494-37765-9
Our file Notre référence
ISBN: 978-0-494-37765-9

Abstract

Development, Implementation and Testing of an Expert System for Detection of Defects in Gas Turbine Engines

Choucri-Gabriel Taraboulsi, Ph.D.
Concordia University, 2008

Unbalance and misalignment are the major causes of vibration in rotating machinery, yet only limited research has been conducted on misalignment. The literature reports that misalignment results in an increase in the vibration at a frequency corresponding to two times the rotating speed (2x responses). The research on misalignment conducted so far has modeled the rotor as two coupled shafts supported on linear and non linear bearings, while misalignment is at the coupler. The results reported to date are inconsistent and the vibration response of a misaligned rotor system is not clearly understood. This dissertation presents a study on the effects of a single shaft misalignment on the dynamic response of a rotor-shaft system. A rotor system supported on two rigid bearings with unbalance and misalignment is modeled using the energy method, and Lagrange formulation is used to establish the equations of motion. The misalignment is modeled through introduction of pre-load and nonlinear shaft stiffness in the direction of pre-load. The model is validated by comparing the natural frequencies predicted using the simulation to the rotor system eigenvalue and the forced response from the simulation is verified using finite element method. A response due to perfectly aligned case is compared with those for parallel and angular misalignments of various magnitudes. Simulations are

carried out for a speed range of 0 to 10,000 rpm, and the response of the rotor at the 2x is carefully examined to establish the effects of various misalignment and non-linear parameters on the response. Experiments are conducted using a rig test to compare with analytically predicted trends. Various gas turbine engine data gathered from the field are also used to confirm the vibration pattern predicted by the simulations. The simulated results are finally used to develop an expert system that can identify unbalance and misalignment in a rotor system. The expert system is developed using Neural Network. Two types of Neural Networks are explored, the back-propagation and the Logicon Projection Network. Finally, both networks are modified, trained and tested using simulation data. The Logicon projection network showed superior performance during training, and was chosen over the back-propagation network. The developed expert system is tested using field test data of gas turbine engines to demonstrate its effectiveness.

Acknowledgements

The author wishes to express his sincere appreciation to his thesis supervisors Dr. A. K. W. Ahmed and Dr. A. Kaushal for providing guidance throughout the course of his investigation.

The author is also deeply indebted to Dr. R.B. Bhat for his constructive advice that was essential for the successful conclusion of this work. Thanks are also due to the members of the supervisory committee for their help in formulating the scope. The author also thanks Rolls-Royce Canada for their support of this work. Finally, the author would like to express his special thanks to his family members for their love, encouragement and support.

Table of Content

List of figures

List of tables

Nomenclature

α	Angular misalignment at the bearing
α_i	Disk angular position due to misalignment
Δ	Parallel misalignment at the bearing
Δ_i	Disk deflection due to misalignment
ω	Rotation speed around the rotation axis.
Ω	Rotation speed
ψ	Rotation angle about the Z axis
$\dot{\psi}$	Rotation speed about the Z axis
ϕ	Rotation angle about the y_1 axis
$\dot{\phi}$	Rotation speed about the y_1 axis
θ	Rotation angle about the x_2 axis
σ_y	Misalignment about the Y axis
σ_z	Misalignment about the Z axis
τ	Angle between the principal axis of the disk and the rotation axis (dynamic unbalance)
a	Distance from left bearing to disk
b	Distance from disk to right bearing
E	Young modulus
e	Distance between center of mass and axis of rotation

F	Force
I_x	Moment of inertia about the shaft x axis
I_{Dx}	Moment of inertia about the disk x axis
I_y	Moment of inertia about the shaft y axis
I_{Dy}	Moment of inertia about the disk y axis
I_z	Moment of inertia about the shaft z axis
I_{Dz}	Moment of inertia about the disk z axis
K	Stiffness terms used in the stiffness matrix
$\mathbf{k}$	Stiffness matrix
$\mathbf{k_n}$	Nonlinear stiffness matrix
l	Length of the shaft
M	Moment
M_D	Disk Mass
t	Time
V	Velocity
y	Displacement along the y axis
$\dot{y}$	Velocity along the y axis
$\ddot{y}$	Acceleration along the y axis
z	Displacement along the z axis
$\dot{z}$	Velocity along the z axis
$\ddot{z}$	Acceleration along z the axis

Chapter 1

1 Introduction and Literature Review

1.1 Introduction

Rotating components are one of the most common elements in mechanical systems. They vary from simple configurations such as in fans, pumps etc. to highly complex ones such as turbine engines. A rotating system typically consists of shafts, bearings, rotors, blades, seals etc., and is required to operate at a fixed speed or over a range of speeds. Such systems are exposed to self induced vibrations due to defects at manufacturing or due to the defects that develop during operations. Simplified models of rotating systems are extensively investigated to examine their dynamic responses. There has been significant development in the methodology to establish the dynamic responses of rotating system under various conditions. The primary causes of vibration response in rotating system are unbalance, and misalignment that are inherent in the system or that may also develop with the usage of the equipment over time. Although these defects may not be crucial for many low speed rotating systems, they can be detrimental for systems that operate at very high speeds. Presence of these defects in numerous possible configurations may lead to excessive deflection and bearing force to cause failure. A diagnostic system with some success has been explored in attempts to identify specific problems while in use. Most studies were, however, limited to only academic interest.

The proposed research focuses on one of the most complex rotating machines, namely gas turbine engines. A gas turbine engine of 50 MW typically costs in excess of 10 million dollars, and consists of multiple shafts rotating relative to each other while attached to many different components. The most common problems with such machines are unbalance and misalignment. Although extra efforts are made to avoid such defects at manufacturing, they may develop during the normal running of the machine. This in turn may lead to excessive vibration and dynamic forces resulting in premature failure if remained undetected. The cost of such repair and unexpected down time for such machinery is excessive.

The objective of this investigation is to analyze the dynamic behavior of a rotor under some common defects, mainly unbalance and misalignment, in order to develop an expert system for on-line monitoring and diagnostic purposes. The research proposes to develop logics based on the dynamic responses that can be utilized for the diagnosis of a specific problem. A properly developed and trained Neural Network (N.N.) can be utilized to establish a reliable expert system. Such a developed tool will be a highly valuable addition to the reliability and operation of a gas turbine engine. Further more, the methodology developed can be easily extended to develop expert system as a diagnostic tool for other rotor defects.

In order to develop the scope of the proposed research, an extensive review of literature on related topics has been carried out. Due to lack of published work on a single uncoupled shaft with misalignment, a rotor system with a single disk and single flexible shaft supported on two bearings is considered for development of model for rotor system with misalignment. A model based on preload due to shaft misalignment and resulting additional non linear stiffness in the direction of misalignment is used in generating rotor responses to unbalance in the presence of varying misalignment. The time domain simulation results were extensively analyzed in frequency domain to examine the influence of misalignment on the rotor responses at multiples of rotating frequency. Experiments were also performed with test rig to validate the response obtained through model simulations. Response data from a real turbine is also collected to aid with the development and testing of the expert system using Neural Network. A Neural Network was developed and trained using simulation data to demonstrate its effectiveness in identifying a specific problem in the rotating system. Finally the trained Neural Network is tested against simulated data and real turbine response data to examine its effectiveness. The proposed research in developing the expert system for identification of unbalance and misalignment in rotor systems is carried out in steps as follows:

1. State of the art relevant to rotor dynamic, neural networks and expert systems were reviewed,

2. A model of an out of balance rotor and a misaligned shaft were developed,
3. The developed models were simulated and validated using a finite element model,
4. The validated model was used to generate time and frequency domain responses for varying misalignments,
5. Results from a rig was used to verify the effect of misalignment on rotor system response,
6. Neural Network (N.N.) was developed and trained to detect unbalance and misalignment based on the responses.
7. The developed N.N. was tested using simulation and engine data.

1.2 Literature Review

The life and usefulness of rotating machinery can be adversely affected by its dynamic behavior. Excessive vibration in rotating machinery could lead to premature failure and loss of availability and reliability of the machine. Rotating machines are thus extensively investigated by researchers to understand the causes and effects of defect in rotor systems. A solution or a monitoring system for rotating machinery is highly sought after by manufacturer and operators of expensive rotating machineries. Such tool can, however, be only developed through in depth understanding of rotor dynamics and response signatures from specific defects. This section of the dissertation presents a detailed review of literature on relevant topics.

The literature review presented deals with three main subjects:

1. Rotor system dynamics,
2. Neural Network,
3. Expert system and their application to gas turbines.

1.3 Rotor System Dynamic

Reliable dynamic analysis is an essential requirement for design of any rotor system. Furthermore, it is a highly complex mechanism consisting of blades, disk, shaft, and multiple bearings that support the assembly. The blade dynamics is studied to determine the natural frequencies and to ensure that an operating condition will not excite any modes that will lead to a failure. Studies of blade only dynamics leads to inaccurate results, because of the simplistic representation of the blade boundary conditions. Disk dynamics is studied for the same reason as blades to ensure that during operation the disk does not fail due to vibration. Similarly, a disk only model does not predict the dynamic behavior accurately because the mass and stiffness of the blade is not taken into account. Hence dynamics of bladed disks have been studied. These models have resulted in better results for both the blades and the disk. These models despite their better accuracy were still not adequate for the requirements imposed on today's rotating machines. This resulted in the study of rotors where the blades, disks, shaft and bearings are modeled and a full system approach is considered.

Hence the literature dealing with the general subject of rotor dynamics could be divided into five distinct sub-topics:

1. Blade dynamics,
2. Disk dynamics,
3. Blade/disk interaction,
4. Rotor dynamics,
5. Misalignment effect on rotor dynamics

The literature dealing with above sub-topics of rotor systems are reviewed in the following sub-sections.

1.3.1 Blade dynamics,

Blade failure on an engine could lead to catastrophic event especially in case of multiple blade failures. The ability to predict blade vibration could help reduce the risks of such failures in gas turbine engines. William Carnegie [1] presents a theoretical expression of the work done due to centrifugal effects when a rotating cantilever blade executes small vibrations. Using Rayleigh's method an equation for the fundamental frequency is established and a solution is deduced for a straight blade of uniform symmetrical cross-section. M. M. Bhat, V. Ramamurti and C Sujatha [2] present in their paper a comparison between blade and bladed disk models and compare the analyzed results with the results obtained from tests performed on a 235 MW steam turbine. The turbine consisted of five high pressures and five low-pressure stages. The results of the research show that a

simple blade alone model fixed at the root gives slightly higher natural frequency than a blade fixed to a disk since it assumes that the blade is rigidly fixed. A single blade disk model gives a more accurate prediction of the natural frequency but cannot predict coupled modes. A model that has more blades can predict the coupled modes more accurately. The paper also presents the effect of lacing wires and lacing chords, which increases the natural frequency as the running speed increases. Depending on the aspect ratios the blade can be modeled as a beam or a plate. R.B. Bhat [3] presents a method to determine the natural frequencies of rectangular plates using a set of beam characteristic orthogonal polynomials in the Rayleigh Ritz method. Natural frequencies calculated using the orthogonal polynomial functions are compared with those obtained using other methods showing that the orthogonal polynomial method yields better results for lower modes, particularly when plates have some of the edges free. Vyas and Rao [4] present a mathematical model of bladed disk rotating at a variable speed. The model takes into account the Coriolis forces. The derived equations are useful in analyzing the dynamics of long slender blades. A.G. Henried [5] presented a computer program to determine the small deflection in a blade subjected to an arbitrary dynamic load. The model of the blade used is developed using a linearly elastic Bernoulli-Euler beam fixed at one end and rotating with constant angular velocity. S.V. Hoa [6] investigates the vibration of a rotating beam with a tip mass. A finite element model is used, and a third order polynomial is assumed for the lateral frequency. The effect of the root radius, the tip mass and the setting angle is incorporated in the finite

element model. The results are compared with results from other investigations using the Myklestad and extended Galerkin methods. The paper shows that the setting angle has a significant effect on the first mode frequencies but not on the high frequencies. The tip mass tends to decrease the frequencies at low speeds of rotation and tends to increase the frequencies at high speed of rotation. R. B. Bhat [7] studies the natural frequencies and mode shapes of a cantilever beam with tip mass using beam characteristic orthogonal polynomial in the Rayleigh-Ritz method. The set of orthogonal polynomials that satisfy the boundary conditions is generated using the Gram-Schmidt process. The results are compared with the results obtained by the Myklestad and extended Galerkin methods and finite element methods.

1.3.2 Disk Dynamics

A disk modeled as a thick plate is used by Sinha [8] to establish the natural frequencies using Rayleigh Ritz method. Celep [9] presents a study on the behavior of a free circular plate subjected to a non-conservative radial load with the purpose of studying the stability of a circular plate. Iwan and Moeller in their paper [10] present an investigation in the effect of a transverse load on the stability of a spinning elastic disk. The investigation shows that the disk is unstable for speeds in a region above the critical speeds of vibration of a spinning disk due to the effects of the load stiffness. Adams in his paper [11] studies the dynamic of a flexible disk. The paper shows that at certain critical

speeds the disk is not able to support arbitrary spatially fixed transverse loads. The paper deals more with flexible disks (floppy disks) and is only mentioned here for reference. Chonan [12] in his paper develops a theory for the vibration of an elastic disk subjected to a conservative load on its edge. The theory shows that a disk under a non-conservative tangential radial load has several flutter instability loads in addition to divergence instability load. Lehmann and Hutton [13] present the results of an experimental and analytical study into the dynamic (vibrational) characteristic of guided rotating saws that are not perfectly flat. Tönshoff and Jendryschik [14] study the dynamical behavior of rotating cutting tool to improve the surface quality after the machining operation. In the paper the dynamic behavior of rotating cutting tools is investigated via experimental and analytical methods.

1.3.3 Blade/disk interaction

In the previous two sections the literature review on blade dynamics and disk dynamics was presented. The interaction of the blades and the disk result in a complex system requiring more extensive modeling. The lack of proper understanding of the dynamic properties of a bladed disk during the design phase of a gas turbine engine could lead to operational problems. Work was done to understand the dynamic properties of a bladed disk. J. T Wagner [15] presents mathematical models of blade attached to a flexible disk and on a rotor with finite mass. The model developed in this paper demonstrates the effect of

coupling on blade frequency and demonstrate that the frequency of the blade is reduced due to the flexibility of the disk. D. J Ewins [16] in his paper presents an analysis of a bladed disk to establish its vibration characteristics. The analysis shows that there are more blade natural frequencies than those predicted by the blade cantilever modes. S. J. Wildheim [17] presents a method to estimate the natural frequencies of a bladed disk using a dynamic sub-structuring method employing the free modes of the disk and the clamped free modes of the blade. V. Omprakash and V. Ramamurti [18] present a Reyleigh Ritz and cyclic symmetry method for the analysis of a rotating bladed disk system. The method predicts the few lowest frequencies accurately. Since the blades mounted on a disk do not alter the rotor response significantly, a bladed disk can be modeled as a simple disk, for the purpose of studying rotor response, as long as the blade masses are accounted for. This modeling method will yield equally good trend in the responses due to unbalance in the rotor and shaft misalignment.

1.3.4 Rotor Dynamics

A shaft supported on a bearing may have multiple critical speeds that the system will pass through before it reaches its operating speed. The design of such a system must ensure that no critical speeds are in the vicinity of the operating speed. The main task of an engineer is to make sure before the execution of the design that the previously stated condition is respected. The dynamic characteristic of a rotor is greatly affected by the support stiffness. In most cases

rotors will be supported on bearings that will contribute to the whole system damping and stiffness. The bearing location and dynamic characteristic could improve or deteriorate the system dynamic behavior. It is therefore very important to model the rotor support in a way that would lead to predicting proper dynamic properties of the whole system during the design phase.

Rajalingham, Xistris and Bhat [19] in their paper investigate the effect of the fluid film bearing and the shaft material damping on the rotor dynamics. Vázquez, Barrett, and Flack [20] present in their paper a study about the effect of bearing support flexibility on the stability and response of a flexible rotor. Lees and Friswell [21] present in their paper a method of evaluating the imbalance of a rotating machine using the measured pedestal vibration. The method requires a good numerical method for the rotor and an approximate model for the bearing behavior. Bansal and Kirk [22] present in their paper a method to calculate the critical speed and stability of a rotor-bearing system. The paper takes into account the effect of bearing and bearing support flexibility. The present study will focus on the effect of shaft misalignment neglecting bearing compliance, since the flexibility of the shaft is significantly less than the flexibility of the bearing support system.

1.3.5 Misalignment effect on rotor dynamics

Misalignment is one of the major causes of machinery vibration in the field, yet only limited research has been conducted on misalignment. The literature reports that misalignment results in an increase in the 2x response (at a frequency two times the rotating frequency) and the presence of harmonics. The research conducted so far has modeled rotor, bearings and coupling using non-linear properties to explain the rotor response due to misalignment.

Al-Hussain [23] in his paper studies the effect of angular misalignment between 2 rigid rotors connected by a flexible coupling on their stability. Xu and Marangoni [24, 25] present a theoretical model of a complete motor-flexible coupling-rotor system. The theoretical model and the experimental validation results are in agreement. They also show that the 2x component is magnified when close to a system natural frequency. The source of the 2x component is the universal joint that is used as a coupling. Sekhar and Prabhu [26] present a rotor bearing system modeled using higher order finite element. The model shows the effect of misalignment on harmonics and the increase of the 2x component. The dominance of the 2x component is attributed to the unbalance excitation that had a second harmonic and the location of the coupling with respect to the bending mode shape. Y.-S. Lee and C.-W. Lee [27] present a rotor-ball bearing system. A dynamic model is derived and experiments are carried out with a laboratory test rig. Both the model and laboratory tests agree in

that the orbit tends to collapse toward a straight line and that the natural frequency of the system associated with the misalignment direction tends to increase due to the bearing non linear stiffness. Rao [28] attributes the response due to misalignment to coupling forces, shaft preload, and bearing nonlinearities. Al-Hussain and Redmond [29] study the effect of parallel misalignment on the lateral and torsional responses of two rotating Jeffcott rotors. The results show that misalignment affects the torsional and lateral responses. The study, however, did not reproduce the effect of misalignment in the form of the 2x component. El-Shafei [30] showed that misalignment affects the second-harmonic using examples from misaligned industrial equipment. Saavedra and Ramirez [31, 32] present a theoretical model of a misaligned rotor coupling system. The coupling stiffness matrix was established using tests. They show that the vibration that resulted from misalignment is due to variation of the coupling stiffness during rotation. Harmonics (1x, 2x, 3x, etc...) are observed in their results. Muszynska [33] in her book attributes the 2x and harmonics to a nonlinear stiffness. The nonlinear stiffness is presented as a function of square of the displacement. The nonlinear stiffness generates 2x and harmonics. A.W. Lees [34] models two misaligned rigidly coupled rotors. In his model, the forces are developed in the coupling due to misalignment. The model shows that misalignment results in the 2x response but does not show harmonics except under certain rotational speeds. The harmonics were explained as an interaction between torsional and flexural effects.

From the review of literature presented thus far it is evident that, the effect of misalignment in a rotor system is not well understood. Clearly, there are discrepancies in establishing the existence of an increase in the 2x component due to misalignment and its natural cause. From the review of literature it is also established that it is adequate to consider a simple rotor modeled as a disc in order to carry out in depth investigation of rotor misalignment and its effect on the rotor responses. A clear understanding of the effect is a prerequisite for developing any expert system using tools such as Neural Network.

1.4 Neural Network

Neurocomputing and Neural Networks (N.N.) in simple terms is an attempt to simulate the human brain. It is however important to mention that in no way the N.N. is a match to the human brain. Human brain is formed of neurons, where each neuron is formed of an input area the dendrites, a processing area the synapse and an output area the axons which is connected to other neurons. Similarly, the N.N. is formed of artificial neurons (A.N.), where each neuron is formed of an input area, a processing element and an output area. A systematically linked network of A.N. is carried out in the construction of N.N. The present research is focused on the application of the advance neurocomputing technology to identify specific vibration problems that could arise in a rotor system.

The beginning of neural computing and N.N. is often considered to be the paper by McCulloh, Walter and Pitts [35]. In their work, although practical application of such work was not apparent, they were able to show that a simple type of N.N. could compute any arithmetic or logical function. Other researchers [36, 37] suggested that research in brain-like computers might have wider applications. D.O. Hebb [38] proposed that the connectivity of the brain neuron is continually changing as an organism learns. He proposed that a specific learning law be introduced for processing area or the synapses of neurons. N.N. is most effective when the problem to be solved depends on many parameters and where physical properties could not be expressed in equations. The theoretical concept of N.N. has been around since 1940s, but its development has been slow due to computational limitations. The first successful neurocomputer (the Mark I Perceptron) was developed during 1957 and 1958 by Frank Rosenblatt, Charles Wightman and others [39]. Following that period, N.N. research went into a quiet phase from 1967 to 1982. With the development of algorithms, programming techniques and fast computers, it gained momentum in the 1980s. In the early 1980s the Defense Advanced Research Projects Agency (DARPA) began funding neurocomputing research. DARPA funding opened the door for neurocomputing to demonstrate its potential and effectiveness in a wide range of applications. Today neurocomputing and N.N. have found their ways into various types of applications like system modeling, control, classification, medical diagnostics, robotics, automation and many other fields. Several articles and books [40, 41, 42, 43] have appeared on various aspects of N.N. algorithms,

applications and software in the 1990s. Zurada [40], Hechlt-Nielsen [41] and Freeman [42] have published books in the area of N.N. These books present a complete introduction to N.N. along with different types and their applications. Some of these N.N. types are:

Adaline and Madaline: has gained application in adaptive signal processing. It is a N.N. algorithm that can be implemented as filters to perform noise removal from information-bearing signals.

Back-propagation: has an application in problems requiring recognition of complex patterns and performing non-trivial mapping. It is a network that adapts itself to "learn" the relationship between a set of example patterns, and is able to apply the same relationship to a new input pattern. Back-propagation network, therefore, has potential application in simulation, control of dynamical systems and reverse dynamics. Taraboulsi [44] successfully applied this method in modeling, simulation and control of vehicle dynamics.

General regression network: is a general-purpose network. It gained applications in system modeling and prediction. A main advantages of general regression network are fast learning, can be used effectively with sparse data and can handle non-stationary data.

Modular neural network: is a generalization of back-propagation neural network. It is applied to system modeling, prediction, classification, and filtering. The modular neural network is a generalization of the back propagation network.

Among various N.N. developed to date, back-propagation network can be easily adapted for application to simulation of dynamical system, control optimization and expert systems. Hunt and Sbarbro [45] present the use of N.N. as a controller. The N.N. is used as a representation framework for modeling nonlinear dynamical systems; it is then possible to use these nonlinear models within nonlinear feedback control structure.

In developing a N.N. application one should take into consideration that success of N.N. to learn is not guaranteed. Sometimes for no apparent reason N.N. might not learn and will not give adequate results [41]. Developing a N.N. application is carried out by trial and error until the best results are obtained. It is important to note that there should be no similar inputs to the N.N. with different outputs; if such a case is presented to the N.N. learning would be impossible.

1.5 Expert system and application to Gas Turbine Engines (GTE)

Gas Turbine Engines (GTE) are highly complex machines with numerous components and are very expensive. It is therefore essential that the GTE function properly and efficiently for a long period of time. GTE could suffer from

mechanical breakdown that could lead to long period of shutdown and costly repairs. For example a bearing failure or blade failure could lead to an engine removal and a long period of shutdown. Today companies rely on Long Term Service Agreement (LTSA) and power/hour performance. It is essential that GTE failure rate be minimized and be predicted. The predictions of a failure ahead of time would give the engineering team an opportunity to schedule proper maintenance and/or engine change out when the engine is not needed. This could be accomplished by the introduction of expert systems that can monitor engine health and diagnose engine problems.

Edwards, Lees and Friswell [46] present a complete literature review of the state of the art in fault diagnosis techniques. The review emphasizes on the use of expert system in the field of rotating machinery. DePold and Gass [47] first present in their paper the application of statistical analysis and neural networks filters to improve data quality collected from a gas turbine engine. They also present the use of neural networks for trend change detection and classification to diagnose engine performance change (loss of power, compressor and turbine efficiency) and finally they present an expert system to diagnose, provide alerts and to rank maintenance action recommendations. Lu, Zhang, Hsu and Zhang [48] present in their paper the use of back-propagation and feed forward neural networks to develop engine condition monitoring and diagnostic tools. Their results indicate that neural networks fault diagnosis cannot achieve more than 50-60% success rate if the data contained high levels of noise. Botros, Kibrya

and Gtover [49] present the successful use of neural networks to perform various data mining on a Rolls-Royce RB-211 gas turbine. Multilayer perceptron, radial basis function and general regression neural networks are used. The radial basis function neural networks are capable of backing up critical engine parameters, detection of sensor faults, prediction of complete engine health with few variables, and estimation of parameters that cannot be measured. Volponi, et al. [50] present a comparative study between the Kalman filter and neural networks for the gas turbine performance diagnostics. The study outlines the pros and cons of each method and that the Kalman filter method have a very slight advantage over neural network. Tan [51] present two novel approaches to the fault classification problem using first Fourier neural networks and second using generalized single hidden layer networks. The networks are used to diagnose multiple modular faults on the F404 engine components. Both methods show successful results and are superior to the back propagation networks at least for this application. Verma, et al. [52] develop a genetic fuzzy system using a linearized model of the gas turbine engine for performing gas turbine fault isolation. A radial basis function neural network is also used to preprocess the measurements taken on the engine before faults isolation. The radial basis function neural network shows significant noise reduction and when combined with the genetic fuzzy system the result is a fault diagnostic tool that is robust against the presence of noise.

Chu and Wang [53] present a method to detect rubbing in rotating machinery and to identify the location of the rub using acoustic emission and wavelet transform. Seibold and Weinert [54] present in their paper a time domain identification algorithm that uses a series of extended Kalman filters to identify crack location. Yang et al. [55] present an ART-Kohonen neural network that performs fault diagnosis on rotating machinery. In their research, a wavelet transform is used instead of a fast Fourier transform (FFT) because it is more tolerant to the presence of noise and drift in sensor response and more effective in terms of data compression. The neural network is trained and tested in a laboratory using a fault generator rig to detect unbalance, misalignment, resonance and, bearing damage. This method relies on the availability of considerable amount of data for different failures, in this case 80 sets of data representing different failure scenarios is used. In gas turbine engines generating such data is not possible. In addition the developed method is only used in a laboratory on a specific machine, and is not tested on real machines. Yang, et al. [56] present an ART-Kohonen (KNN) neural network that is integrated with a case-base reasoning to enhance fault diagnosis. The ART-KNN is used to make hypotheses and to guide the case base reasoning to learn based on the findings that are commonly observed for each diagnosis considered. This in turn is used to guide the case base reasoning module in the search for similar cases. Hend and Nor [57] propose a method of detecting bearing damage using sound and vibration signals. These signals are analyzed using statistical methods to identify bearing problems. The methods developed are successfully validated and tested

on a rig. Krodkiewski, et al. [58] present in their paper a method of identifying a change in the unbalance of a rotor using a non-linear mathematical model coupled with change in the displacement of the rotor. The method allows the identification of the amount of unbalance and its location, assuming it is in one plane. The method furthermore, provides the modification required to reduce the unbalance. Openheimer and Dubowsky [59] present in their paper a method for predicting the noise and vibration of machines and their support structures. Hoffman and Merwe [60] evaluate in their paper three different neural network classification techniques to detect bearing problem and unbalance. The three techniques are Kohonen self organizing maps, nearest neighbor rule classifiers, and radial basis function. Among the techniques self organizing maps yields the best results when compared to the other methods. The validation tests are conducted on a rig.

Literatures found in the field deals with theoretical methods of detecting rotating machine problems and are based on simple pattern identification. In addition, most of the papers present experiment done in labs in a controlled environment. These experiments rarely represent a real environment where a lot of noise is present in the signal recorded from the transducer. Hu, et al. [61] present in their paper a feed forward N.N. using back propagation, node decoupled extended Kalman filter (NDEKF) and support vector machines to create an inverse dynamic model of a propulsion system rotor that is capable to identify unbalance and its location. A simulation is used to provide the data to train and test the NN.

Filippetti, et al. [62] present in their paper a NN trained and tested using a mathematical model of an electric machine to identify rotor problems. In this work, four models are used, three to train the network and one to test it. Tse and Wang [63] present in their paper a combination of recurrent back-propagation (RBP) NN and fuzzy adaptive resonance theory to create a machine condition forecaster and classifier that is able to detect fault through vibration monitoring. The developed method was used on compressor connected to an electrical motor. Crupi, et al. [64] present in their paper a method to diagnose rotating machinery using NN. The method proposed consists of two sections; the first is an analysis section using self organizing map and the second a diagnostic section using radial basis function - probabilistic neural network. The method was used in the diagnosis of an overhung fan used at the refinery of Milazzo. McCormik and Nandi [65] present in their paper a N.N. that provides the mean of capturing stationary statistical information about machine vibrations in the form of non-linear autoregressive models. These models are then used as one step predictors allowing comparison of signals for the purposes of fault detection and diagnosis. The experimental setup used to generate vibration time series for this work consists of a small electric motor that drives a shaft with a flywheel. Two faults are introduced; unbalance and rubbing. Li, et al. [66] present in their paper a back propagation neural network to detect mass unbalance. The expert system uses acoustic signals as input. The system is tested and validated using a rig in a lab using proximity probes and acoustic signal. The system performs as expected but has some limitations in discriminating between faults near the

natural frequencies. Şeker, et al. [67] present a study on the use of recurrent neural network (RNN) for condition monitoring and diagnosis of nuclear power plant system. Their study is split into two parts; the first part presents the use of RNN in detection of anomalies in simulated power operation of a high temperature gas cooled nuclear reactor. The second part presents the use of RNN in the diagnosis of bearing problems on a 5 HP electric induction motor.

1.6 Scope and Objective of the Present Research

It is evident from the above literature review, that there have been numerous attempts in using N.N. for expert system in applications to diagnostics. There also has been limited success in its applications where it is tested using simulation results or very simple test rig in controlled laboratory environment. Some literature present methods and application for rotor system unbalance. However, there is no evidence of any significant attempts in the diagnosis of misalignment in a rotor system. Furthermore, the author did not find any literature that directly addresses the vibration problems associated with a GTE. The proposed research will focus on an expert system that will be developed using NN and that will be applied for identification of engine problems using available engine data from engines running in the field.

Reports from the field show that shaft misalignment results in a shaft response that has a 2x component as well as harmonics. The first objective of this

research is thus aimed at developing a rotor model with unbalance and misalignment to examine their effects. Shaft misalignment regardless of being parallel or angular essentially introduces a preload and nonlinear stiffness to the shaft. This nonlinear stiffness is proportional to the misalignment magnitude and will introduce a response at a frequency two times the rotational speed commonly referred to as 2x response. This is accomplished by modeling a rotor in a way to emphasize the effect of the nonlinear stiffness. The second objective of this research is to develop an expert system that can identify unbalance and misalignment using N.N. The developed N.N. trained off-line will allow its implementation on any engine. In addition, the method developed can be extended to detect other defects in a rotating system or other systems. The final objective of the proposed research is to test the developed expert system for diagnosis based on field data obtained from a GTE.

1.6.1 Organization of the Thesis

In chapter 2, the different strain and kinetic energy equations that are needed to develop the mathematical model of a rotor system are presented. The stiffness matrix for different shaft configurations is also established in this chapter.

Chapter 3 is devoted to the development of equations of motion for three different configurations. The first sets of equations of motion are developed for a perfectly aligned rotor supported on two rigid bearings, ignoring the higher order

terms. The second sets of equations of motion including higher order terms are developed in order to examine their influence. The third sets of equations of motion are developed for a misaligned rotor supported on two rigid bearings.

In chapter 4, the equations of motion are solved theoretically to establish the natural frequencies of the rotor at different speeds. The natural frequencies obtained from the solution of the equations are used to validate the simulation results in time domain. The effect of the second order terms is then studied and the rotor response with and without the second order terms are compared. Finally the simulations are validated against a finite element model and the limitation of the finite element model to simulate the effect of misalignment on the rotor response is examined.

In chapter 5 a study is carried out on the effect of nonlinear stiffness and damping on the rotor response. The nonlinear stiffness and damping for the rotor are chosen and simulations are carried for the rotor system with and without misalignment to systematically examine the effect of misalignment on the rotor response. The simulated results of rotor responses due to misalignment are discussed in details.

Chapter 6 is devoted to laboratory experiment using an available test rig. The test results are obtained for misaligned shaft in terms of responses at the bearing. The test results are compared with those established in chapter 4.

Chapter 6 also presents field test data from real GT Engines which are known to have a shaft misalignment.

An introduction to neural network is presented in chapter 7. Back-propagation and logicon projection, the two neural network used to develop the expert system are presented in detail. The different parameters used to develop the neural networks are also discussed and presented in this chapter. Finally, the steps adopted in developing the expert system using the N.N. are discussed and presented.

In Chapter 8, the detection logic is developed and the method to filter the data is presented. Two neural networks presented in chapter 7 are developed and trained using simulation data. The developed neural networks are then tested using data from the simulation as well as field test data of a GTE. The performance of both developed neural networks is compared.

Finally chapter 9 presents general and specific conclusions related to the present study. A list of recommendation for further work is also included in this chapter.

Chapter 2

2 Energy Formulation for a Rotor System

2.1 Introduction

A rotor system consists of a rigid disc within the span of a shaft which is flexible. The shaft in turn may be supported at one or both ends on a set of bearings. The bearings in reality are also flexible elements that can be represented by spring and damper with linear or non linear characteristics. In considering response due to misalignment in the shaft support system, where misalignment introduces a nonlinear stiffness to the shaft, it would be more meaningful to consider the bearings as rigid. The proposed rotor model thus consists of flexible shaft with a rigid disk and rigid bearings.

The most general approach for formulating the mathematical model for the rotor system is the Lagrange's equation based on energy. The energy method is used in this study to formulate the equation of motion due to its simplicity and generality. To be able to formulate the equation of motion using the Lagrangian all the energy terms need to be established. This chapter presents the strain and kinetic energy terms that are required to formulate the Lagrangian for a rotor. In chapter 3, the energy terms formulated in this section are used to formulate the equations of motion. Expressions for strain energy for the shaft and kinetic energy for the disk with and without unbalance are developed in this chapter for a rotor system with misalignment.

2.2 Strain Energy

2.2.1 Strain Energy of Shaft

In this section, the strain energy for a simple flexible shaft subjected to bending is formulated. Bending of the shaft attributed to force and moment acting at the rotor location is used to obtain the energy expressions. Based on the deflection at the disk location the stiffness matrix for the shaft under a given boundary condition can be established.

2.2.1.1 Strain energy of a shaft due to bending

When a flexible shaft is subjected to vertical / lateral force or moment, the strain energy in term of deflection and stiffness is:

$$U = \frac{1}{2}\{y\}'[k]\{y\} \qquad 2\text{-}1$$

Where $\{y\}$ is the displacement vector and $\{k\}$ is the stiffness matrix and ' denotes the vector transpose. Furthermore, the deflection of the shaft can be related to the moment (M) within the elastic limit by:

$$\frac{d^2y}{dx^2} = -\frac{M}{EI_y} \qquad 2\text{-}2$$

For a simple rotor system supported on two bearings, the reaction to a force F at the disk is shown in Figure 2-1. Similarly the reaction forces due to pure

moment acting at the rotor are shown in Figure 2-2. Using the moment expression along the shaft in Figure 2-1, equation (2-2) can be expressed as:

$$EI_y \frac{d^2y}{dx^2} = -\frac{Fb}{a+b}x \qquad 0 \le x < a \qquad 2\text{-}3$$

And

$$EI_y \frac{d^2y}{dx^2} = -\frac{Fb}{a+b}x + F(x-a) \qquad a \le x < b \qquad 2\text{-}4$$

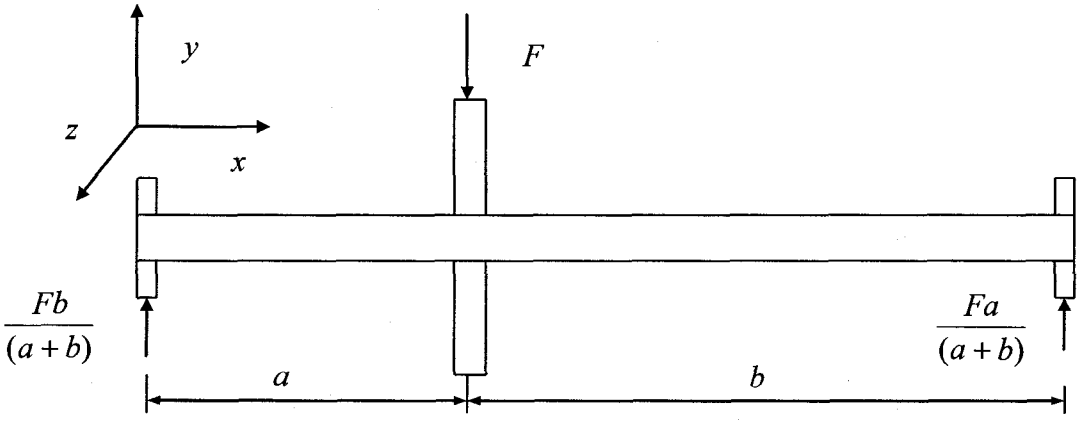

Figure 2-1 Rotor subjected to a force

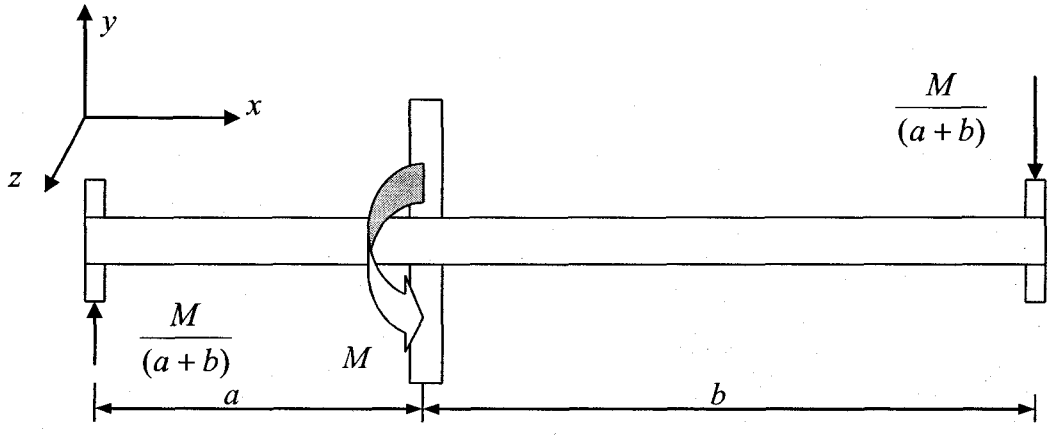

Figure 2-2 Rotor subjected to a Moment

The slope and deflection at any point along the shaft can be established by integrating the expressions in equations (2-3) and (2-4). The integration constant can then be established using the boundary conditions and validity of both equations at $x = a$. In doing so, the deflection and slope of the shaft due to force F valid for $0 \le x \le a$ are:

$$y = \frac{Fbx}{6(a+b)EI_y}(a^2 + 2ab - x^2) \qquad 0 \le x < a \qquad 2\text{-}5$$

$$\phi = \frac{dy}{dx} = \frac{Fb}{6(a+b)EI_y}(a^2 + 2ab - 3x^2) \qquad 0 \le x < a \qquad 2\text{-}6$$

At the disk, for $x = a$, the deflection and slope due to F is:

$$y = \frac{Fa^2b^2}{3(a+b)EI_y} \qquad 2\text{-}7$$

$$\theta = \frac{Fba}{3(a+b)EI_y}(b-a) \qquad 2\text{-}8$$

Similarly for the shaft subjected to a pure moment (M) as shown in Figure 2-2, the deflection and slope at the disk location are:

$$y = \frac{Mba}{3(a+b)EI_y}(b-a) \qquad 2\text{-}9$$

$$\phi = \frac{M}{3(a+b)EI_y}(a^2 + b^2 - ab) \qquad 2\text{-}10$$

The total deflection of a shaft subjected to a force F and moment M at location a is:

$$\begin{bmatrix} y \\ \phi \end{bmatrix} = \begin{bmatrix} \frac{a^2b^2}{3lEI_y} & \frac{ba(b-a)}{3lEI_y} \\ \frac{ba(b-a)}{3lEI_y} & \frac{(a^2+b^2-ab)}{3lEI_y} \end{bmatrix} \begin{bmatrix} F \\ M \end{bmatrix} \qquad 2\text{-}11$$

where $l = a + b$.

From the above equation the stiffness matrix of the simply supported rotor is:

$$\begin{bmatrix} F \\ M \end{bmatrix} = \begin{bmatrix} \frac{3lEI_y(a^2+b^2-ab)}{a^3b^3} & \frac{3lEI_y(a-b)}{a^2b^2} \\ \frac{3lEI_y(a-b)}{a^2b^2} & \frac{3lEI_y}{ab} \end{bmatrix} \begin{bmatrix} y \\ \phi \end{bmatrix} \qquad 2\text{-}12$$

Following the same procedure, one can find the stiffness matrix for a shaft with one end fixed and one end simply supported to be:

$$\begin{bmatrix} F \\ M \end{bmatrix} = \begin{bmatrix} \frac{3EI_y(a^3+4b^3)}{a^3b^3} & \frac{3EI_y(a^2-2b^2)}{a^2b^2} \\ \frac{3EI_y(a^2-2b^2)}{a^2b^2} & \frac{EI_y(3a+4b)}{ab} \end{bmatrix} \begin{bmatrix} y \\ \phi \end{bmatrix} \qquad 2\text{-}13$$

Similarly, for fixed boundary conditions at both bearings the stiffness matrix is established as:

$$\begin{bmatrix} F \\ M \end{bmatrix} = \begin{bmatrix} \frac{12lEI_y(a^2-ab+b^2)}{a^3b^3} & \frac{6lEI_y(a-b)}{a^2b^2} \\ \frac{6lEI_y(a-b)}{a^2b^2} & \frac{4lEI_y}{ab} \end{bmatrix} \begin{bmatrix} y \\ \phi \end{bmatrix} \qquad 2\text{-}14$$

In general, the stiffness matrices given by (2-12), (2-13), (2-14) can be written as:

$$\begin{bmatrix} F \\ M \end{bmatrix} = \begin{bmatrix} K_{11} & K_{12} \\ K_{21} & K_{22} \end{bmatrix} \begin{bmatrix} y \\ \phi \end{bmatrix} \qquad 2\text{-}15$$

Since the rotor is free to move along the y and z directions, the total strain energy using equation (2-1) must be expressed as:

$$U = \frac{1}{2}\{y\}'[k]\{y\} + \frac{1}{2}\{z\}'[k]\{z\} \qquad 2\text{-}16$$

For symmetric stiffness matrices ($K_{21} = K_{12}$), the total strain energy for the shaft is:

$$U = \frac{1}{2}(K_{11}y^2 + 2K_{12}\phi\, y + K_{22}\phi^2) + \frac{1}{2}(K_{11}z^2 + 2K_{12}\psi\, z + K_{22}\psi^2) \qquad 2\text{-}17$$

where ϕ represents the slope corresponding to deflection y and ψ represents slope corresponding to deflection z.

2.3 Kinetic Energy

2.3.1 Kinetic Energy in a Disk

The kinetic energy in a disk will be caused by its linear and rotational velocities. The disk shown in Figure 2-3 rotates about the x_3 axis along the shaft. Due to the flexibility of the shaft the disc is further free to rotate about y_3 and z_3 axis. For linear motion the disk is free to move laterally in the y_3 and z_3 direction due to self excitations. To establish the instantaneous rotational speed around the three main axes, Euler angles are used. In Figure 2-3, first the disk rotates by an angle ψ around the Z axis, then by an angle ϕ around the y_1 axis and finally by an angle θ around the x_2 axis. The rotation matrix for the 3 described rotations are [70, 71]:

$$A = rot(x_2, \theta) = \begin{bmatrix} 1 & 0 & 0 \\ 0 & \cos(\theta) & -\sin(\theta) \\ 0 & \sin(\theta) & \cos(\theta) \end{bmatrix}, \qquad 2\text{-}18$$

$$B = rot(y_1, \phi) = \begin{bmatrix} \cos(\phi) & 0 & \sin(\phi) \\ 0 & 1 & 0 \\ -\sin(\phi) & 0 & \cos(\phi) \end{bmatrix} \qquad 2\text{-}19$$

and

$$C = rot(Z, \psi) = \begin{bmatrix} \cos(\psi) & -\sin(\psi) & 0 \\ \sin(\psi) & \cos(\psi) & 0 \\ 0 & 0 & 1 \end{bmatrix} \qquad 2\text{-}20$$

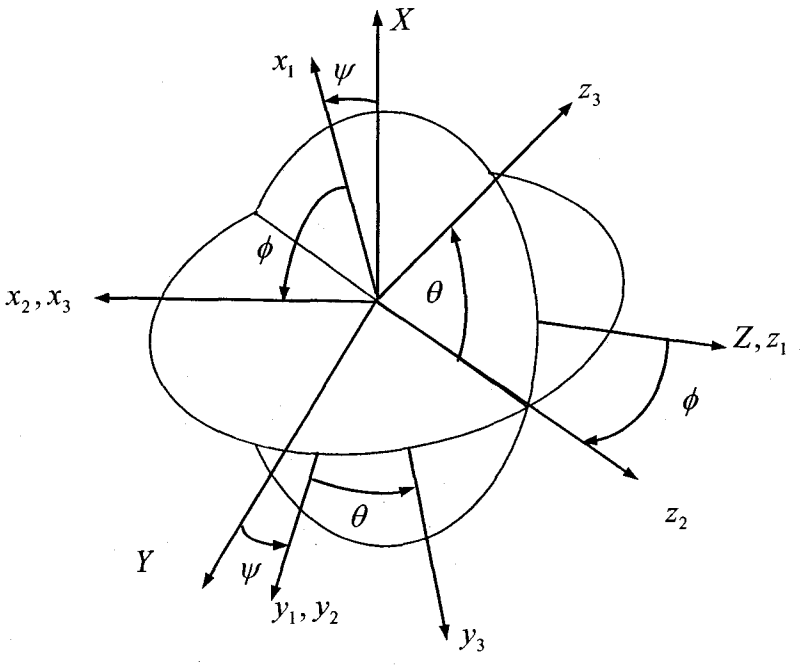

Figure 2-3 Reference frames for a disk rotating around the x axis

The instantaneous angular velocity of the $x_3y_3z_3$ frame is:

$$\omega = \dot{\psi}\, Z + \dot{\phi}\, y_1 + \dot{\theta}\, x_2 \qquad 2\text{-}21$$

In order to calculate the kinetic energy of the disk about its center of mass, it is necessary to establish the angular speeds using frame $x_3y_3z_3$, as:

$$\omega_{x_3y_3z_3} = \begin{bmatrix} \omega_{x_3} \\ \omega_{y_3} \\ \omega_{z_3} \end{bmatrix} \tag{2-22}$$

Each component of the angular speeds in equation (2-22) are obtained in the following manner. The first angular rotation ψ about the Z axis occurs at an angular velocity of $\dot{\psi}$:

$$\omega_{z_a} = C\begin{bmatrix} 0 \\ 0 \\ \dot{\psi} \end{bmatrix} = \begin{bmatrix} 0 \\ 0 \\ \dot{\psi} \end{bmatrix} \tag{2-23}$$

Where C is the rotational matrix given by equation (2-20).

The second rotation is then about the y_1 axis:

$$\omega_{z_b} = B\omega_{za} = B\begin{bmatrix} 0 \\ 0 \\ \dot{\psi} \end{bmatrix} = \begin{bmatrix} \dot{\psi}\sin(\phi) \\ 0 \\ \dot{\psi}\cos(\phi) \end{bmatrix} \tag{2-24}$$

where the rotational matrix B is presented in equation (2-19). The third rotation for ψ is about the x_2 axis:

$$\omega_{z_c} = C\omega_{z_b} = C\begin{bmatrix} -\dot{\psi}\sin(\phi) \\ 0 \\ \dot{\psi}\cos(\phi) \end{bmatrix} = \begin{bmatrix} \dot{\psi}\sin(\phi) \\ -\dot{\psi}\sin(\theta)\cos(\phi) \\ \dot{\psi}\cos(\theta)\cos(\phi) \end{bmatrix} \tag{2-25}$$

Similarly the first rotation ϕ about the y_1 occurs at an angular velocity of $\dot{\phi}$:

$$\omega_{y_b} = B\begin{bmatrix} 0 \\ \dot{\phi} \\ 0 \end{bmatrix} = \begin{bmatrix} 0 \\ \dot{\phi} \\ 0 \end{bmatrix} \tag{2-26}$$

The second rotation is about the x_2 axis:

$$\omega_{y_c} = C\omega_{y_b} = A\begin{bmatrix}0\\ \dot{\phi}\\ 0\end{bmatrix} = \begin{bmatrix}0\\ \dot{\phi}\cos(\theta)\\ \dot{\phi}\sin(\theta)\end{bmatrix} \qquad 2\text{-}27$$

Finally, the rotation θ occurs around the x_2 axis at an angular velocity of $\dot{\theta}$:

$$\omega_{x_c} = A\begin{bmatrix}\dot{\theta}\\ 0\\ 0\end{bmatrix} = \begin{bmatrix}\dot{\theta}\\ 0\\ 0\end{bmatrix} \qquad 2\text{-}28$$

The total angular velocity for the disk can now be expressed using equation (2-22) as:

$$\omega_{x_3y_3z_3} = \begin{bmatrix}\omega_{x_3}\\ \omega_{y_3}\\ \omega_{z_3}\end{bmatrix} = \omega_{x_c} + \omega_{y_c} + \omega_{z_c} \qquad 2\text{-}29$$

Substituting for the components from equations (2-25), (2-27) and (2-28) yields:

$$\omega_{x_3y_3z_3} = \begin{bmatrix}\omega_{x_3}\\ \omega_{y_3}\\ \omega_{z_3}\end{bmatrix} = \begin{bmatrix}\dot{\theta} + \dot{\psi}\sin(\phi)\\ \dot{\phi}\cos(\theta) - \dot{\psi}\sin(\theta)\cos(\phi)\\ \dot{\phi}\sin(\theta) + \dot{\psi}\cos(\theta)\cos(\phi)\end{bmatrix} \qquad 2\text{-}30$$

Along with the above three rotational motions, the disk is also allowed to move in the y and z directions. Hence the total kinetic energy assuming no dynamic or static unbalance of the disk is defined as:

$$T_D = \frac{1}{2}M_D(\dot{y}^2 + \dot{z}^2) + \frac{1}{2}(I_{Dx}\omega_{x_3}^2 + I_{Dy}\omega_{y_3}^2 + I_{Dz}\omega_{z_3}^2) \qquad 2\text{-}31$$

For a symmetrical disk $I_{Dy} = I_{Dz}$. Assuming small angles ψ and ϕ and that the angular velocity of the disc is constant i.e. $\Omega = \dot{\theta}$, equation (2-31) becomes:

$$T_D = \frac{1}{2}M_D(\dot{y}^2 + \dot{z}^2) + \frac{1}{2}I_{Dy}(\dot{\phi}^2 + \dot{\psi}^2) + \frac{1}{2}I_{Dx}(\Omega^2 + 2\Omega\dot{\psi}\phi) \qquad 2\text{-}32$$

The term $I_{Dx}\Omega\dot{\psi}\phi$ in equation (2-32) represents the gyroscopic (Coriolis) effect.

2.3.2 Kinetic energy of the disk with unbalance forces and moments.

The unbalance force on a rotor is due to the imperfect manufacturing and/or assembly of the rotor system. There are 2 types of unbalance:

1. Static unbalance that is due to the center of gravity of the disk not coinciding with the center of rotation of the shaft,
2. Dynamic unbalance that is due to the disk not rotating around the major axis of inertia.

1. Static unbalance:

During rotation the mass will exert a centrifugal force on the shaft that is proportional to its mass and the square of the rotational speed. Figure 2-4 shows a shaft rotating around the X axis while the center of the disc is at C. The instantaneous location of the rotor mass due to static unbalance is at D. The position of the rotor mass centre is defined by the vector:

$$OD = \begin{bmatrix} x \\ y + e\cos(\dot{\theta}\, t) \\ z + e\sin(\dot{\theta}\, t) \end{bmatrix} \qquad 2\text{-}33$$

The velocity of the rotor mass with unbalance is:

$$V = \frac{d(OD)}{dt} = \begin{bmatrix} 0 \\ \dot{y} - e\dot{\theta}\sin(\dot{\theta}t) \\ \dot{z} + e\dot{\theta}\cos(\dot{\theta}t) \end{bmatrix} \qquad 2\text{-}34$$

The kinetic energy of the disc mass due to linear motion represented by first part of equation (2-31) is thus:

$$T = \frac{1}{2}M_D V^2 = \frac{1}{2}M_D(\dot{y}^2 + \dot{z}^2 + \dot{\theta}^2 e^2 - 2\dot{\theta}\, e\dot{y}\sin(\dot{\theta}t) + 2\dot{\theta}\, e\dot{z}\cos(\dot{\theta}t)) \qquad 2\text{-}35$$

where e represents the eccentricity from the mass center due to static unbalance.

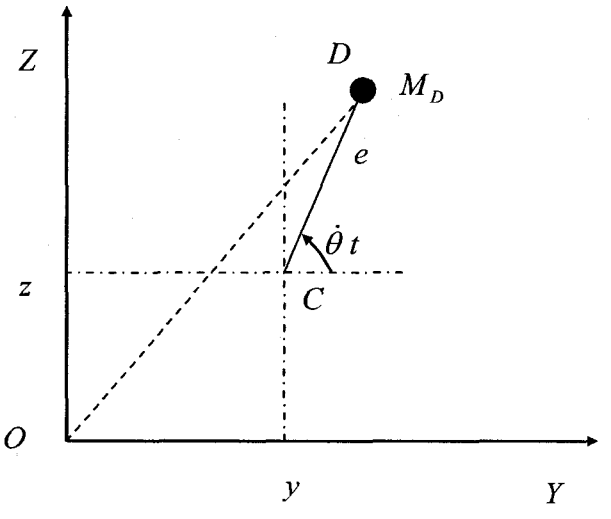

Figure 2-4 Mass unbalance on shaft rotating around the X axis

2. Dynamic unbalance

The dynamic unbalance is due to the rotor not rotating around the principal axis of the rotor as shown in Figure 2-5. In that case there is an angle τ between the

disk principal axis and the rotation axis. Assuming that at the beginning of the motion the y_3' axis coincide with y_3 axis and the angular velocity is defined by equation (2-30) presented earlier.

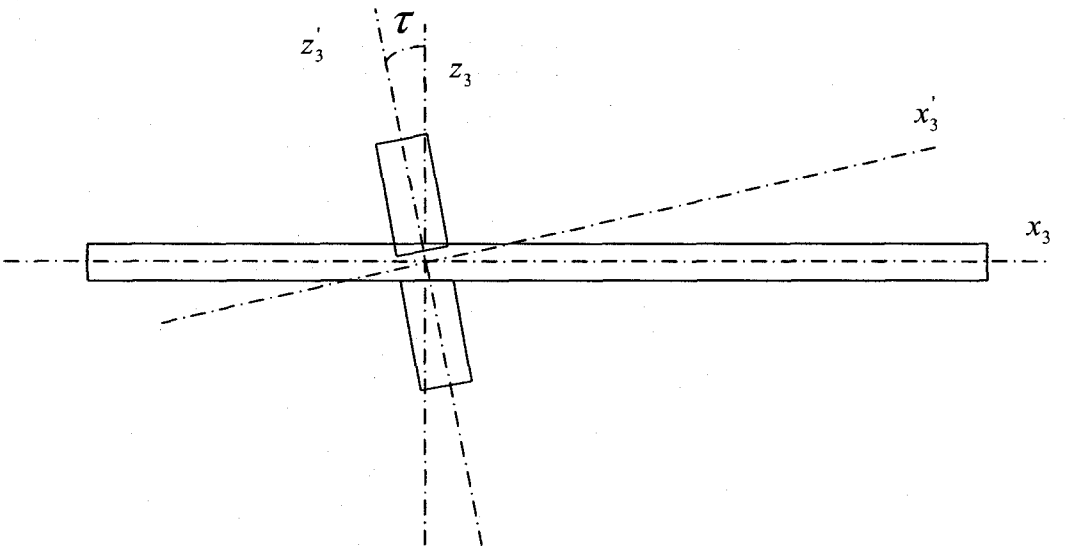

Figure 2-5 Dynamic unbalance

In order to include the dynamic unbalance parameter τ, the rotation matrix around the y_3 axis is defined as:

$$rot(y_3,\tau)=\begin{bmatrix}\cos(\tau) & 0 & \sin(\tau)\\ 0 & 1 & 0\\ -\sin(\tau) & 0 & \cos(\tau)\end{bmatrix} \qquad 2\text{-}36$$

The angular velocity matrix can now be established by multiplying equation (2-30) by the matrix (2-36) to yield:

$$\begin{bmatrix}\omega_{x_3}\\ \omega_{y_3}\\ \omega_{z_3}\end{bmatrix}=\begin{bmatrix}\cos(\tau)(\dot{\theta}+\dot{\psi}\sin(\phi))+\sin(\tau)(\dot{\phi}\sin(\theta)+\dot{\psi}\cos(\theta)\cos(\phi))\\ \dot{\phi}\cos(\theta)-\dot{\psi}\sin(\theta)\cos(\phi)\\ -\sin(\tau)(\dot{\theta}+\dot{\psi}\sin(\phi))+\cos(\tau)(\dot{\phi}\sin(\theta)+\dot{\psi}\cos(\theta)\cos(\phi))\end{bmatrix} \qquad 2\text{-}37$$

The total kinetic energy of the disc for the presence of static and dynamic unbalance with misalignment is thus given by:

$$T_D = \frac{1}{2} M_D V^2 = \frac{1}{2} M_D (\dot{y}^2 + \dot{z}^2 + \dot{\theta}^2 e^2 + 2\dot{\theta}\, e\dot{y}\cos(\dot{\theta}\, t) - 2\dot{\theta}\, e\dot{z}\sin(\dot{\theta}\, t)) + \frac{1}{2}(I_{Dx}\omega_{x_3}^2 + I_{Dy}\omega_{y_3}^2 + I_{Dz}\omega_{z_3}^2) \quad \text{2-38}$$

where the angular velocity terms in equation (2-38) is given in equation (2-37) for a disc with dynamic unbalance.

2.4 Summary

In order to formulate the equations of motion for a rotor system using Lagrange, the necessary energy equations were derived in this section. Assuming the shaft as mass less, the strain energy of the shaft from its flexibility as a result of force and moment applied at disc location was formulated. The resulting stiffness matrix for the shaft was also established. The kinetic energy associated with the disc motions in two linear and three angular directions had been formulated for rotor with unbalance while the shaft is misaligned. The energy expressions are used in the next chapter for developing the equations of motion for the rotor system.

Chapter 3

3 Rotor System Analytical Model

3.1 Introduction

The equations of motion for the rotor system are developed in this chapter using the energy expressions developed for the shaft and rotor in the previous chapter. The primary objectives in deriving the equation are to examine the effect of misalignment in the shaft support systems. This can be achieved by comparing the responses of a perfectly aligned shaft to that of misaligned shaft. The misalignment can further be parallel or angular misalignment. The possible contribution of higher order terms typically neglected in such investigation are also considered in this study in order to examine the consequences of their presence.

In order to facilitate the objectives, three sets of equation of motion are developed. The first set represents a perfectly aligned shaft where higher order terms are neglected. The second set includes the higher order terms due to dynamic unbalance that can be readily compared with the first set. Finally equations are developed for misalignment introduced between support bearings. As discussed earlier, the misalignment in this study introduces a preload and nonlinear stiffness to the shaft. Equations of motion are developed taking into consideration the non linear stiffness and the damping. The initial position of the

disk is derived using the shaft properties. All the equations are derived and discussed in the following sub sections. These equations are used in the next chapter for simulations of response.

3.2 Equation of Motion for Aligned Rotor System

Figure 3-1 presents a rotor system supported on two bearings. The flexible shaft of length l is attached to a rotor at a distance a and b from the left and right support, respectively. The rotor is free to move along y and z directions while rotates about the x axis at an angular velocity ω. The rotor is also free to generate angular motions about y and z axes represented by ϕ and ψ, respectively. For constant angular velocity of the rotor, the four equations of motion can be derived using Lagrangian defined as:

$$L = T - U \tag{3-1}$$

where T and U are the total kinetic and strain energy of the system.

Using the above Lagrangian the equations of motion are derived from the general expression:

$$\frac{d}{dt}\left(\frac{\partial L}{\partial \dot{\delta}_n}\right) - \frac{\partial L}{\partial \delta_n} = 0 \tag{3-2}$$

where δ_n is the general response vector for the rotor given as:

$$\delta_n = \begin{bmatrix} y_n \\ z_n \\ \phi_n \\ \psi_n \end{bmatrix} \qquad 3\text{-}3$$

For the case of one rotor considered, n is equal to 1.

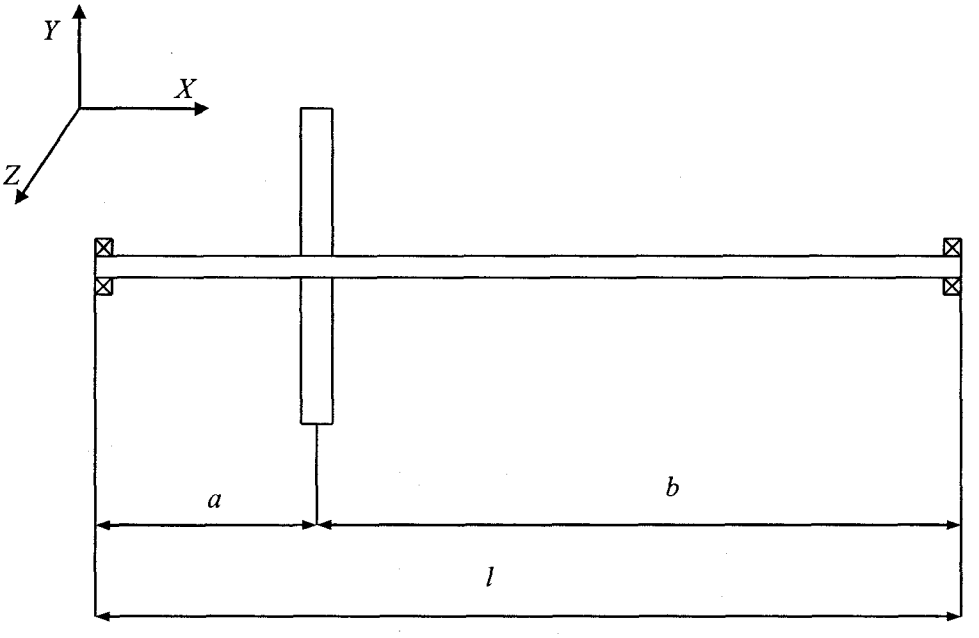

Figure 3-1 Simple shaft with no misalignment

Using the energy terms derived in chapter 2 the Lagrangian (Equation 3-1) is expressed as:

$$\begin{aligned} L = \frac{1}{2} M_D (\dot{y}^2 + \dot{z}^2 + \Omega^2 e^2 + 2\Omega e \dot{y} \cos(\Omega t) - 2\Omega e \dot{z} \sin(\Omega t)) \\ + \frac{1}{2} (I_{Dx} \omega_{x_3}^2 + I_{Dy} \omega_{y_3}^2 + I_{Dz} \omega_{z_3}^2) \\ - \left(\frac{1}{2} \left(K_{11} y^2 + 2K_{12} \phi y + K_{22} \phi^2 \right) + \frac{1}{2} \left(K_{11} z^2 + 2K_{12} \psi z + K_{22} \psi^2 \right) \right) \end{aligned} \qquad 3\text{-}4$$

Where the angular velocity terms are given by equation (2-30) when there is no unbalance. In the presence of unbalance, the angular velocity terms are represented by equation (2-37).

3.2.1 Equations of Motion for a Perfectly Aligned Shaft Neglecting Higher Order Terms

In majority of dynamic studies, the high order terms are neglected assuming that their contribution is small. For the present study of rotor system with unbalance and misalignment, its validity is explored to ensure that the influence of high order terms do not influence the responses. For this, the equations of motion are first derived here assuming that all the terms that are raised to a power greater than 1 are equal to zero. Furthermore it is assumed that all angles associated with motion and rotor unbalance are small. The equation of motion are obtained by applying equation (3-2) to equation (3-4) where the angular velocity term for perfectly aligned shaft is given in equation (2-37). In doing so, the equations of motion are found to be:

$$M_D\ddot{y} + K_{11}y + K_{12}\phi = M_D\omega^2 e\cos(\omega t + \beta) \qquad 3\text{-}5$$

$$M_D\ddot{z} + K_{11}z + K_{12}\psi = M_D\omega^2 e\sin(\omega t + \beta) \qquad 3\text{-}6$$

$$I_{Dy_3}\ddot{\phi} - I_{Dx_3}\omega\dot{\psi} + K_{21}y + K_{22}\phi = -(I_{Dx_3} - I_{Dy_3})\omega^2\tau\cos(\omega t) \qquad 3\text{-}7$$

$$I_{Dz_3}\ddot{\psi} + I_{Dx_3}\omega\dot{\phi} + K_{21}z + K_{22}\psi = (I_{Dx_3} - I_{Dz_3})\omega^2\tau\sin(\omega t) \qquad 3\text{-}8$$

Where distance e and angle β define the position of mass center for the unbalanced rotor as shown in Figure 3-2.

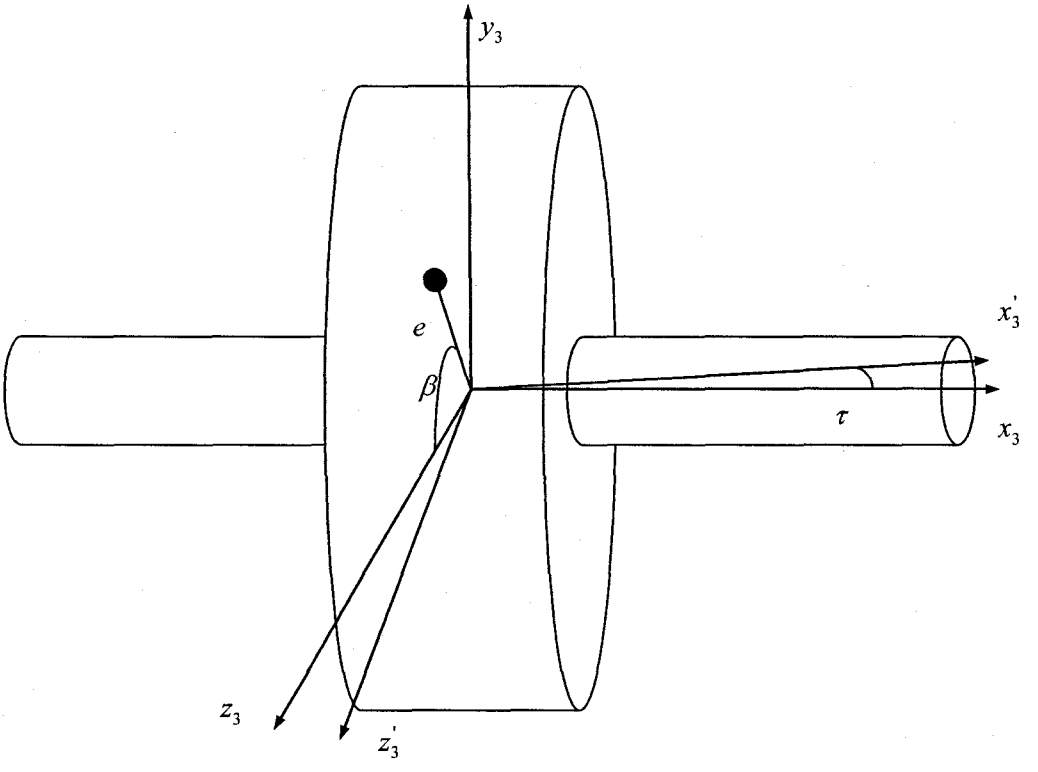

Figure 3-2 Unbalance phase angle β

3.2.2 Equations of Motion for a Perfectly Aligned Shaft with Higher Order Dynamic Unbalance Terms

The next set of equations of motion are developed assuming that all terms raised to a power greater than one are equal to zero except the dynamic unbalance term τ. The equations of motion are derived again following the steps outlined in section 3.2.1. For small angle assumption, the equations of motion are found to be:

$$M_D\ddot{y} + K_{11}y + K_{12}\phi = M_D\omega^2 e\cos(\omega t + \beta) \quad \text{3-9}$$

$$M_D\ddot{z} + K_{11}z + K_{12}\psi = M_D\omega^2 e\sin(\omega t + \beta) \quad \text{3-10}$$

$$\begin{aligned} &I_{Dy_3}\ddot{\phi} - I_{Dx_3}\omega\dot{\psi} + K_{21}y + K_{22}\phi = -(I_{Dx_3} - I_{Dy_3})\omega^2\tau\cos(\omega t) \\ &+ I_{Dy_3}(\phi\tau\ddot{\psi}\sin(\omega t) - \tau\dot{\psi}^2\cos(\omega t) + \omega\tau^2\dot{\psi} + \omega\phi\tau\dot{\psi}\cos(\omega t)) \\ &+ I_{Dx_3}(\tau^2\omega\dot{\psi} + \tau\dot{\psi}^2\cos(\omega t) - \tau\varphi\ddot{\psi}\sin(\omega t) - \tau^2\ddot{\phi} - \tau\phi\dot{\psi}\omega\cos(\omega t) \\ &+ \tau^2\ddot{\phi}\cos^2(\omega t) - \tau^2\ddot{\psi}\sin(\omega t)\cos(\omega t) - 2\tau^2\dot{\psi}\omega\cos^2(\omega t) \\ &- \tau^2\dot{\phi}\omega\sin(2\omega t)) \end{aligned} \quad \text{3-11}$$

$$\begin{aligned} &I_{Dz_3}\ddot{\psi} + I_{Dx_3}\omega\dot{\phi} + K_{21}z + K_{22}\psi = (I_{Dx_3} - I_{Dz_3})\omega^2\tau\sin(\omega t) \\ &+ I_{Dz_3}(\dot{\phi}^2\tau\sin(\omega t) + \phi\tau\omega\dot{\phi}\cos(\omega t) + \phi\tau\ddot{\phi}\sin(\omega t) + 2\tau\dot{\phi}\dot{\psi}\cos(\omega t) \\ &+ 2\phi\tau\ddot{\psi}\cos(\omega t) - 2\phi\tau\dot{\psi}\omega\sin(\omega t) - \tau^2\omega\dot{\phi}) + I_{Dx_3}(\tau^2\omega\dot{\phi} - \dot{\phi}^2\tau\sin(\omega t) \\ &- \tau^2\ddot{\psi}\cos^2(\omega t) - \phi\tau\omega\dot{\phi}\cos(\omega t) - \phi\tau\ddot{\phi}\sin(\omega t) - 2\tau\dot{\phi}\dot{\psi}\cos(\omega t) \\ &- 2\phi\tau\ddot{\psi}\cos(\omega t) + 2\phi\tau\omega\dot{\psi}\sin(\omega t) - 2\tau^2\omega\dot{\phi}\cos^2(\omega t) \\ &- \tau^2\ddot{\phi}\sin(\omega t)\cos(\omega t) + \tau^2\omega\dot{\psi}\sin(2\omega t)) \end{aligned} \quad \text{3-12}$$

3.3 Equation of Motion for a Misaligned Shaft

Figure 3-3 and Figure 3-4 show the models for a misaligned shaft. The misalignment can be defined by an offset of one of the bearing with respect to the other. This is referred to as parallel misalignment as shown in Figure 3-3. The level of parallel misalignment is designated by an offset Δ. The angular misalignment shown in Figure 3-4 is the result of an angle α for the bearing support with respect to the vertical plane. For a rigidly supported rotor system it is assumed that the shaft is supported on 2 bearings that are infinitely stiff. Due to either parallel and/or angular misalignment, the shaft is subjected to bending and deflection.

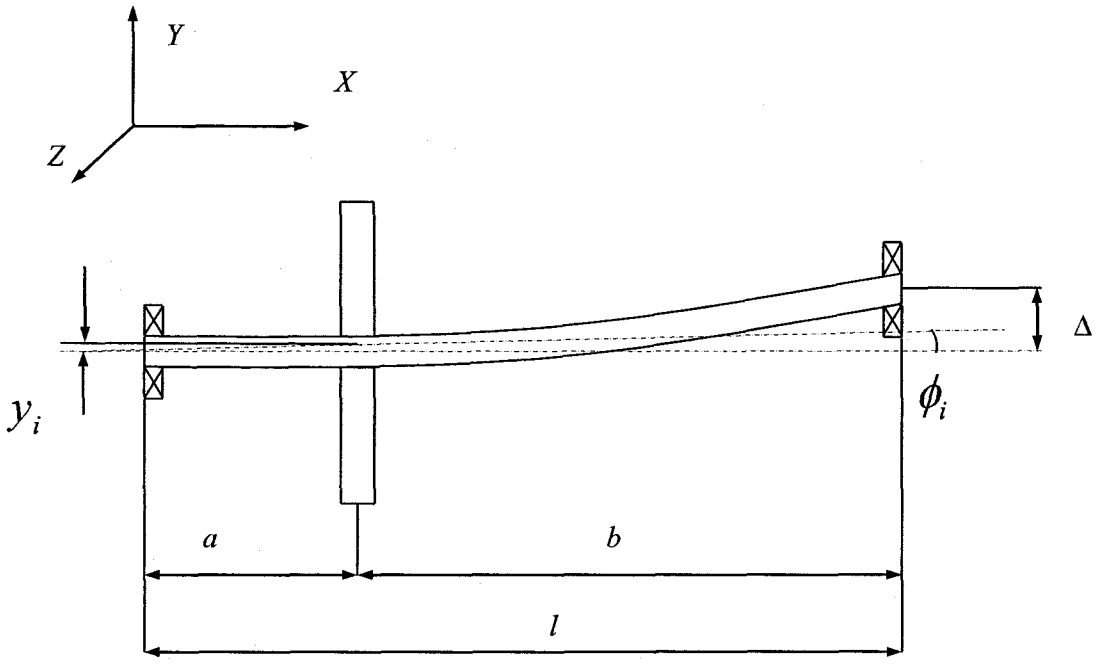

Figure 3-3 Rotor model with parallel misalignment

The resulting deflection and bending at the disk location as shown in Figure 3-3 and Figure 3-4 are designated by y_i and ϕ_i, respectively. The shaft is deformed due to misalignment, and an internal force and moment are created in the shaft due to the misalignment.

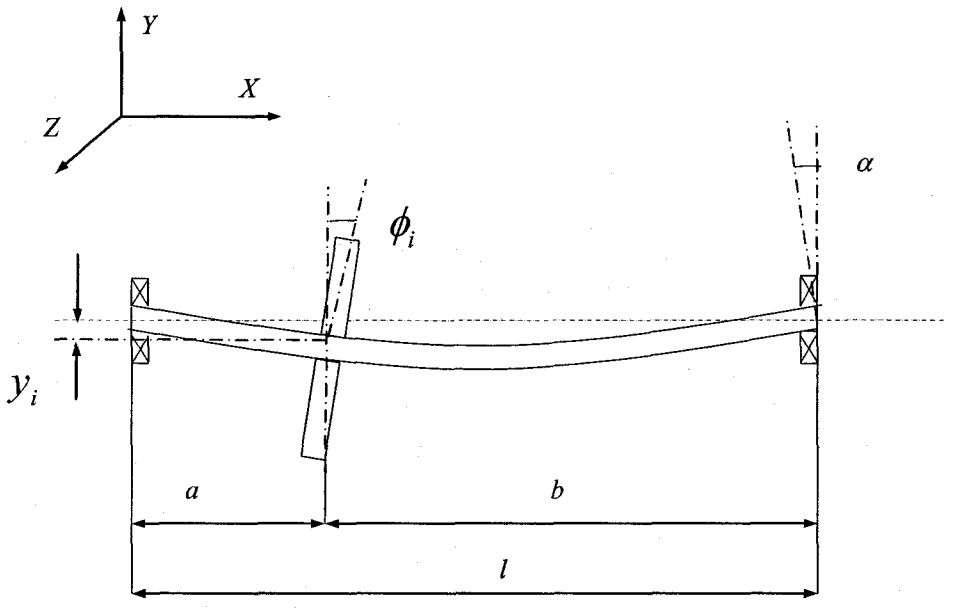

Figure 3-4 Rotor with angular misalignment

The internal force and moments are calculated using the shaft properties and boundary conditions. Depending on the bearing support system used, a misaligned shaft may have one of three possible boundary conditions. It can be either simply supported, or fixed-simply supported or fixed-fixed. For the simply supported case there are no internal loads that develop due to bearing misalignment hence this case is not considered. The internal forces and moments developed due to misalignment for the fixed-simply supported and fixed-fixed boundary conditions are evaluated and summarized in the following:

1) Fixed-Simply Supported Boundary Condition

For a simple rotor system, if one side of the shaft is supported on a fixed bearing while the other side is mounted on self aligning bearing, it can be modeled as a fixed-simply supported boundary configuration. This geometry for misalignment Δ as shown in Figure 3-5 (i) where the misaligned end of the shaft will tend to develop a slope as misalignment is introduced. The misalignment in turn will introduce a preload on the shaft in the form of a shear force and moment. The force and moment at end A of the shaft are:

$$F_a = -\frac{3EI\Delta}{l^3} \qquad 3\text{-}13$$

$$M_a = -\frac{3EI\Delta}{l^2} \qquad 3\text{-}14$$

Similarly for end B, the forces and moments are:

$$F_b = \frac{3EI\Delta}{l^3} \qquad 3\text{-}15$$

$$M_b = 0 \qquad 3\text{-}16$$

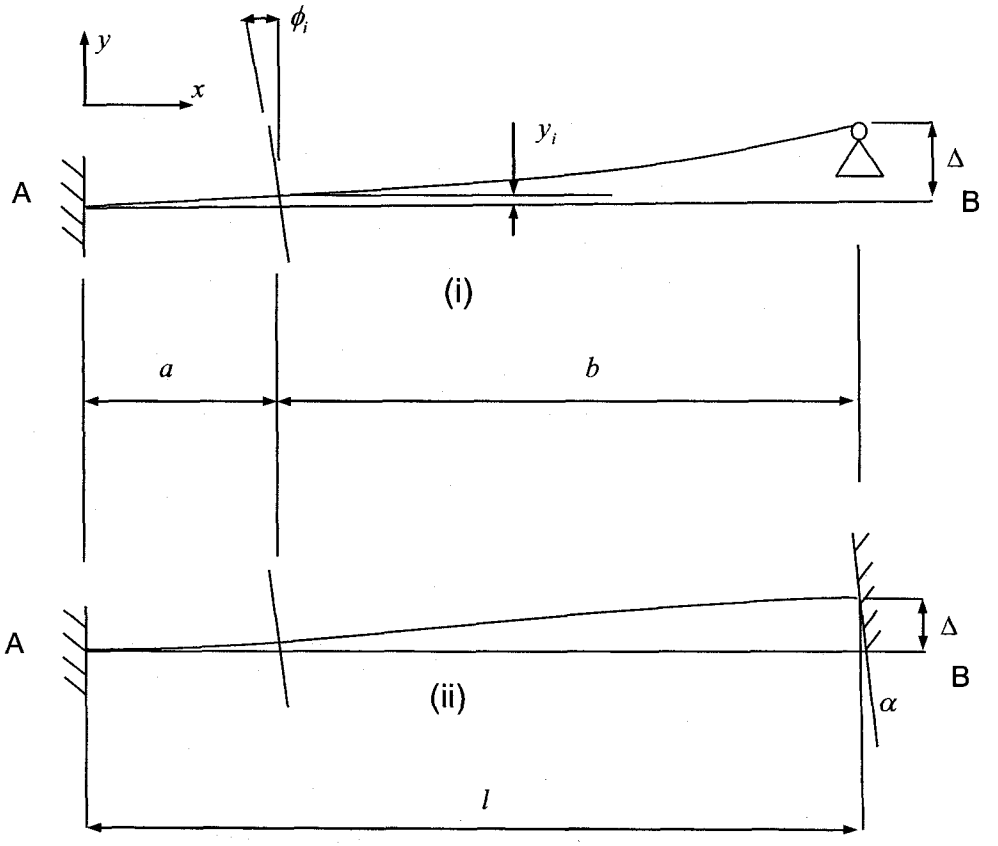

Figure 3-5 Shaft geometries for different boundary conditions

The force and moment at the disk location due to misalignment Δ can be used to establish the initial position of the disk. The initial position of the disk is defined in terms of deflection and slope at the disk location of the shaft and is given by:

$$y_i = \frac{\Delta a^2 (3l - a)}{2l^3} \qquad 3\text{-}17$$

$$\phi_i = \frac{3\Delta a (2l - a)}{2l^3} \qquad 3\text{-}18$$

The preload force and moment at the disk are calculated using the stiffness of the shaft developed in chapter 2 along with the disk initial displacement and rotation.

Combining equations (3-17) and (3-18) with equation (2-13) and substituting l for $a+b$ the preload forces and moments at disk location are:

$$\begin{bmatrix} F \\ M \end{bmatrix} = \begin{bmatrix} \frac{3IE\Delta}{b^3} \\ \frac{3IE\Delta}{b^2} \end{bmatrix} \qquad 3\text{-}19$$

The above preload force and moment are due to misalignment in a shaft with fixed and simply supported boundary condition. The present investigation will, however consider bearing support system where the boundary condition is fixed-fixed.

2) Fixed-Fixed Boundary Condition.

The shaft geometry for both ends with fixed support is shown in Figure 3-5 (ii). In this case the misalignment is represented by parallel offset Δ and an angle α as shown in the figure. The parallel and/or angular misalignment will lead to a force and moment along the shaft length. For the support at A, the force and moment as function of misalignment are:

$$F_a = -\frac{12EI\Delta}{l^3} + \frac{6EI\alpha}{l^2} \qquad 3\text{-}20$$

$$M_a = -\frac{6EI\Delta}{l^2} + \frac{2EI\alpha}{l} \qquad 3\text{-}21$$

Similarly at support B the force and moment are:

$$F_b = \frac{12EI\Delta}{l^3} - \frac{6EI\alpha}{l^2} \qquad 3\text{-}22$$

$$M_b = -\frac{6EI\Delta}{l^2} + \frac{4EI\alpha}{l} \qquad 3\text{-}23$$

The initial position of the disk in terms of deflection and slope due to misalignment Δ and α are:

$$y_i = \frac{a^2(3l\Delta - \alpha l^2 - 2a\Delta + a\alpha l)}{l^3} \qquad 3\text{-}24$$

$$\phi_i = \frac{a(6l\Delta - 2\alpha l^2 - 6a\Delta + 3a\alpha l)}{l^3} \qquad 3\text{-}25$$

The preload force and moment at the disk can now be calculated using the stiffness of the shaft established in chapter 2 along with the disk initial displacement and rotation and substituting $l = a + b$:

$$\begin{bmatrix} F \\ M \end{bmatrix} = \begin{bmatrix} \frac{6IE(2\Delta - \alpha b)}{b^3} \\ \frac{2IE(3\Delta - \alpha b)}{b^2} \end{bmatrix} \qquad 3\text{-}26$$

As discussed above, the misalignment, regardless of parallel and/or angular, essentially introduces a preload and moment in the shaft. This in turn introduces a change in the equilibrium position of the disk by an initial position and angle of the disk due to the misalignment. In addition, the preload introduces additional stiffness to the shaft in the direction of misalignment. This stiffness denoted by K_n is known to be nonlinear [33] and should be function of misalignment magnitude. The misalignment feature can, therefore, be introduced to the equations of motion derived in equations (3-5) to (3-8) by introducing the preload and corresponding nonlinear stiffness parameter K_n. Furthermore it is essential to introduce damping to the rotor system to account for material and possible

bearing damping to ensure stable finite response of the rotor system simulations. The equations of motion for the misaligned rotor system are thus finally obtained by modifying the equations (3-5) to (3-8) in the following manner:

$$M_D\ddot{y} + K_{11}y + K_{12}\phi + K_{n11}y^2 + K_{n12}\phi^2 + C_{11}\dot{y} + C_{12}\dot{\phi} = M_D\omega^2 e\cos(\omega t + \beta) + F_{\mathrm{Pr}\,y} \tag{3-27}$$

$$M_D\ddot{z} + K_{11}z + K_{12}\psi + K_{n11}z^2 + K_{n12}\psi^2 + C_{11}\dot{z} + C_{12}\dot{\psi} = M_D\omega^2 e\sin(\omega t + \beta) + F_{\mathrm{Pr}\,z} \tag{3-28}$$

$$I_{Dy_3}\ddot{\phi} - I_{Dx_3}\omega\dot{\psi} + K_{21}y + K_{22}\phi + K_{n21}y^2 + K_{n22}\phi^2 + C_{21}\dot{y} + C_{22}\dot{\phi} = -\omega^2(I_{Dx_3} - I_{Dy_3})(\tau\cos(\omega t)) + M_{\mathrm{Pr}\,y} \tag{3-29}$$

$$I_{Dy_3}\ddot{\psi} + I_{Dx_3}\omega\dot{\phi} + K_{21}z + K_{22}\psi + K_{n21}z^2 + K_{n22}\psi^2 + C_{21}\dot{z} + C_{22}\dot{\psi} = \omega^2(I_{Dx_3} - I_{Dy_3})(\tau\sin(\omega t)) + M_{\mathrm{Pr}\,z} \tag{3-30}$$

Where K_n is a non linear stiffness, C is the damping coefficient and F_{Pr} and M_{Pr} are the forces and moments developed due to parallel and/or angular misalignment that can be established from the following equations:

$$\begin{bmatrix} F_{\mathrm{Pr}\,y} \\ M_{\mathrm{Pr}\,y} \end{bmatrix} = \begin{bmatrix} K_{11} & K_{12} \\ K_{21} & K_{22} \end{bmatrix}\begin{bmatrix} y_i \\ \phi_i \end{bmatrix} + \begin{bmatrix} K_{n11} & K_{n12} \\ K_{n21} & K_{n22} \end{bmatrix}\begin{bmatrix} y_i^2 \\ \phi_i^2 \end{bmatrix} \tag{3-31}$$

$$\begin{bmatrix} F_{\mathrm{Pr}\,z} \\ M_{\mathrm{Pr}\,z} \end{bmatrix} = \begin{bmatrix} K_{11} & K_{12} \\ K_{21} & K_{22} \end{bmatrix}\begin{bmatrix} z_i \\ \psi_i \end{bmatrix} + \begin{bmatrix} K_{n11} & K_{n12} \\ K_{n21} & K_{n22} \end{bmatrix}\begin{bmatrix} z_i^2 \\ \psi_i^2 \end{bmatrix} \tag{3-32}$$

Selection of K_n and its influence on the rotor responses will be discussed in chapter 5.

3.4 Summary

In this chapter the kinetic energy and potential energy terms for a shaft and rotor developed in chapter 2, were used to formulate the Lagrangian. Using the energy method the equations of motion were developed for a perfectly aligned shaft first ignoring the second order terms for the unbalance and then taking into account the second order terms. In addition, the equations of motion were developed for a misaligned shaft. For misaligned shaft, equations were developed to model fixed-simply supported as well as fixed-fixed boundary conditions. The equations of motion for the misaligned shaft were obtained by introducing preload force and moment to the shaft, modifying the equilibrium position of the disk due to misalignment and introducing additional nonlinear stiffness for the shaft. The equations of motion developed in this chapter are simulated in the next chapter in the time domain, and are analyzed both in time and frequency domain. Attempts are made in the next chapter to validate the developed lumped mass time domain model by comparing the results with those of eigenvalue solutions and finite element analysis of the rotor system.

Chapter 4

4 Model Validation

4.1 Introduction

The rotor system considered in this investigation consists of a flexible shaft supported at each end by rigid bearings. The shaft in turn carries a thick disk with static and dynamic unbalance. The equations of motion for the rotor system were developed using Lagrange's energy method. For this, the energy terms form the shaft deflections and disk motions were derived in chapter 2. Assuming constant shaft speed, the disk is assigned four degrees of freedom. The final equations of motion for the rotor were developed in chapter 3 using the energy expressions presented in chapter 2. In developing the model, one of the objectives was to examine the influence of high order terms due to unbalance on the rotor system responses. For this, the first set of equations were developed neglecting all the higher order terms. The higher order terms due to rotor unbalance were retained in the second set of equations, which can be readily compared with the first set. Finally, equations of motion were derived from the rotor system incorporating both unbalance and misalignment.

This chapter is devoted to validation of the rotor system model developed in chapter 3 for time domain simulations. Prior to any simulations, eigenvalues formulation is used to establish the system natural frequencies as function of

speed. The eigen solutions are compared with dynamic model simulation results in time domain. The FFT of time domain response is then validated against the eigenvalues solutions.

Further attempt of validation is made against the finite element analysis (FEA) of the rotor system considered. The software used to construct the geometry and mesh is Patran and the software used to analyze the finite element model is Nastran. The data for the FEA is carefully selected to closely resemble the model developed for time domain simulation. The analysis is used to establish both the natural frequencies and mode shapes. The results are compared with those established from eigenvalue solutions and time domain responses. Finally an attempt is made to introduce misalignment in the shaft for FE model to examine its effectiveness for such simulations.

4.2 Identification of the natural frequencies

The natural frequencies of the rotor system are established for a perfectly aligned shaft. Further assumptions include negligible mass of the shaft where all mass is due to the rotor and that the bearings are rigid. An eigenvalue formulation is thus carried out using the equations of motion from aligned shaft presents in equations (3-5) to 3-8) with all forcing functions set to zero:

$$M_D\ddot{y} + K_{11}y + K_{12}\phi = 0 \qquad 4\text{-}1$$

$$M_D\ddot{z} + K_{11}z + K_{12}\psi = 0 \qquad 4\text{-}2$$

$$I_{Dy_3}\ddot{\phi} - I_{Dx_3}\omega\dot{\psi} + K_{21}y + K_{22}\phi = 0 \qquad 4\text{-}3$$

$$I_{Dy_3}\ddot{\psi} + I_{Dx_3}\omega\dot{\phi} + K_{21}z + K_{22}\psi = 0 \qquad 4\text{-}4$$

Based on the coordinate system used, the phase between $y, z, \phi,$ and ψ are known. The motion y and z are 90° out of phase while ϕ and ψ are in phase with y and z, respectively. Therefore we can assume that the solutions for free oscillations are of the form:

$$y = A\sin(\omega_n t + \zeta) \qquad 4\text{-}5$$

$$z = A\cos(\omega_n t + \zeta) \qquad 4\text{-}6$$

$$\phi = B\sin(\omega_n t + \zeta) \qquad 4\text{-}7$$

$$\psi = B\cos(\omega_n t + \zeta) \qquad 4\text{-}8$$

Substituting equations (4-5) to (4-8) and their derivatives into equations (4-1) to 4-4) will yield:

$$-M_D A\omega_n^2 \sin(\omega_n t + \zeta) + K_{11}A\sin(\omega_n t + \zeta) + K_{12}B\sin(\omega_n t + \zeta) = 0 \qquad 4\text{-}9$$

$$-M_D A\omega_n^2 \cos(\omega_n t + \xi) + K_{11}A\cos(\omega_n t + \zeta) + K_{12}B\cos(\omega_n t + \zeta) = 0 \qquad 4\text{-}10$$

$$\begin{aligned} &-I_{Dy_3}B\omega_n^2 \sin(\omega_n t + \zeta) + I_{Dx_3}\omega B\omega_n \sin(\omega_n t + \zeta) \\ &+ K_{21}A\sin(\omega_n t + \zeta) + K_{22}B\sin(\omega_n t + \zeta) = 0 \end{aligned} \qquad 4\text{-}11$$

$$\begin{aligned} &-I_{Dy_3}B\omega_n^2 \cos(\omega_n t + \zeta) + I_{Dx_3}\omega B\omega_n \cos(\omega_n t + \zeta) \\ &+ K_{21}A\cos(\omega_n t + \zeta) + K_{22}B\cos(\omega_n t + \zeta) = 0 \end{aligned} \qquad 4\text{-}12$$

For a symmetric rotor system, equations (4-9) and (4-10) simplifies to:

$$-M_D A\omega_n^2 + K_{11}A + K_{12}B = 0 \qquad 4\text{-}13$$

While equations (4-11) and (4-12) simplifies to:

$$-I_{Dy_3}B\omega_n^2 + I_{Dx_3}\omega B\omega_n + K_{21}A + K_{22}B = 0 \qquad 4\text{-}14$$

Writing the above equations (4-13) and (4-14) in a matrix form lead to eigenvalue problem:

$$\begin{bmatrix} -M_D\omega_n^2 + K_{11} & K_{12} \\ K_{21} & -I_{Dy_3}\omega_n^2 + I_{Dx_3}\omega\,\omega_n + K_{22} \end{bmatrix}\begin{bmatrix} A \\ B \end{bmatrix} = \begin{bmatrix} 0 \\ 0 \end{bmatrix} \qquad 4\text{-}15$$

The natural frequencies of the system can now be easily determined from the roots of the characteristic equation:

$$(-M_D\omega_n^2 + K_{11})(-I_{Dy_3}\omega_n^2 + I_{Dx_3}\omega\omega_n + K_{22}) - K_{12}^2 = 0 \qquad 4\text{-}16$$

Equation 4-16 yields four values for the natural frequencies. Two of these values are negative and correspond to the backward whirl frequencies and two positive corresponding to the forward whirl frequencies. Using rotor system baseline parameters presented in Table 4-1, equation (4-16) is solved for different shaft speed. The computed natural frequencies for different shaft speeds are plotted in Figure 4-1. As seen from the figure the natural frequency of the shaft will change with the rotational speed due to the Coriolis or gyroscopic effect.

4.3 Validation of Time Domain Simulation

Sine the equations of motion derived for shaft with misalignment are nonlinear, all simulations are to be carried out in time domain. For this, Simulink in Matlab is adopted using Runge-Kutta for solution of differential equations. A code is

written in Matlab to perform an FFT and extract the amplitude corresponding to the first and second order rotating speeds. The rotor acceleration response is thus obtained for various shaft speeds. Sample results of frequency response at 3000 and 9000 rpm are shown in Figure 4-2 and Figure 4-3, respectively.

Table 4-1 Rotor physical properties

Physical property	Value
Distance from Bearing A to rotor (a)	0.160 m
Distance from Bearing A to rotor (b)	0.200 m
Rotor Diameter	0.075 m
Rotor width	0.024 mm
Shaft diameter	0.010 m
Young Modulus	2E11 N/ m^2
Material Density	8000 kg/m^3
e Disk CG offset from geometrical center	0.45E-3 m
τ Angle between disk and shaft	0 Degree

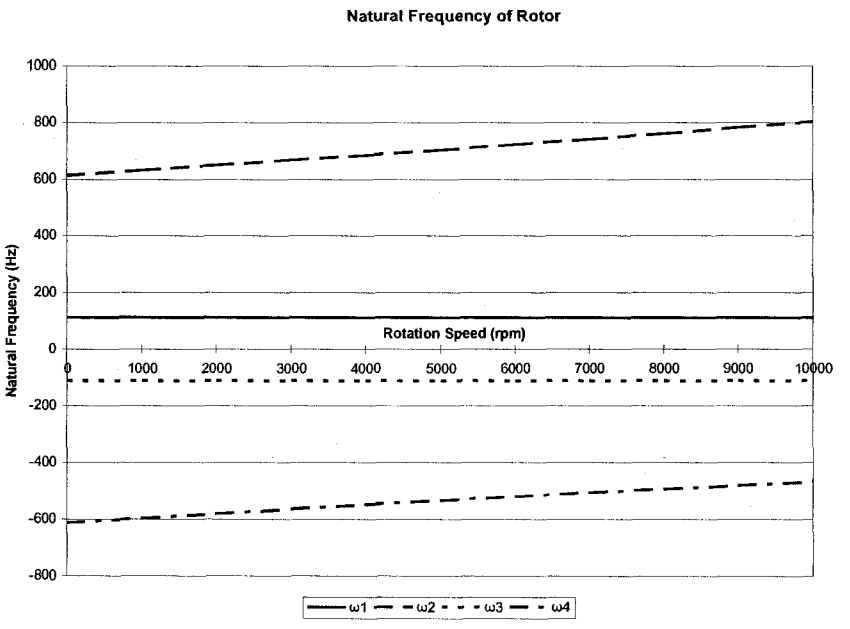

Figure 4-1 Rotor natural frequency versus shaft speed in rpm

As shown in the figures five distinct peaks could be clearly identified from the frequency responses obtained from the simulations. One of the peaks in these responses corresponds to the frequency of the rotation speed. The other four are identified as the rotor system natural frequencies.

The natural frequencies identified from the time domain simulation and FFT analysis at two selected speed are compared with those obtained earlier from eigenvalue solution referred to as analytical results. A quantitative comparison of the natural frequency results is presented in Table 4-2

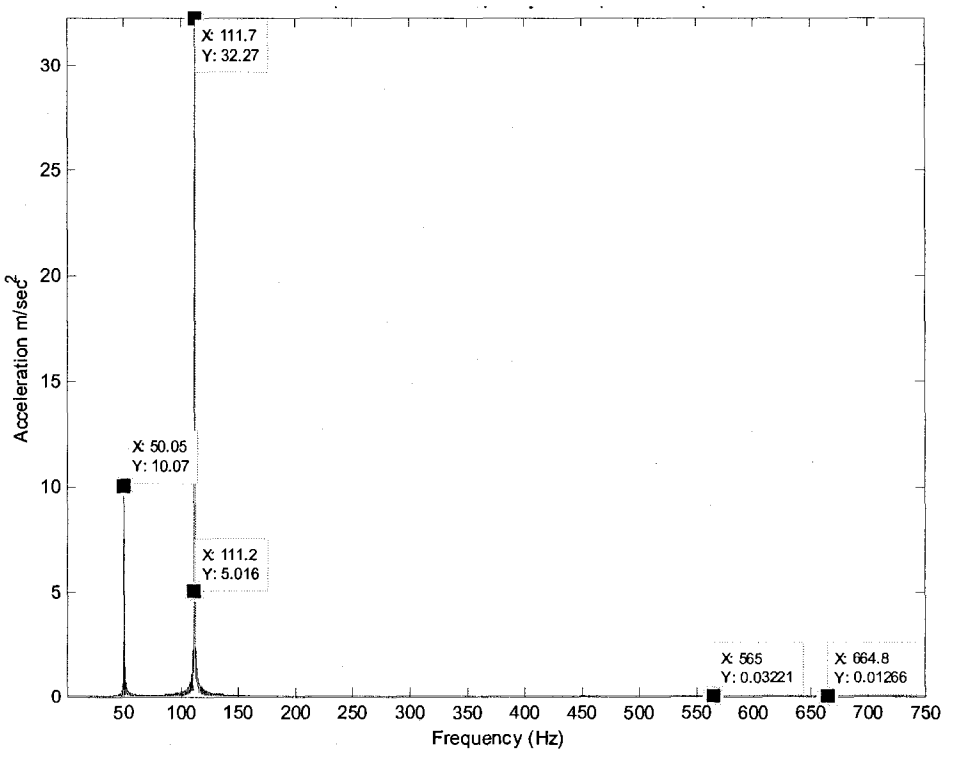

Figure 4-2 Amplitude versus frequency for the rotor at 3000 rpm

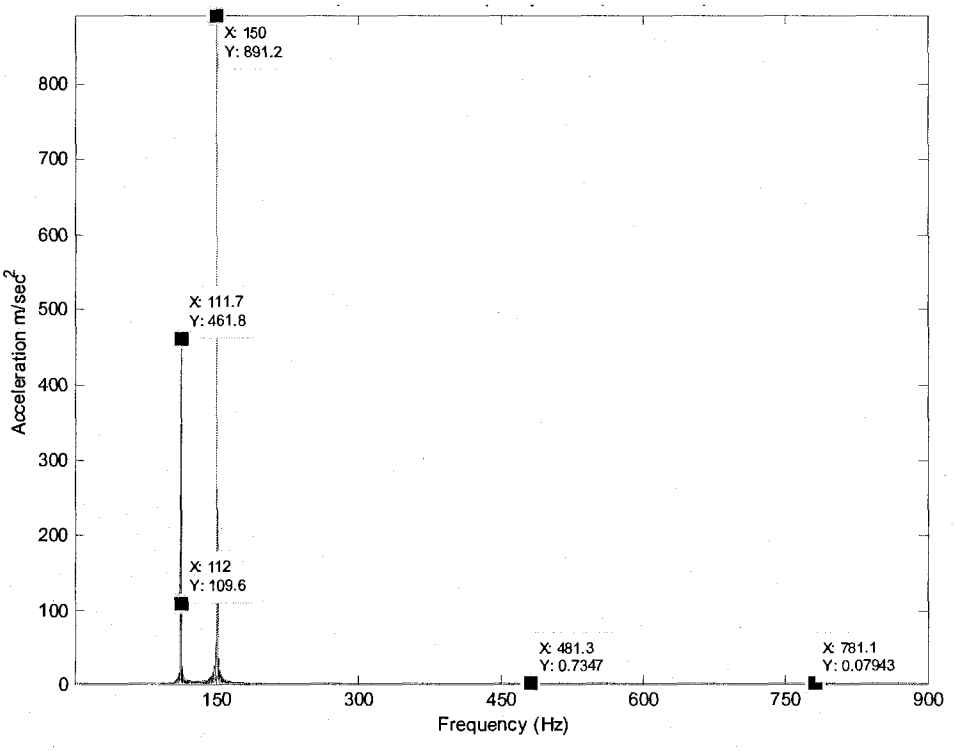

Figure 4-3 Amplitude versus frequency for the rotor at 9000 rpm

Table 4-2 Natural frequencies computed using analytical method and simulation results.

	3000 rpm		9000 rpm	
	Analytically	Simulation	Analytically	Simulation
First Mode (Hz)	111.76	111.2	111.62	111.7
Second Mode (Hz)	111.89	111.7	112.02	112
Third Mode (Hz)	565.08	565	481.31	481.3
Fourth Mode (Hz)	664.95	664.8	780.91	781.1

The comparison between the simulation and the analytical model shows that the simulation predicts the rotor natural frequencies that are similar to those predicted by eigenvalue solution.

4.4 Effect of second order terms on the simulation results

It is clear from the surveyed literature that the equations of motion for a rotor ignore the second order terms and assume that the higher order terms are negligible based on the fact that the higher orders of a small term are too small to contribute in the shaft response compared to other terms. Due to conflicting results in literature in the presence of misalignment, the present investigation reconsidered the higher order unbalance terms to examine its effect on responses at two times the rotating speed. Equations (3-9) to (3-12) developed in chapter 3 take into account the second order terms for dynamic unbalance. Simulations are carried out using equations (3-9) to (3-12) and equations (3-5) to (3-8) in order to compare responses with and without higher order terms,

respectively. Identical parameters as presented in Table 4-1 are used in both cases where the dynamic unbalance parameter τ was assigned a value of 0.1 degree, for shaft speeds in the range of 0 to 10,000 rpm.

In each case, the acceleration response of the rotor is established in time domain. The rotor exhibits a response at a frequency that corresponds to the shaft rotational speed. For example, a shaft rotating at 3,000 rpm will have a forced excitation that corresponds to 50 Hz due to the inherent unbalance in the rotor. The amplitude that corresponds to this frequency is called the 1x response. Similarly the shaft could have amplitude that corresponds to twice the rotational speed (2x response) if the rotor has a natural frequency close to twice the rotation speed, and so on.

Figure 4-4 shows the 1x shaft response against the shaft rotational speed for a rotor model where the higher order terms are ignored. A similar plot is shown in Figure 4-5 for a rotor model that takes into account the higher order terms and hence could be considered more accurate. A comparison of the results clearly shows that the higher order terms do not contribute to the rotor 1x response. It should be pointed out that the significantly large response near system natural frequencies is the result of considering an undamped system.

Similarly Figure 4-6 and Figure 4-7 show, respectively, the 2x response for a rotor model where the second order terms are ignored and for the rotor model

where the second order terms are included. Similar to the 1x response, the 2x response for both the models are found to be identical throughout the speed range.

In order to have a quantitative assessment, the percentage error due to neglecting the higher order terms is established for both 1x and 2x responses as shown in Figure 4-8. The results confirm that there is hardly any error in the 1x response when higher order terms are ignored in the equations of motion.

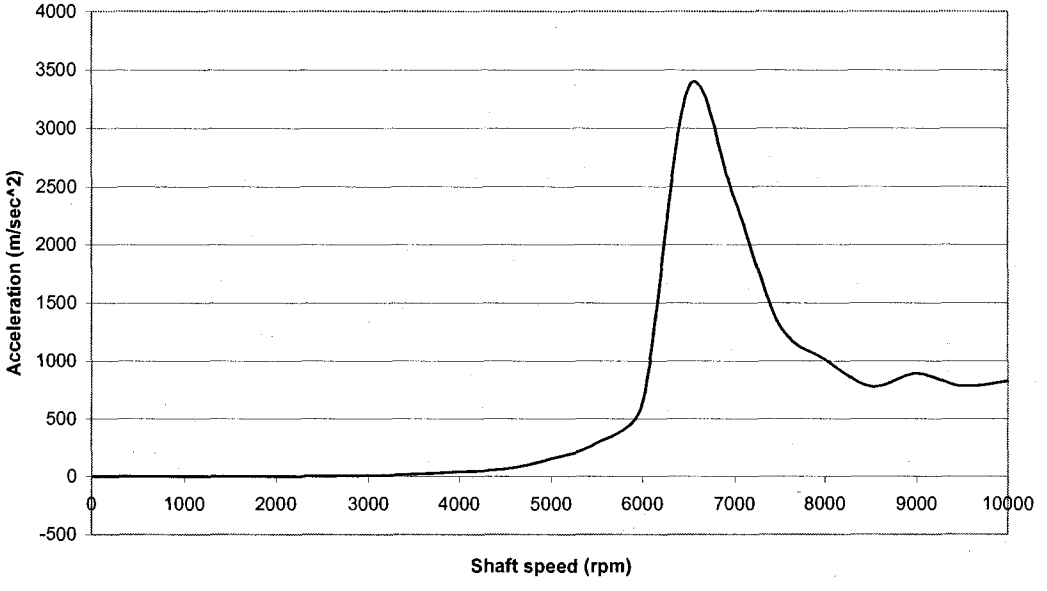

Figure 4-4 Rotor 1x response neglecting higher order terms

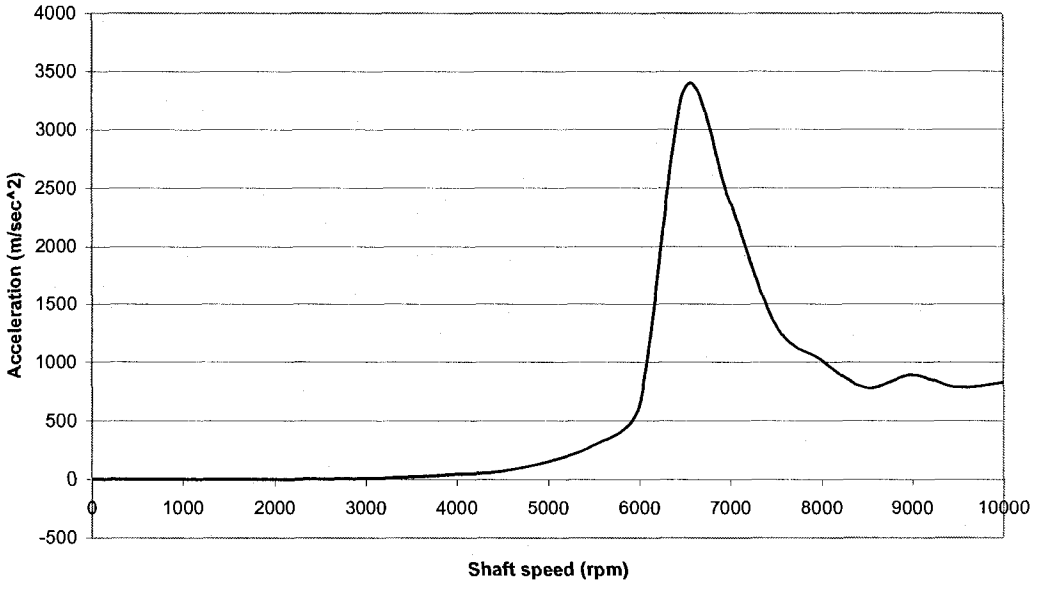

Figure 4-5 Rotor 1x response with higher order terms

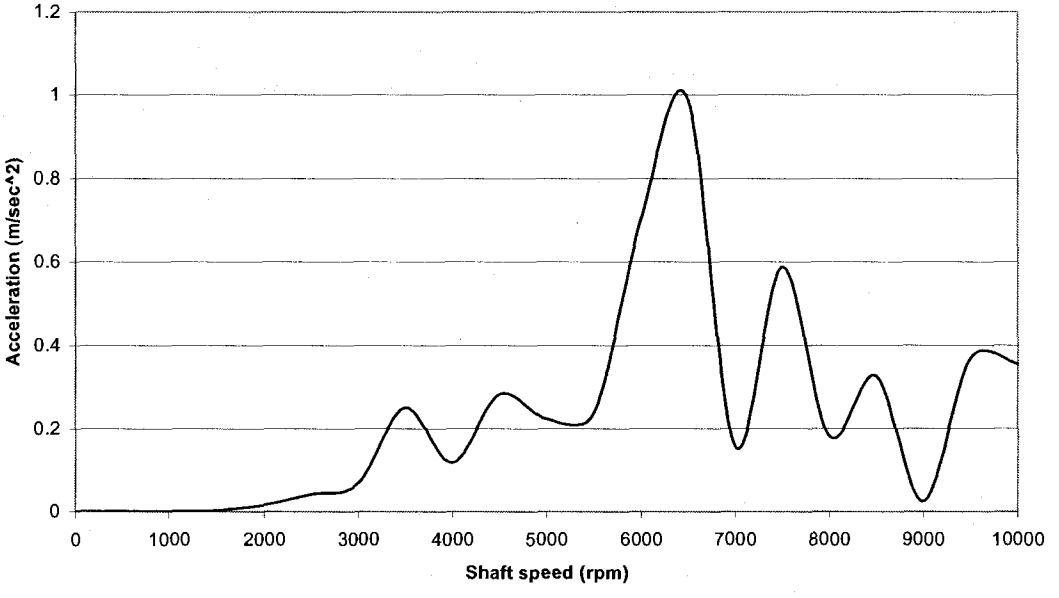

Figure 4-6 2x Rotor response neglecting higher order terms

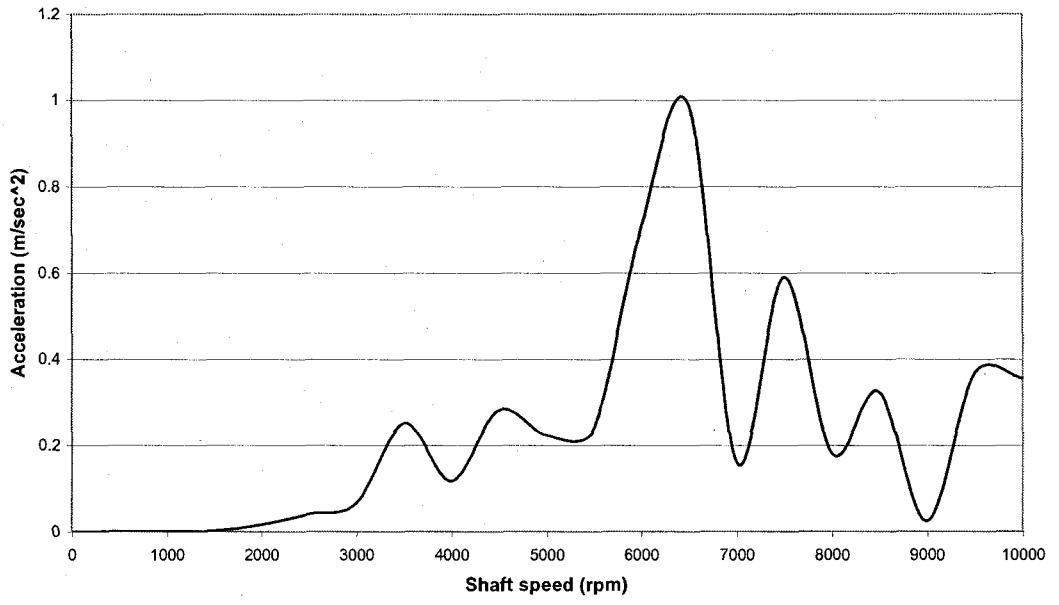

Figure 4-7 2x Rotor response with higher order terms

The results further show that there are small errors in the 2x responses throughout the speed range considered. The change in the 2x response is due to the introduction of the $\sin(2\omega t)$ term in equations 3-11 and 3-12. The error however remains less than 1% except around 7,000 rpm where it is found to be just above 2%. The increase in relative error for 2x response, compared to 1x response is the fact that relatively smaller response amplitude at 2x response contribute to an increase in percentage error. Such magnitude of error, however, can be neglected in a study involving extensive numerical computations.

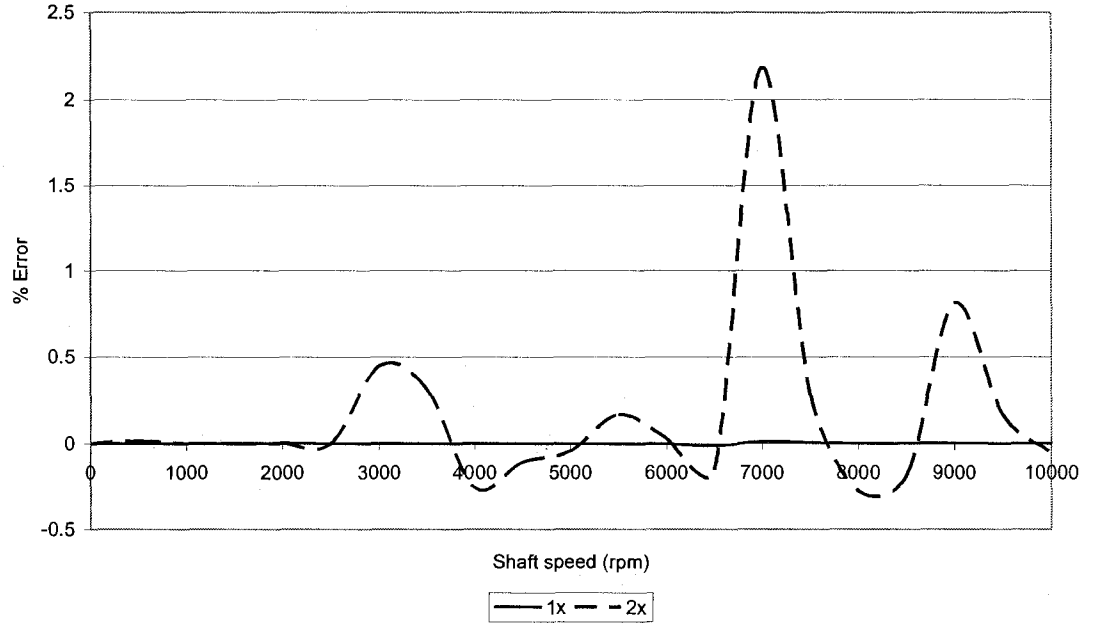

Figure 4-8 Percentage error for 1x and 2x

It is therefore, concluded that higher order terms due to unbalance can be neglected without any effect on the responses due to shaft misalignment.

4.5 Finite Element Analysis

The simplified parametric model developed for this investigation is next validated against a Finite Element (FE) model of the rotor system. A geometrically identical model to the one described by parameters in Table 4-1 is constructed using Patran.

The shaft is meshed using bar elements and each element is given a circular cross section. The disk is meshed using quadratic elements and the elements

are given a thickness representing the disk thickness. The shaft is assigned a material with zero density and the disk is assigned a material with a density of 8000 kg/m^3. The mass of the rotor and inertia matrix, calculated from the finite element model and those used in the simulation, are compared and the comparison is shown in Table 4-3. Figure 4-9 shows the finite element model created in Patran. The finite element model consists of 36 bar elements representing the shaft and 215 elements representing the disk. The extremities of the shaft were fixed to the ground via very rigid springs to replicate the fixed-fixed boundary condition.

4.5.1 Natural Frequencies of the Rotor

The created model in Patran is analyzed using Nastran to find the eigenvalues. A subroutine is used to include the gyroscopic effect. Solution 107 [74] is used, which calculates the rotor natural frequencies at different rotating speed and takes into account the gyroscopic effect. The natural frequencies are compared to the natural frequencies established in section 4.2 and 4.3 for rotor speeds 3000 and 9000 rpm. The three sets of natural frequencies calculated from eigenvalue analysis referred to as "Analytical", from time domain simulation of lumped parameter model referred to as "Sim" and finite element method referred to as "FEM" are presented in Table 4-4. The results show that all three methods predict very similar natural frequencies for the first two modes. For higher modes, all the methods generate comparable results, where FEM generated

slightly lower values. This can be easily attributed to the fact that the mass and stiffness generated by FEM are not identical to lumped parameter model due to geometry approximation. Figure 4-10 to Figure 4-13 show respectively the first four mode shapes for the rotor rotating at 3000 rpm. The first two frequencies shown in Figure 4-10 and Figure 4-11, are the first bending modes. The third and fourth frequencies shown in Figure 4-12 and Figure 4-13, are disk modes.

Table 4-3 Comparison between FEM model and Simulation model

	FEM Model	Simulation Model
Mass (Kg)	0.8458	0.8482
Ip ($Kg\text{-}m^2$)	5.93E-04	5.96E-04
I ($Kg\text{-}m^2$)	2.965E-04	2.98E-04

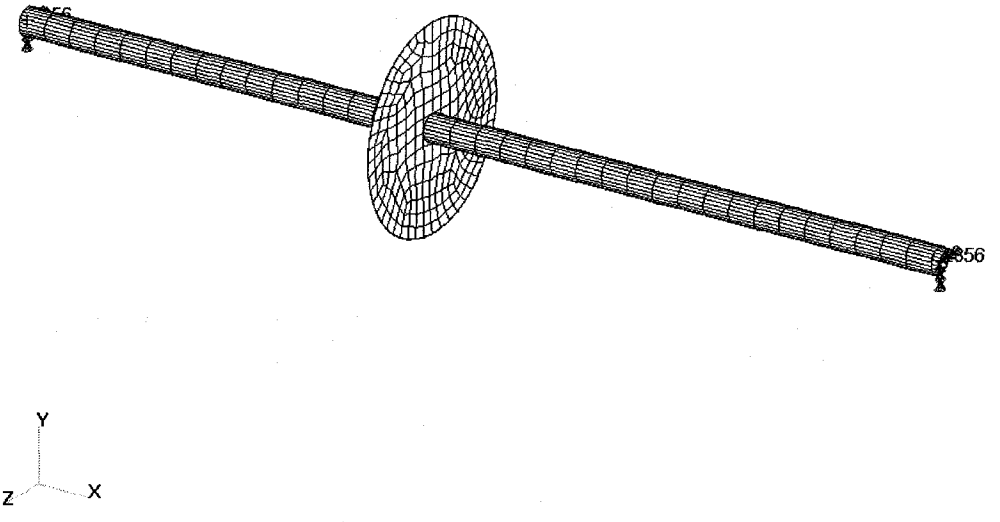

Figure 4-9 Finite element model

Table 4-4 Comparison of natural frequency using different methods of calculation

	3000 rpm			9000 rpm		
	Analytical	Sim.	FEM	Analytical	Sim.	FEM
First Mode (Hz)	111.76	111.2	111.38	111.62	111.7	111.4
Second Mode (Hz)	111.89	111.7	111.51	112.02	112	111.8
Third Mode (Hz)	565.08	565	557.9	481.31	481.3	476.8
Fourth Mode (Hz)	664.95	664.8	654.3	780.91	781.1	765.7

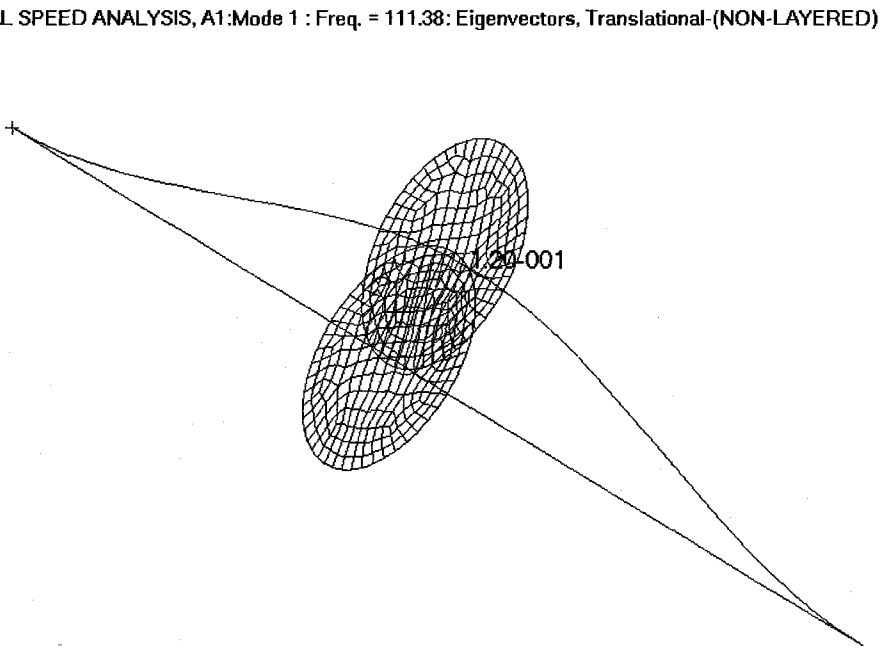

Figure 4-10 Mode shape for first frequency.

SC1:CRITICAL SPEED ANALYSIS, A1:Mode 3 : Freq. = 111.51: Eigenvectors, Translational-(NON-LAYERED)

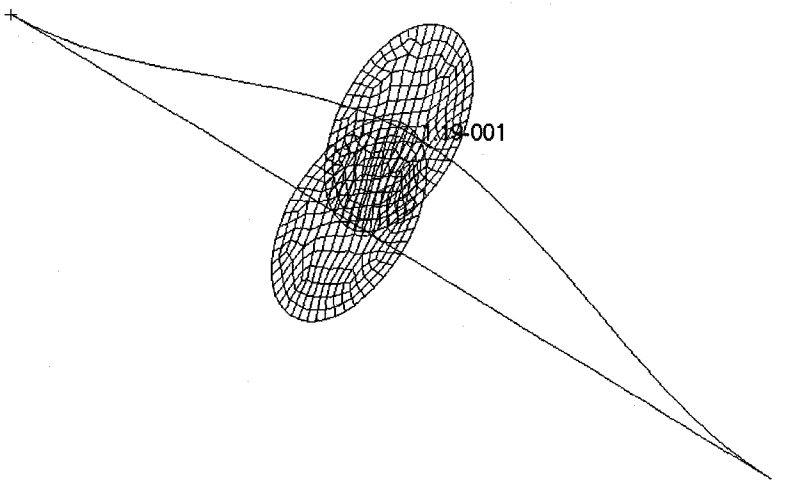

Figure 4-11 Mode shape for second frequency

SC1:CRITICAL SPEED ANALYSIS, A1:Mode 5 : Freq. = 557.96: Eigenvectors, Translational-(NON-LAYERED)

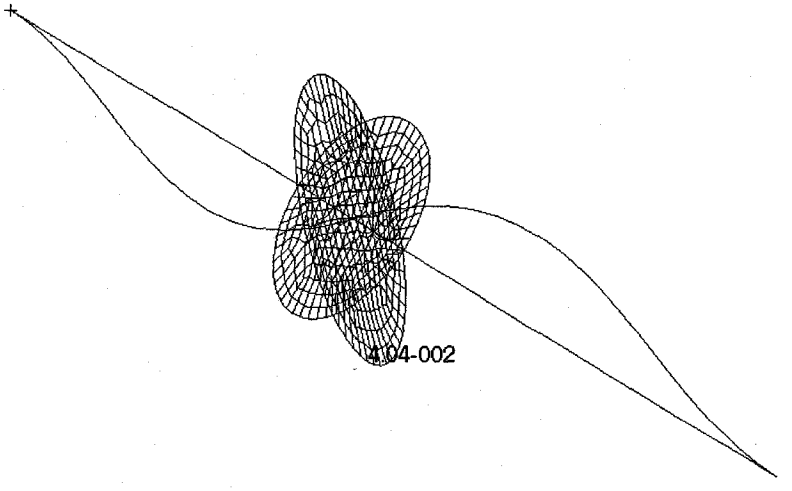

Figure 4-12 Mode shape for third frequency

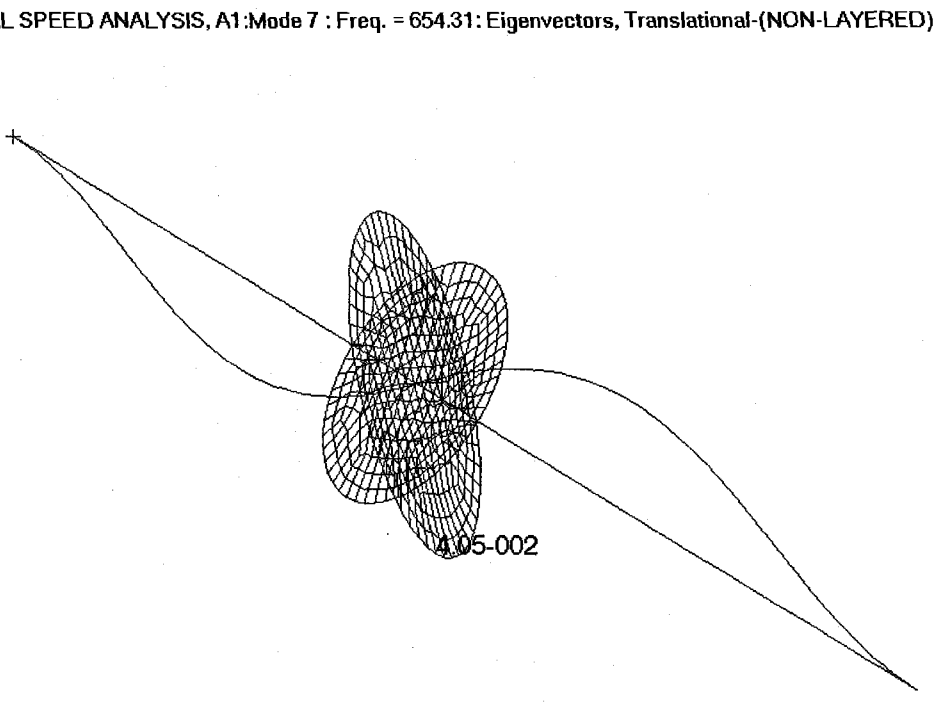

Figure 4-13 Mode shape for the fourth frequency.

4.5.2 Dynamic Response of the Rotor

The FEM model, developed in the previous section, is modified to study its dynamic response. An unbalance is introduced and the model was run in the time domain assuming that the shaft is perfectly aligned. The time domain data is imported into Matlab and then transferred to the frequency domain using FFT. The analysis method used is modal transient response (solution 129 [74]). The unbalance used corresponds to $3.81e^{-4}$ kg m similar to the unbalance used in the Matlab/Simulink simulation. A sample frequency response result for rotor speed 3000 rpm is presented in Figure 4-14 for a perfectly aligned shaft. This result can be readily compared with those from lumped parameter simulation model

presented in Figure 4-2. As these results show, both models predict very similar response amplitude for the rotor at a selected speed.

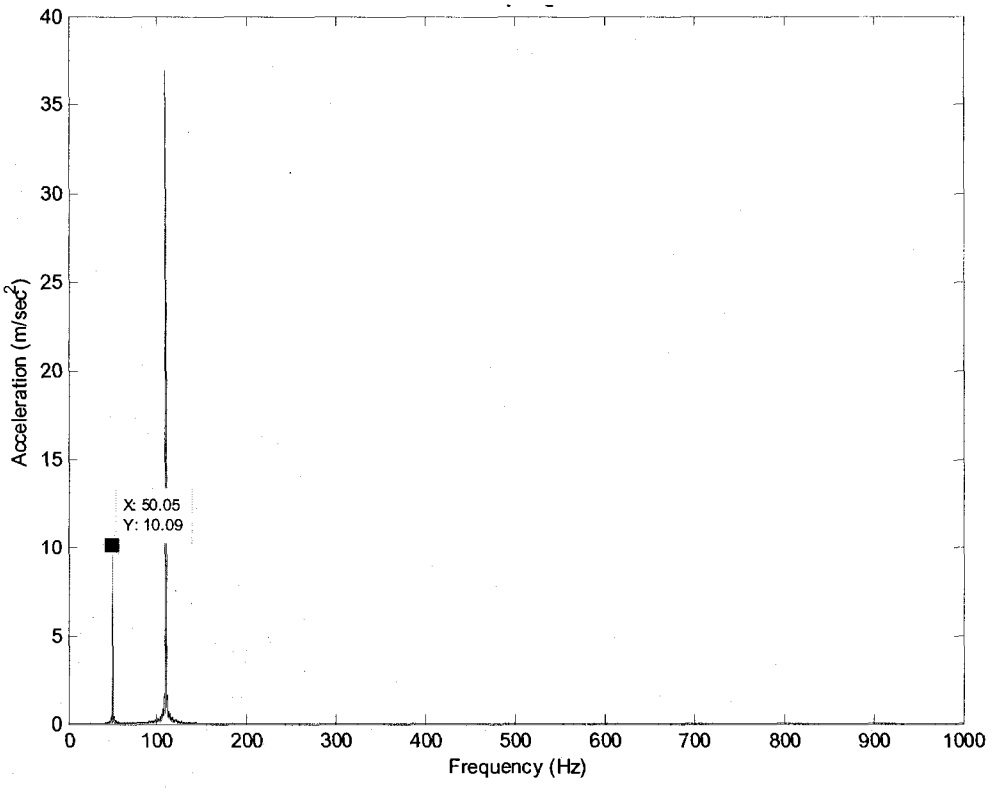

Figure 4-14 Perfectly aligned rotor response using FEM

Finally, in order to examine the applicability of the FEA for misaligned shaft the FEM model developed for validation is extended to include misalignment. This is achieved by introducing a linear displacement at one end of the shaft by 0.1 mm in the y direction. Similarly to frequency response for aligned shaft in Figure 4-14, Figure 4-15 presents the frequency response for the misaligned shaft.

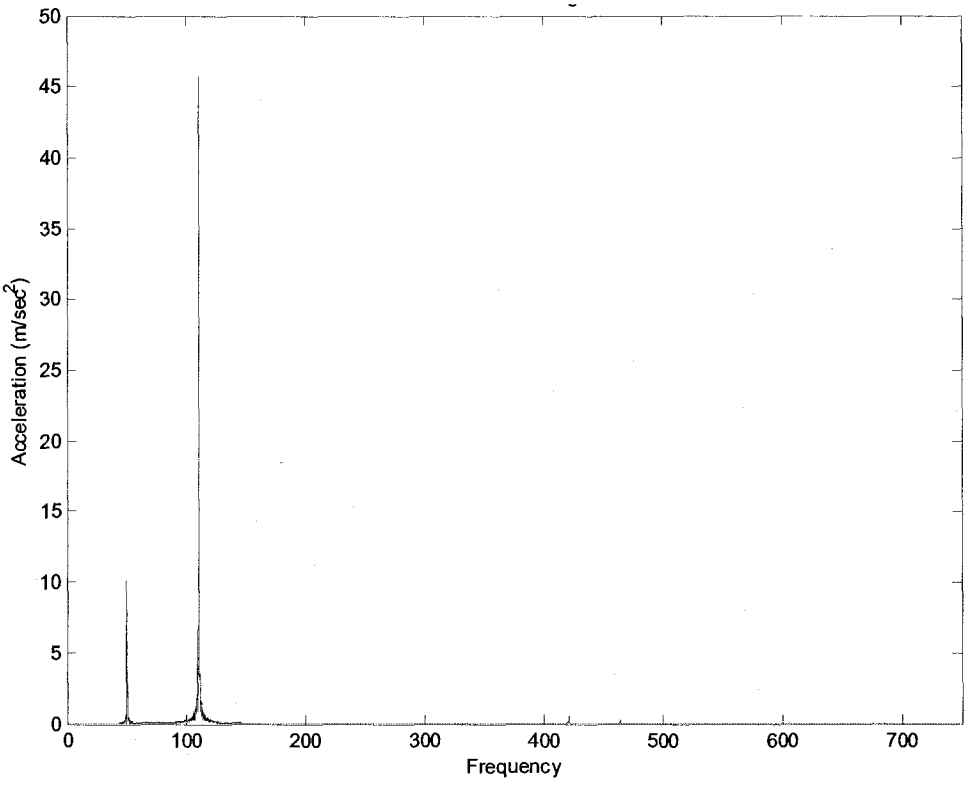

Figure 4-15 Shaft response with 0.1 mm using FEM

As the results show, misalignment in FEM leads to slightly higher response amplitude at the same frequency as the perfectly aligned shaft. More importantly FEM with misalignment do not exhibit response at harmonics which is frequently observed in field [28, 29, 30]. The failure of FEM model in exhibiting misalignment rotor behavior is also reported in the literature [29].

4.6 Summary

The rotor system model developed in chapter 3 was validated by comparing the natural frequencies of the system with those predicted through eigenvalue analysis. For further validation of the model in frequency domain, a finite element of the rotor system was developed using Patran and analyzed using Nastran. Best effort was made to ensure that the finite element model represents the developed model.

The natural frequencies predicted from eigenvalue analysis, finite element analysis and frequency response of lumped parameter model in time domain simulation was used to validate the model. Comparable results were obtained by all three methods over a speed range of 0 to 10,000 rpm. The finite element model was also used to generate time domain response for a given unbalance to compare the response of the developed model. Both models were found to give comparable results both in terms of magnitude and frequency.

A section in the chapter is also devoted to examining the influence of higher order unbalance terms in the equations of motion. The results in terms of 1x and 2x response over the speed range showed that the higher order terms had negligible influence on the above responses of interest and hence could be safely neglected for the purpose of this study. Finally in this chapter, the

effectiveness of finite element method in simulating shaft with misalignment was examined. The results showed that the introduction of misalignment in finite element model had little effect on the amplitude response. However, it failed to exhibit responses at harmonics which have been reported in literature based on experimental tests and field studies.

Chapter 5

5 Dynamic Response of Rotor System Due to Misalignment

5.1 Introduction

In chapter 4, the lumped parameter model of the rotor system was validated against eigenvalue solution as well as comparison with natural frequencies and responses of an equivalent finite element model (FEM). In chapter 4 it was also shown that FEM can not predict the known trend in the response of a rotor system in the presence of misalignment.

The validated lumped parameter model in chapter 3 was extended to include shaft misalignment, which could be parallel and/or angular or combined type. The equation of motion for the misaligned rotor system developed as equations (3-27) to (3-30) in chapter 3 included preload force, nonlinear stiffness K_n and damping C. While the preload force that due to a given parallel and/or angular misalignment, is well defined, there is a lack of methodology in establishing a value for K_n. In the literature [33] the nonlinear stiffness is acknowledged to fluid film bearing properties. Furthermore, the values for damping parameter C, which is essential for stable response, is difficult to estimate accurately. The first part of the misaligned rotor study is thus devoted to a sensitivity analysis of the parameters K_n and C on the rotor responses of interest.

Based on literature review, the most general and useful response of rotor system to misalignment is considered to be 1x, 2x, ... nx responses at a selected rotational speed. For the nonlinear rotor model, it is obtained by time domain simulation of the model for a selected rotational speed followed by FFT of the steady state response. The magnitude of acceleration response of the rotor at frequency corresponding to rotational frequency is referred to as 1x response. Similarly, the response at frequency corresponding to n times the rotational speed is referred to as nx response. Since dominant responses are found only at 1x and 2x frequencies, only 1x and 2x responses are considered in this investigation as response measures for the rotor system.

The sensitivity analysis to K_n and C on the response measure is carried out in the next subsection is used to establish the parameters K_n and C for this investigation.

The following subsections use these parameters for a detailed investigation of response measures for different levels of misalignment. The results obtained in this chapter for misalignment are compared with those without misalignment and are compared with experimental and field test data in chapter 6.

5.2 Sensitivity of nonlinear stiffness and damping

The equations of motion derived for the rotor system with misalignment contain a nonlinear stiffness term K_n and damping parameter C. Prior to examining the influence of misalignment, it is necessary to establish these two parameters. Although, the existence of K_n is acknowledged and attributed to bearing properties [33], an effective value of this parameter has not been explored. This section is thus devoted to examination of its effect on the 1x and 2x responses of the rotor system with misalignment. For this, the rotor system parameters used are same as those presented in Table 4-1, with dynamic unbalance (τ) being 0.15 degrees.

When misalignment is introduced at one of the bearing support, a preload is introduced in the shaft due to its deformation. This preload in the form of a force F and a moment M at the disc location can be established following the derivations presented in section 3.3 by equation (3-26) for a fixed-fixed boundary condition. The total preload in the shaft, as defined in the equations of motion (3-27) to (3-30) is the summation of the preload due to shaft bending and the preload due to the non-linear stiffness as described in the equations (3-31) and (3-32). Since there are no guidelines to establish the value of the nonlinear stiffness K_n it is assumed that the nonlinear stiffness parameter is a percentage

of the preload due to the shaft misalignment. As a starting point, for a parallel misalignment, the values of K_{nij} can be established from:

$$K_{n11} = A\left(\frac{K_{11}}{y_i}\right) \quad 5\text{-}1$$

$$K_{n12} = K_{n21} = 0 \quad 5\text{-}2$$

$$K_{n22} = A\left(\frac{K_{22}}{\phi_i}\right) \quad 5\text{-}3$$

Where A represents a percentage ratio, y_i and ϕ_i are respectively the displacement and slope at the disk location due to a given parallel misalignment. For parallel misalignment of 0.1E-03 m and A taken as 0.008, the initial value of K_n are established as:

$$K_n = \begin{bmatrix} K_{n11} & 0 \\ 0 & K_{n22} \end{bmatrix} = \begin{bmatrix} 8.4684E+07 & 0 \\ 0 & 86957 \end{bmatrix} \quad 5\text{-}4$$

In order to examine the influence of K_n the matrix shown in equation (5-4) is varied from:

$$\mathbf{K_n} = \begin{bmatrix} 8.4684E6 & 0 \\ 0 & 8696 \end{bmatrix} \text{ to } \begin{bmatrix} 1.6937E8 & 0 \\ 0 & 173916 \end{bmatrix} \quad 5\text{-}5$$

Where the ratio $\frac{K_{n11}}{K_{n22}} = 9.74 \times 10^2$ is maintained as a constant.

The damping parameter for the rotor system is selected in order to realize a reasonable damping ratio. For this, the effect of the damping ratio in the range of 1% to 10% is considered. The damping coefficients are thus established using:

$$\mathbf{C} = \begin{bmatrix} B(2\sqrt{K_{11}M_D}) & 0 \\ 0 & B(2\sqrt{K_{22}I_{Dy_3}}) \end{bmatrix} \qquad 5\text{-}6$$

Where K_{11} and K_{22} are elements of stiffness matrix in equation (2-14) established for fixed-fixed boundary condition. The parameter B in equation (5-6) is the damping ratio.

Simulations are carried out for rotor speed 2000 rpm using baseline parameters and 5% damping for K_n in the range of 8.5E6 to 1.7E8, where K_n refers to K_{n11}, while K_{n22} is obtained by maintaining the ratio $\frac{K_{n11}}{K_{n22}}$ constant. The 1x and 2x frequency response at 2000 rpm computed from the steady state time history for the range of K_n is presented in Figure 5-1.

The 1x response for the simulation presented in Figure 5-1 shows that while there is a small 1x response of the rotor at this speed, there is no noticeable effect of K_n on its magnitude. The 2x response at 2000 rpm shown in the same figure indicates that there is negligible response at 2x frequency while effect of K_n is also negligible. This is expected due to relatively small unbalance force at this rotor speed.

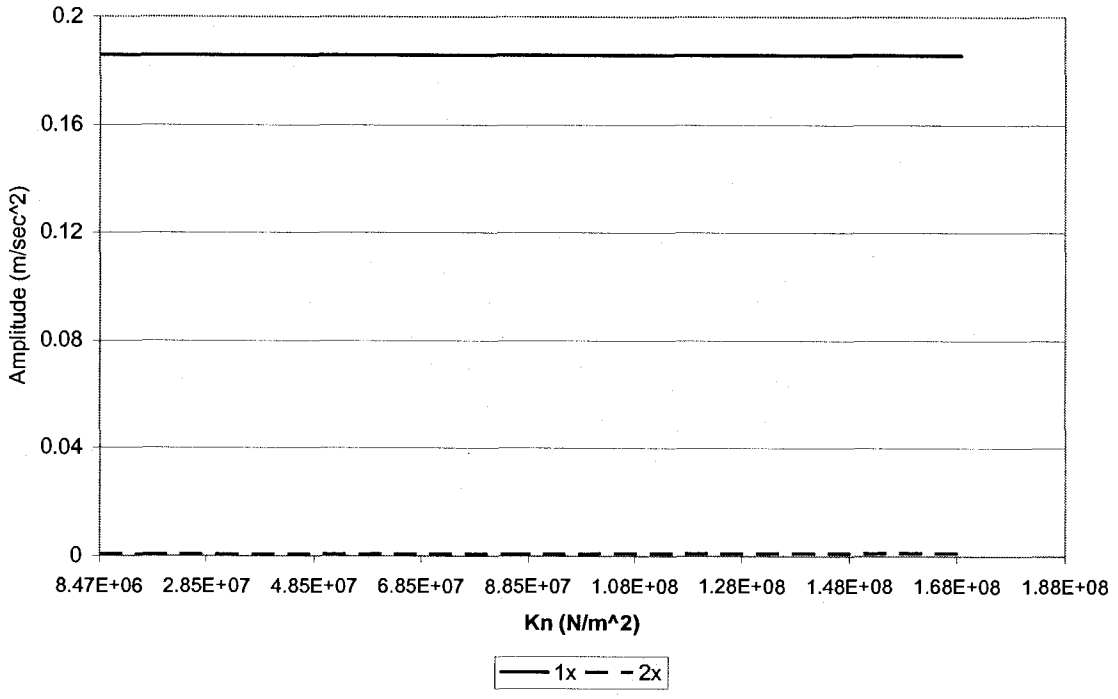

Figure 5-1 1x and 2x Responses at 2000 rpm for different K_n at 5% damping.

Similar results generated for rotor speed 4000 rpm is shown in Figure 5-2. The results show that as the speed is increased, the 1x response of the rotor increases significantly due to increase of the unbalance force. However, the 1x response remains relatively unaffected as the value of K_n is increased. The results further show that at this speed, the 2x response appears and tend to increase steadily as the value of K_n is increased.

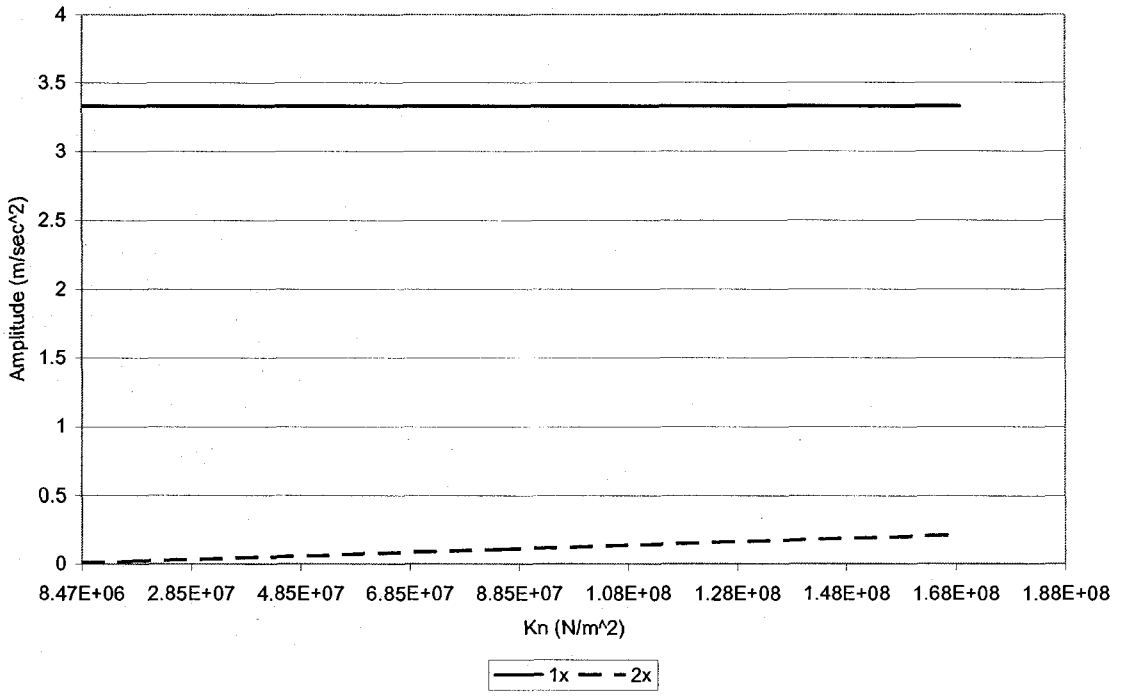

Figure 5-2 1x and 2x responses at 4000 rpm for different K_n at 5% damping.

The 1x and 2x responses for identical simulations carried out fro 6000 rpm are shown in Figure 5-3 and Figure 5-4. The results for 1x response as a function of K_n presented in Figure 5-3 show significantly larger response for the damping considered. It further shows that there is a slight increase in the 1x response as the parameter K_n is increased. The 2x response at 6000 rpm as shown in Figure 5-4 is found to increase significantly with the increase in nonlinear parameter K_n. At this speed the 2x response is also found to be significantly larger than at other rotational speeds.

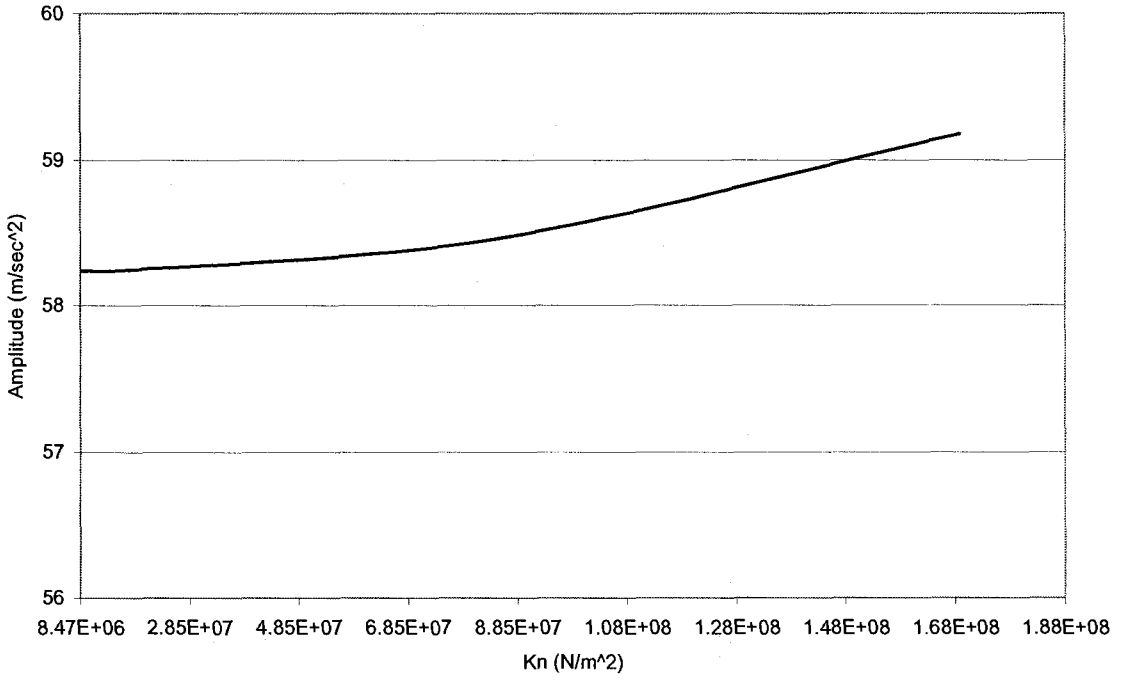

Figure 5-3 1x response at 6000 rpm for different K_n at 5% damping

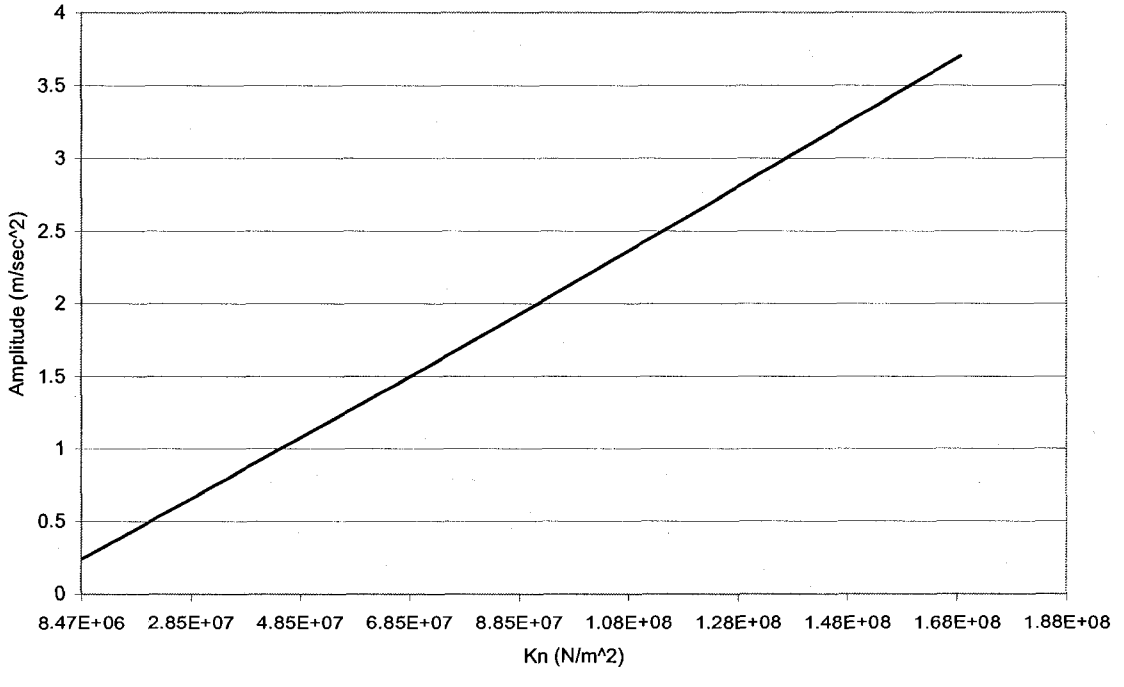

Figure 5-4 2x response at 6000 rpm for different K_n at 5% damping

The 1x response at a higher speed of 8000 rpm, shown in Figure 5-5, exhibits even a higher response due to larger unbalance force. As far as the effect of K_n is concerned, the results in Figure 5-5 show that the 1x response of the rotor decreases slightly as the magnitude of K_n is increased. Although the decrease is minimum, a general trend in 1x response can be noted as the following.

At lower speeds 1x response is low due to low unbalance force, and the 1x response increases with the increase in the rotational speed. Furthermore, K_n has negligible influence on the 1x response for low speeds. As the speed is increased, K_n tends to increase the 1x response very slightly until around 6000 rpm is used. For the considered rotor, speeds beyond 6000 rpm an increase in K_n tend to reduce the 1x response very slightly. It should be noted that 6000 rpm for the considered rotor system is in the vicinity of the rotor system critical speed.

The 2x response at the higher speed of 8000 rpm is presented in Figure 5-6. Once again the 2x response as shown is found to increase with an increase in the K_n value. When compared to the 2x response at 6000 rpm it is evident that the 2x response at 8000 rpm is lower than that observed at 6000 rpm.

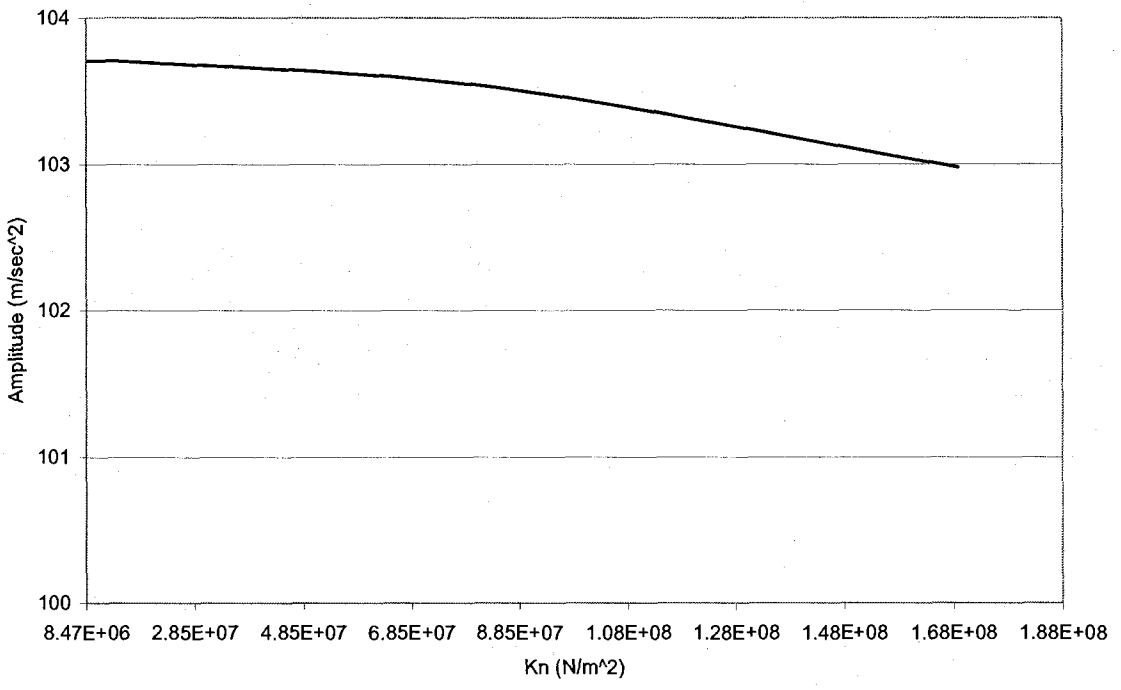

Figure 5-5 1x response at 8000 rpm for different K_n at 5% damping

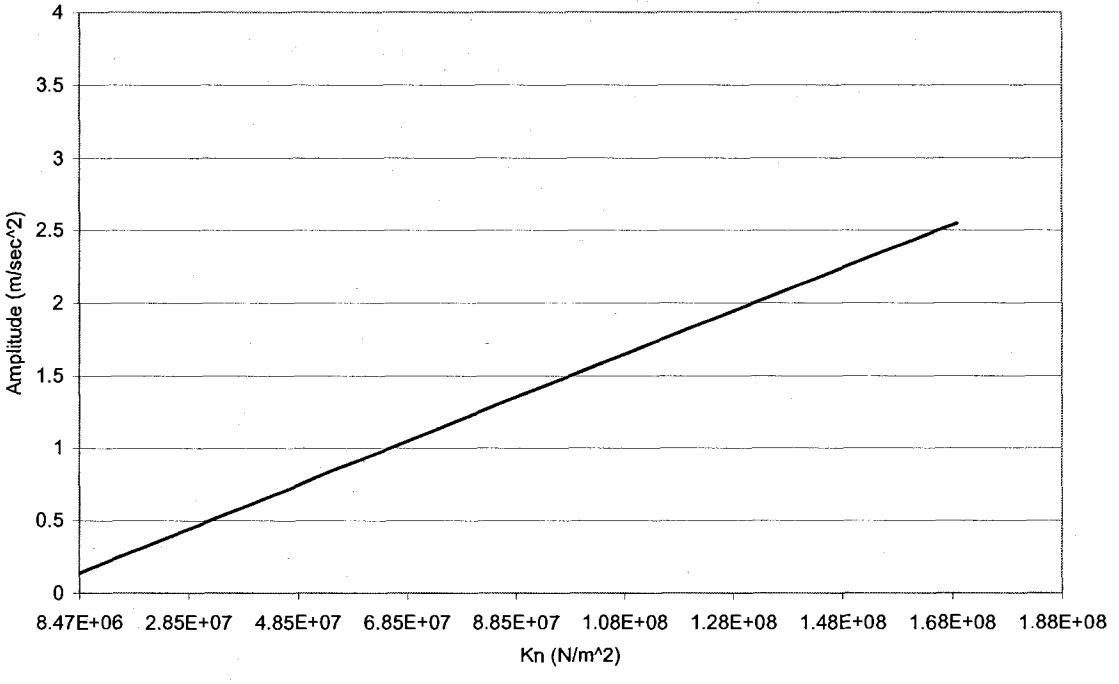

Figure 5-6 2x response at 8000 rpm for different K_n at 5% damping

Again a general trend in the 2x response as function of speed and magnitude of K_n can be noted as follows.

At lower speeds, the 2x response is not present where K_n also shows no influence. As the speed and resulting unbalance force is increased in the presence of misalignment, the 2x response appears even for lower end of K_n values. The 2x response also increases as the value of K_n is increased. It is also observed that near 6000 rpm, the 2x response is most prominent with most sensitivity to K_n values where the response increases significantly as K_n is increased. At speeds higher than 6000 rpm or as the speed increases beyond the system critical speed, the 2x response decreases and the sensitivity to K_n is lower than that near the critical speed.

The above simulation results presented are for a 5% damping. The influence of damping parameter on the response sensitivity of K_n is next examined. The damping parameter is selected for damping ratio of 1, 5, and 10% based on equation (5-6).

The effect of K_n on the 1x and 2x responses for the three damping parameters are shown in Figure 5-7 and Figure 5-8. It was found that typically the response at 1x and 2x will reduce with the increase in damping while the slope of the response with respect to K_n will reduce with the increase of the damping ratio.

The sensitivity of K_n to the 2x response thus reduces significantly when the damping is large. For further investigation of responses due to misalignment the damping parameter is taken to yield 5% damping to account for structural and bearing damping. This is accomplished by equating parameter B in equation (5-6) to 0.05

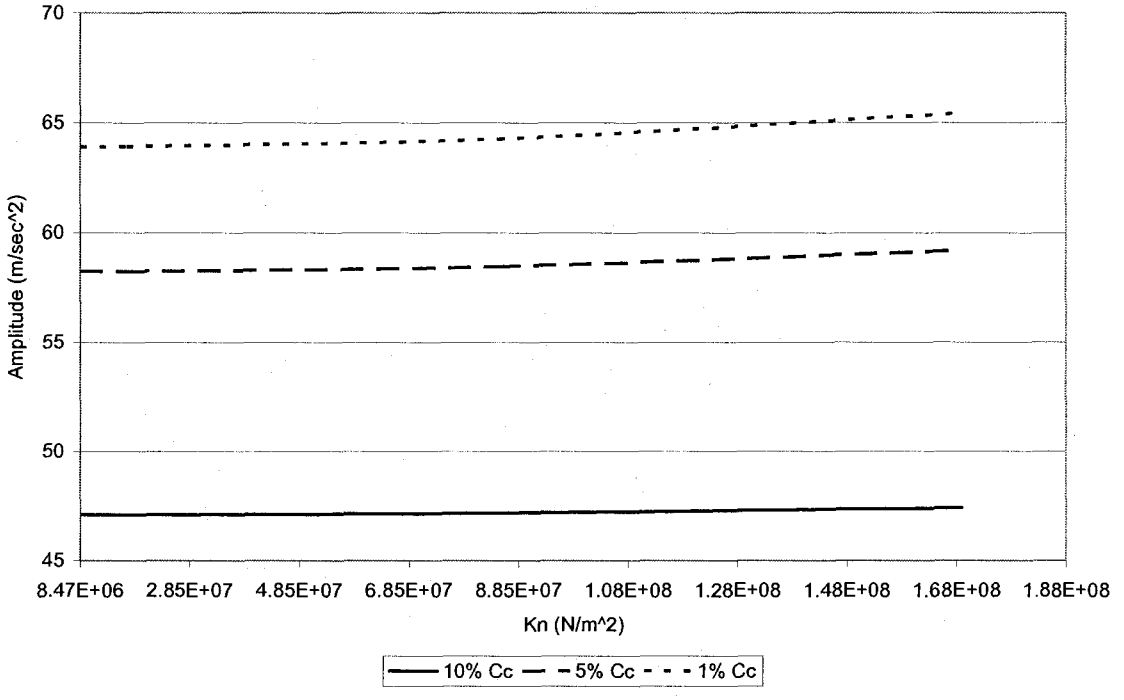

Figure 5-7 1x response for different damping at 6000 rpm

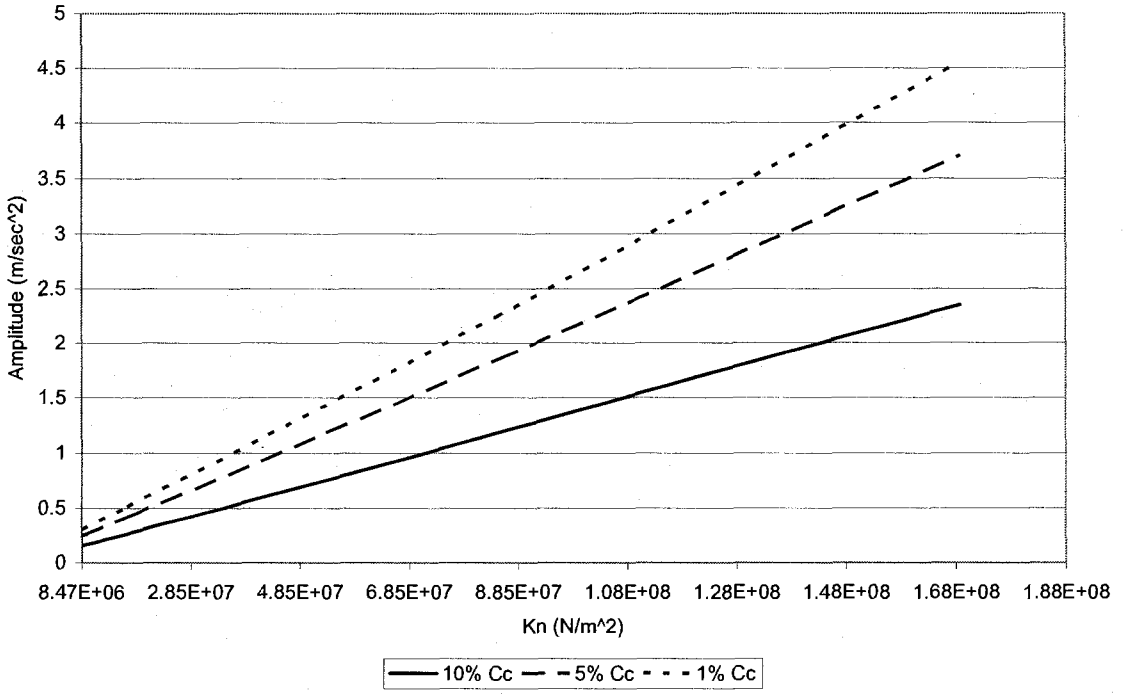

Figure 5-8 2x response for different damping at 6000 rpm

The introduction of the damping terms in the equations of motion will alter the dynamic properties of the rotor. To evaluate the effect of damping ($B = 0.05$ in equation 5-6) on the natural frequency of the rotor the equations of motion (4-1) to (4-4) were rewritten with the introduction of the damping terms:

$$M_D\ddot{y} + K_{11}y + K_{12}\phi + C_{11}\dot{y} + C_{12}\dot{\phi} = 0 \qquad 5\text{-}7$$

$$M_D\ddot{z} + K_{11}z + K_{12}\psi + C_{11}\dot{z} + C_{12}\dot{\psi} = 0 \qquad 5\text{-}8$$

$$I_{Dy_3}\ddot{\phi} - I_{Dx_3}\omega\dot{\psi} + K_{21}y + K_{22}\phi + C_{21}\dot{y} + C_{22}\dot{\phi} = 0 \qquad 5\text{-}9$$

$$I_{Dy_3}\ddot{\psi} + I_{Dx_3}\omega\dot{\phi} + K_{21}z + K_{22}\psi + C_{21}\dot{z} + C_{22}\dot{\psi} = 0 \qquad 5\text{-}10$$

The complex eigenvalues for the above equations were calculated using the rotor properties shown in Table 4-1. The results were compared to the natural frequency of the systems and the damping ratio was calculated for each mode. Table 5-1 shows in the first column the natural frequency of the system without damping, the second column shows the natural frequency of the damped rotor and finally the third column shows the damping ratio for each mode. The result show that the damped frequency does not change significantly due to the introduction of the damping. It is also important to note that the rotation speed does not affect the damping ratio significantly.

Table 5-1 Comparison of the effect of damping on natural frequency

	3000 rpm			9000 rpm		
	Natural Freq. (Hz)	Damp. Natural Freq. (Hz)	ξ	Natural Freq. (Hz)	Damp. Natural Freq. (Hz)	ξ
First Mode	111.76	111.61	0.051	111.62	111.4	0.051
Second Mode	111.89	111.75	0.051	112.02	111.8	0.051
Third Mode	565.02	564.32	0.049	481.18	476.8	0.048
Fourth Mode	665.01	664.19	0.049	781.13	765.7	0.048

5.3 Rotor Response with Misalignment

Prior to any simulation of misaligned rotor system it is essential to determine a methodology to select appropriate value for nonlinear stiffness K_n as a function

of preload. In general the analysis on the sensitivity of K_n presented in section 5.2 indicates that at the lower end of K_n values used the 1x response of the rotor is relatively unaffected while the 2x response is always found to increase. Based on the literature review and experimental studies presented in chapter 1, it is clear that misalignment invariably results in an increase in the 2x component of the response while 1x is relatively unaffected. Furthermore, the increase in the 2x response is known to be a function of misalignment magnitude. Hence it was decided to adopt the value for K_n as a function of misalignment while K_n will be in the lower range of the range considered in section 5.2.

For this, K_n is established using equation (5-1) to (5-3) for parameter A taken as 0.0014, with a parallel misalignment of 0.1 mm at bearing B as shown in Figure 3-5 (ii), the deflection and slope at disk location are found to be:

$$\begin{bmatrix} y_i \\ \phi_i \end{bmatrix} = \begin{bmatrix} 4.17E\text{-}5\,(\text{m}) \\ 4.12E\text{-}4(\text{rad}) \end{bmatrix} \qquad 5\text{-}11$$

And the corresponding value of K_n is established as:

$$K_n = \begin{bmatrix} 1.4114E+07 & 0 \\ 0 & 1449.28 \end{bmatrix} \qquad 5\text{-}12$$

For other magnitudes of misalignment, the computed values of deflection and angle at rotor location is used to establish the new K_n matrix. For this the new location of the disk y_{Di} and slope ϕ_{Di} is calculated. Then the K_n matrix is modified using the following equation:

$$K_n = \begin{bmatrix} 1.4114E+07\frac{y_{Di}}{y_i} & 0 \\ 0 & 1449.28\frac{\phi_{Di}}{\phi_i} \end{bmatrix} \qquad 5\text{-}13$$

Where y_i and ϕ_i are defined in equation (5-11).

Simulations are carried out with different misalignment magnitude to show the effect of misalignment on the 1x and 2x responses. Similar to the previous sections the differential equations of motion are solved in time domain using Runge Kutta method. The time domain data is then transferred to the frequency domain. The simulation is run at different rotation speed and the amplitude at 1x and 2x are plotted.

The first two simulations examine the effect of parallel misalignment on the 1x and 2 x responses. Two misalignment are introduced the first being 0.2E-3 m and the second 0.4E-3 m. Figure 5-9 shows the 1x rotor response at different rotational speed. As the result shows, the introduction of misalignment dies not change the response significantly. In fact the response remains identical regardless of the level of misalignment except in the vicinity of the critical speed, where there is a slight change in the response. The effect of parallel misalignment on the 2x response is shown in Figure 5-10, which clearly shows a significant increase of the 2x response due to misalignment. The 2x responses observed from the simulation show that as misalignment is introduced a dominating 2x response appear over a wide speed range where the response is

largest when the rotational speed corresponds to the critical speed. The results further show that the increase in this response is significantly more for larger magnitude of misalignment. This trend is in line with the experimental observations reported in the literature.

The next set of simulations examines the effect of angular misalignment on the rotor response. For this an angular misalignment of 0.2 and 0.4 degree is introduced at bearing B. Similar to the response observed for parallel misalignment the 1x response shown in Figure 5-11 does not change significantly with the introduction of the angular misalignment. The 2x response, shown in Figure 5-12, on the other hand increases with the increase in misalignment magnitude; this is in line with the response observed due to parallel misalignment.

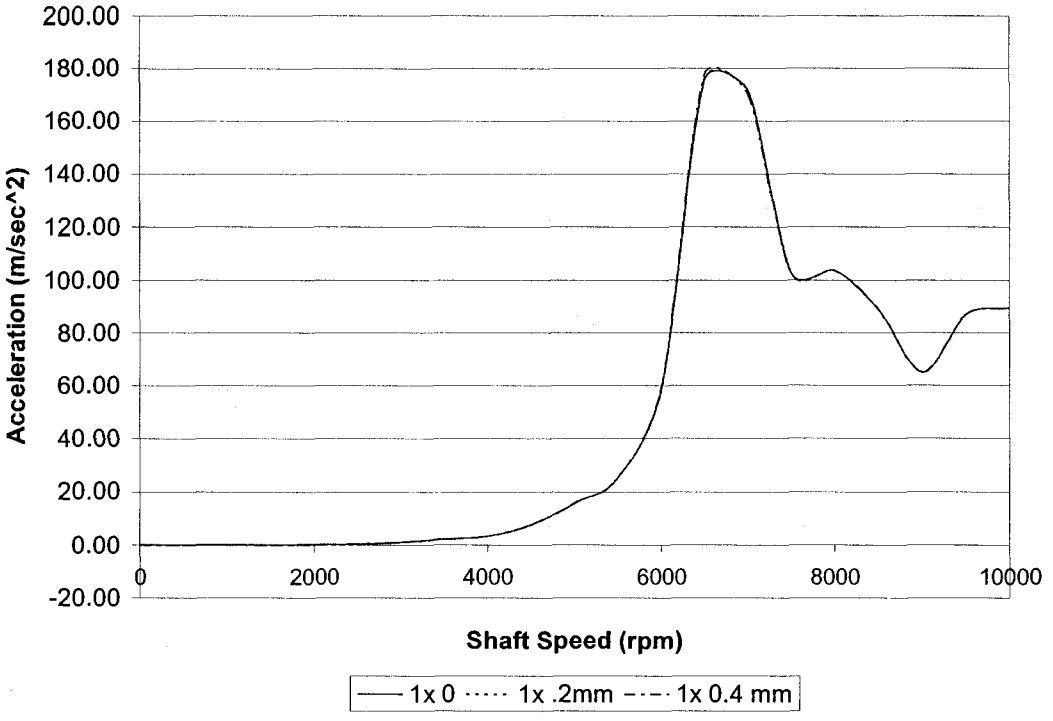

Figure 5-9 1x Disk response versus shaft speed for parallel misalignment

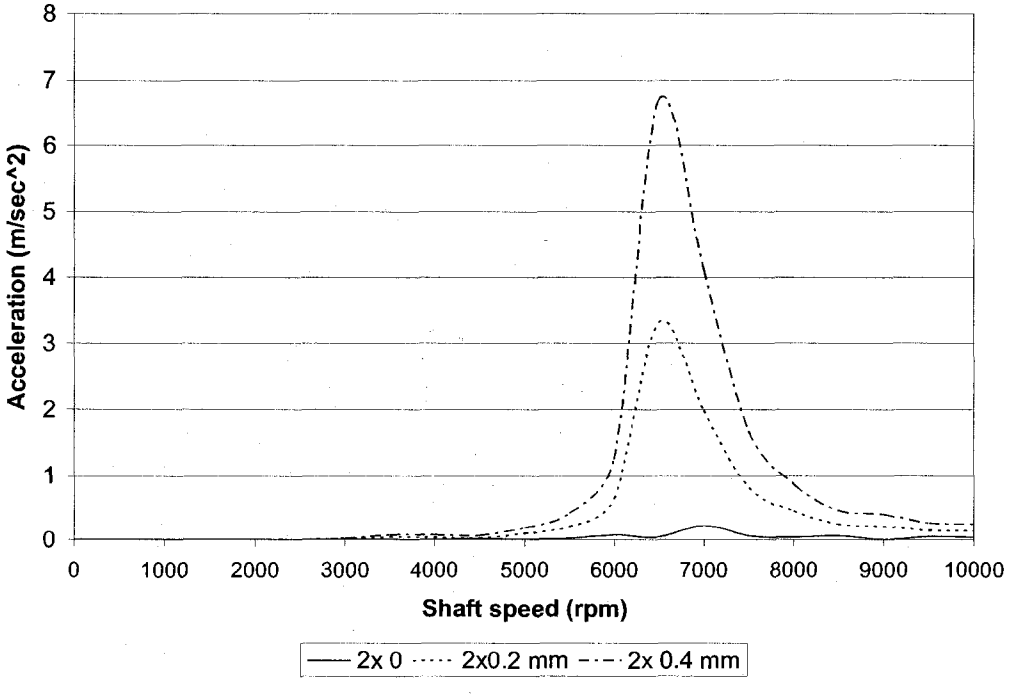

Figure 5-10 2x Disk response versus shaft speed for parallel misalignment

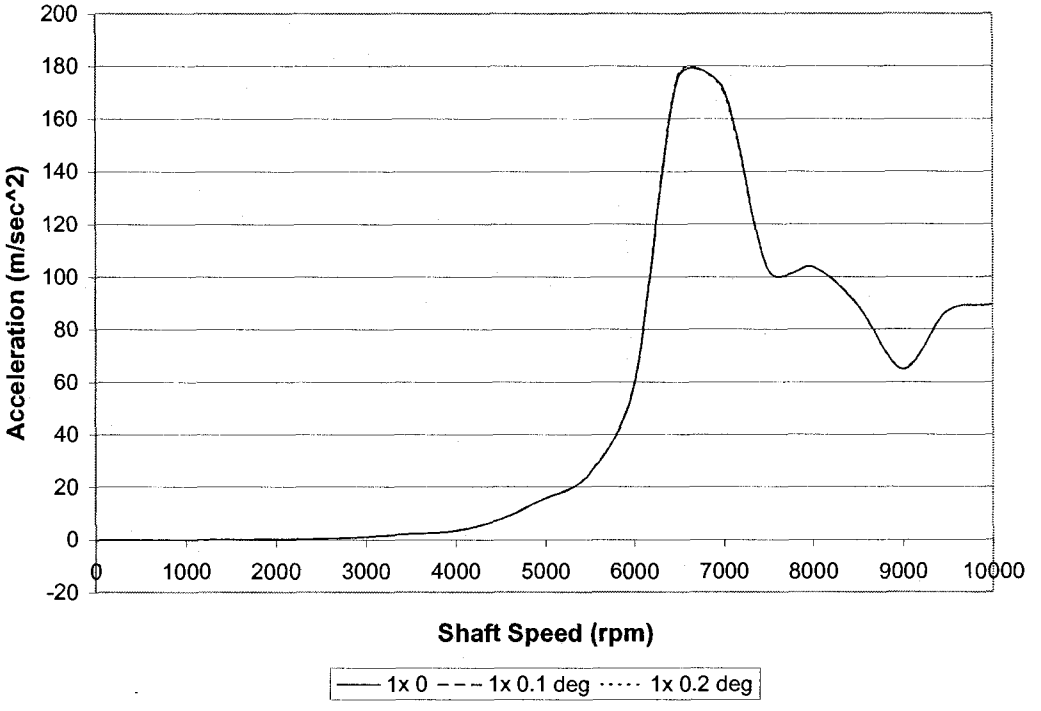

Figure 5-11 1x Disk response versus shaft speed for angular misalignment

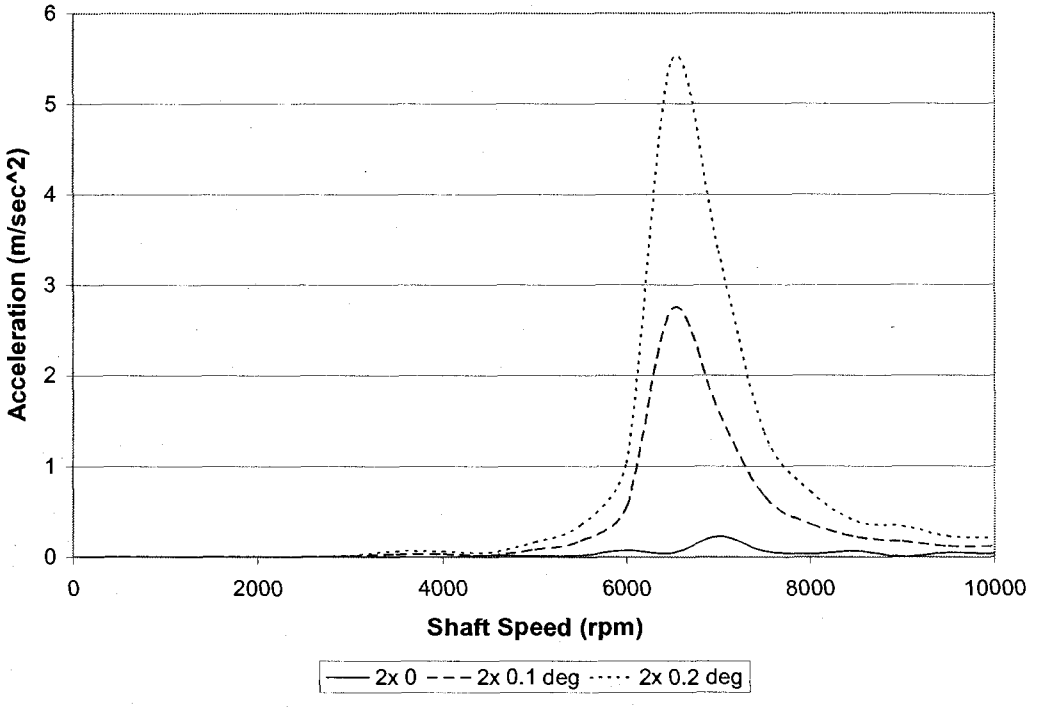

Figure 5-12 2x Disk response versus shaft speed for angular misalignment

It should be pointed out that both parallel and angular misalignment essentially introduce a preload in the shaft with resulting deflection and slope at the disk location. Hence a very similar rotor response is expected in both parallel and/or angular misalignment.

The next case examines the effect of the combined parallel and angular misalignment on the rotor response. To accomplish this, the simulation is run with a combined parallel misalignment of 0.2E-3 m and angular misalignment of 0.2 degree. The 1x response is shown in Figure 5-13, and again for the misalignment values used the 1x response does not show any change due to misalignment. The 2x response on the other hand, shown in Figure 5-14 indicates a sharp increase in the 2x response in the presence of misalignment.

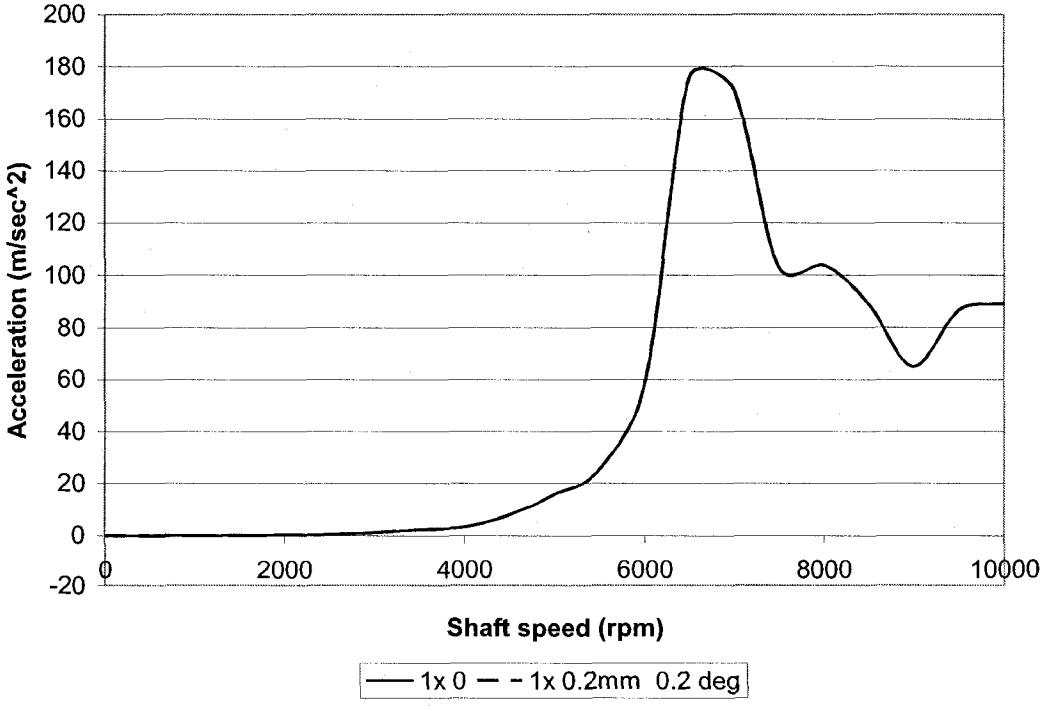

Figure 5-13 Rotor 1x response due to combined angular and parallel misalignment

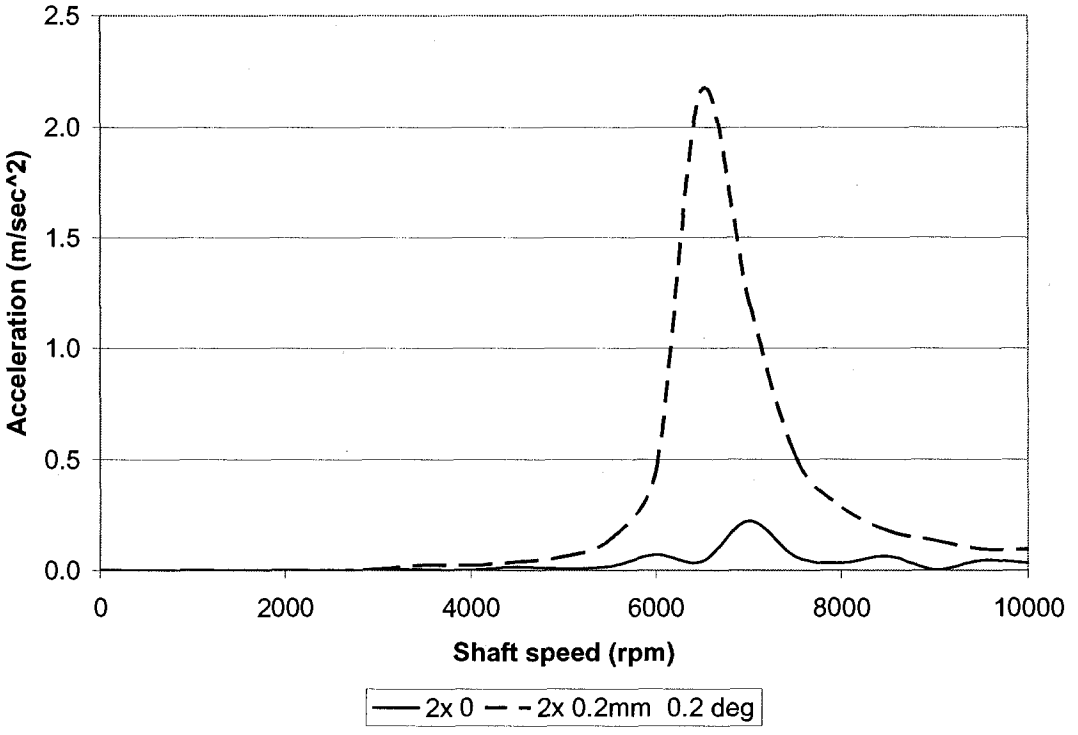

Figure 5-14 Rotor 2x response due to combined angular and parallel misalignment

This result, when compared to 2x response due to pure parallel (0.2 mm) misalignment (Figure 5-10) or pure angular (0.2 deg) misalignment (Figure 5-12), show relatively smaller 2x response when both are present at the same time. This is attributed to the fact that the preload created by a parallel misalignment in this case was reduced by the considered angular misalignment.

Finally to investigate the effect of severe misalignment, a simulation is run with a misalignment of 0.005 m and without misalignment. The FFT of the rotor response at 6500 rpm is shown in Figure 5-15 and Figure 5-16, for aligned and misaligned rotor system, respectively.

The aligned rotor response shown in Figure 5-15 shows only one peak that occurs at the rotation speed, there is no sign of other peaks at 2x or 3x. On the other hand, the response of the misaligned shaft, shown in Figure 5-16 shows clearly a distinctive 1x, 2x and 3x. Comparing the frequency response between the aligned rotor and the misaligned rotor indicates that the 1x frequency may decrease to some extent due to sever misalignment while a significant 2x response is introduced by misalignment. At the same time higher harmonics such as 3x response may be present when the misalignment is severe. Such behavior is also considered with some reported experimental results.

For a close look on the effect of severe misalignment on the 1x and 2x response over a wider rotational speed range the response results are presented in Figure 5-17 and Figure 5-18 for 5 mm misalignment. These results clearly show significant decrease in the 1x response with very significant increase in the 2x response over a wide rotational speed range.

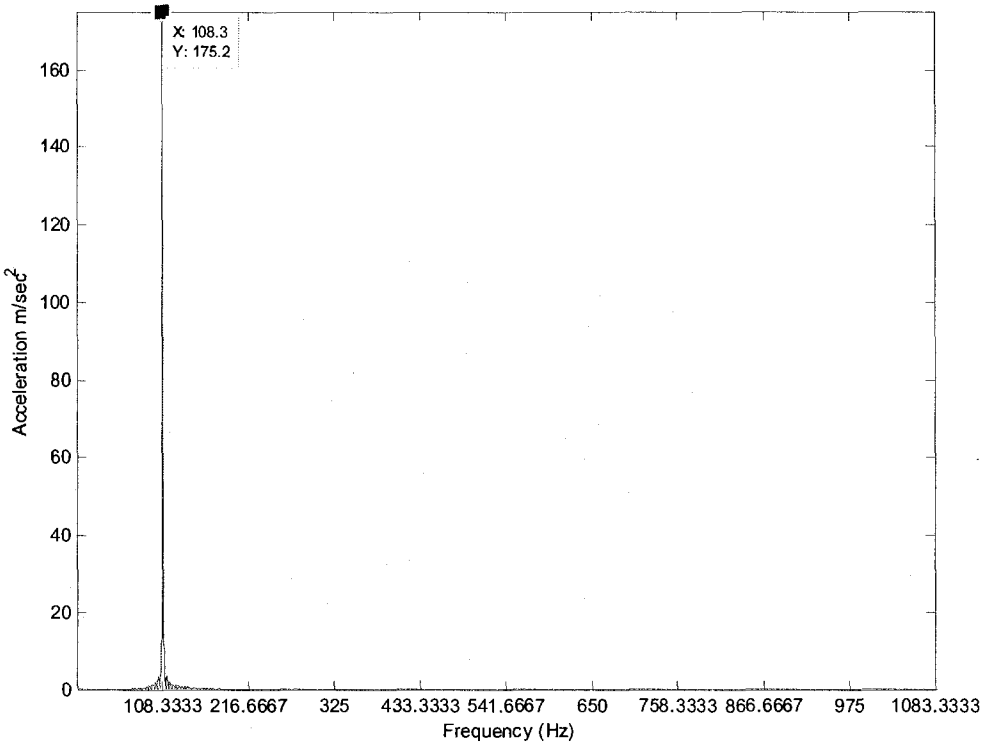

Figure 5-15 FFT of rotor response at 6500 rpm without misalignment

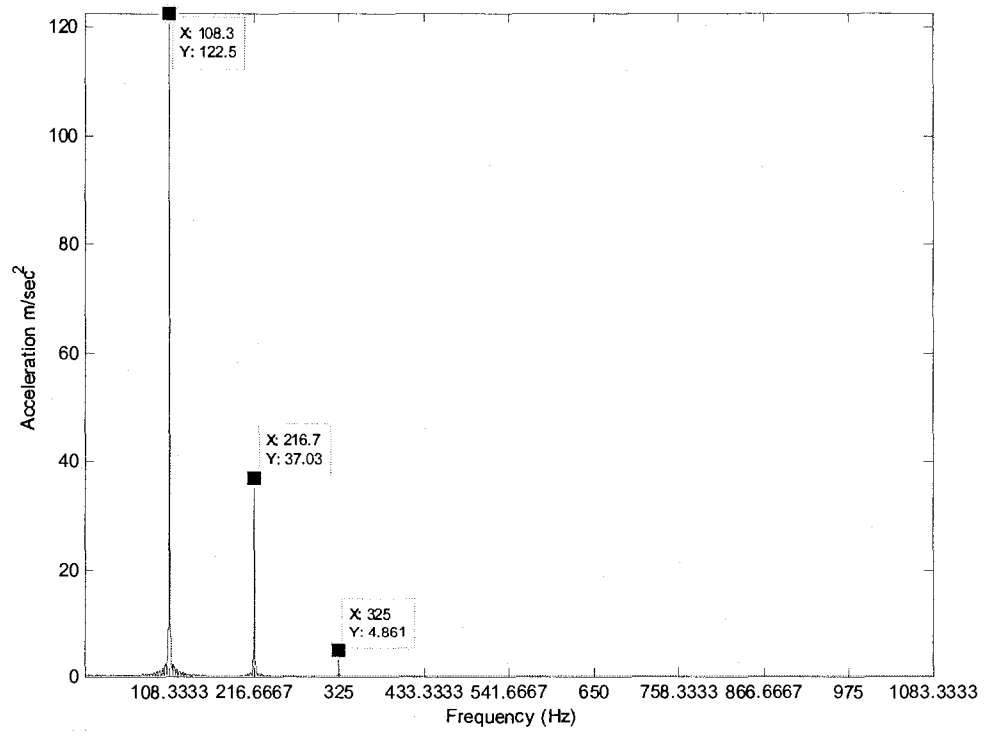

Figure 5-16 FFT of rotor response at 6500 rpm with 0.005 m misalignment

The results obtained so far indicate that in a perfectly aligned rotor system there will be no significant 2x response. If there is a misalignment, it will be accompanied by a significant increase of the 2x components. An increase in the 2x component is a clear indication of an increase in the misalignment. Furthermore if the misalignment is severe, there will be a change in the 1x response with significant 2x response along with nx response.

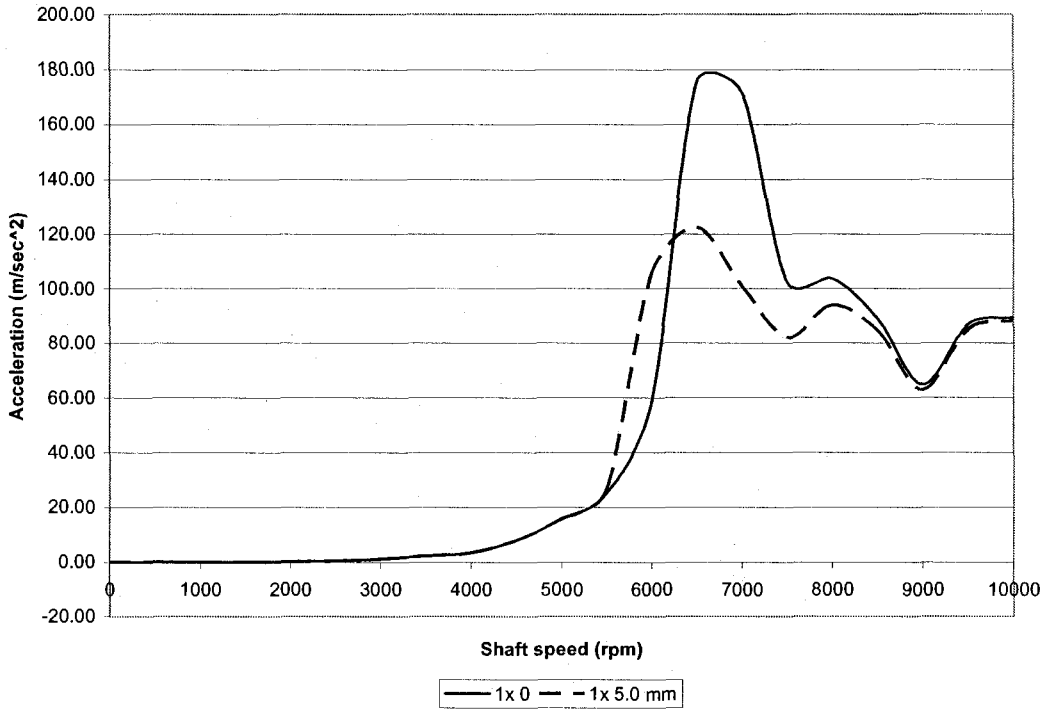

Figure 5-17 1x rotor response due to 0.005 m misalignment

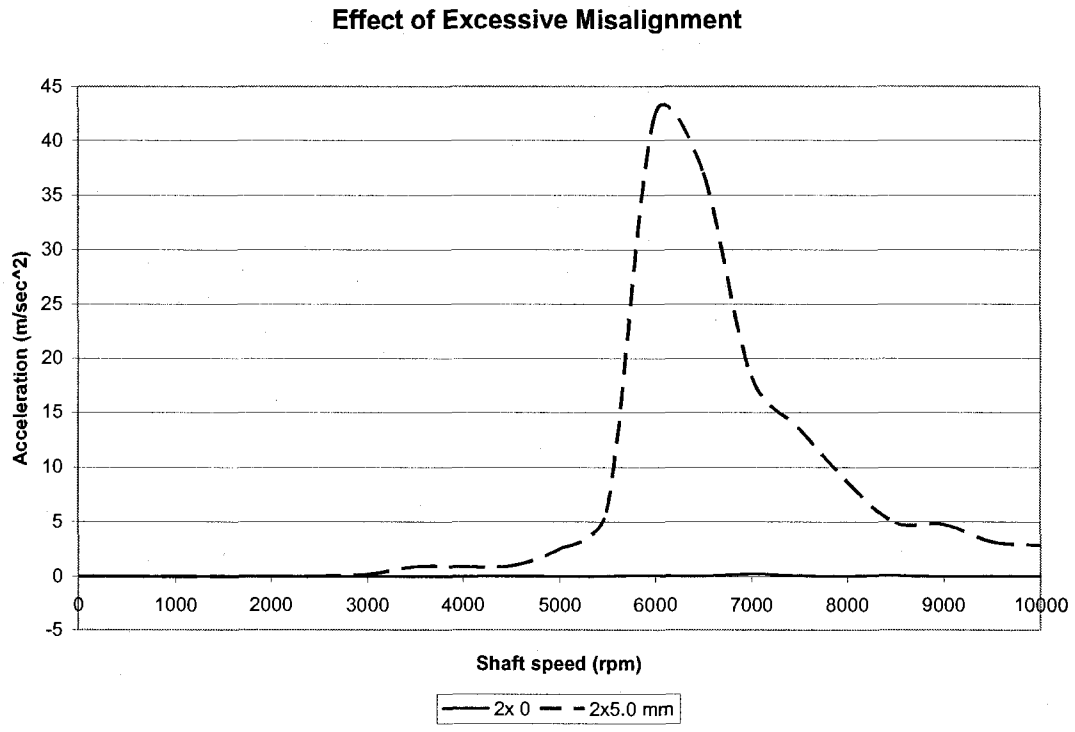

Figure 5-18 2x response due to 0.005 m misalignment

The final set of results in this section present the time domain steady state response in absence and presence of misalignment. Figure 5-19 presents the rotor response time history at 6500 rpm when there is no misalignment. As expected the response is due to unbalance and results in a pure sinusoidal response of the rotor. For the same rotor system, the introduction of 5 mm misalignment leads to a time history response shown in Figure 5-20. This result clearly shows that the misalignment and resulting preload and nonlinear stiffness causes an offset and clipping of the response which yields the higher harmonics in the response in frequency domain.

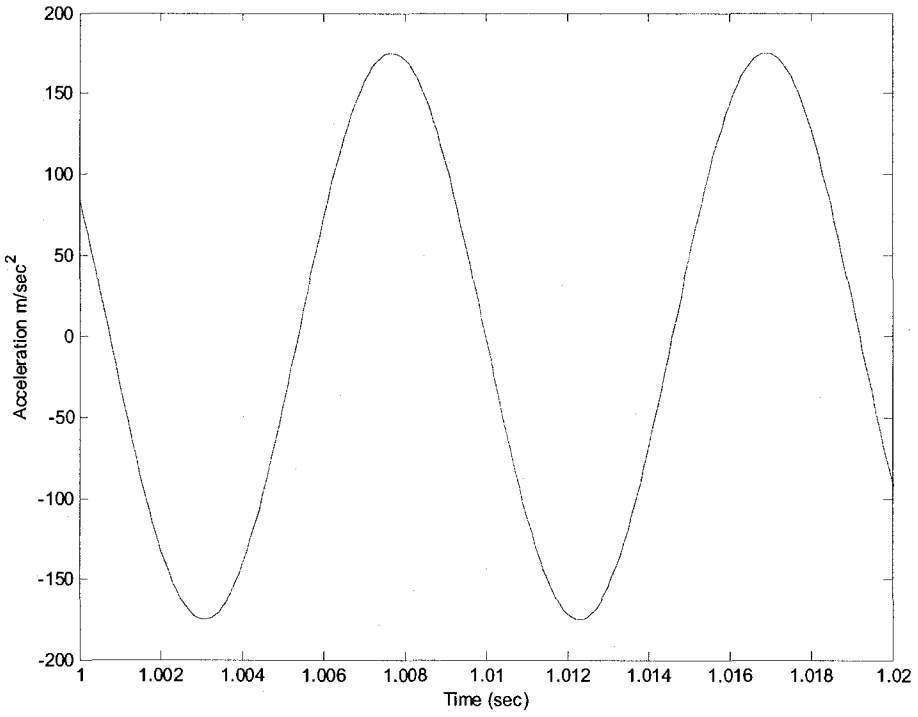

Figure 5-19 Rotor response without misalignment at 6500 rpm in time domain

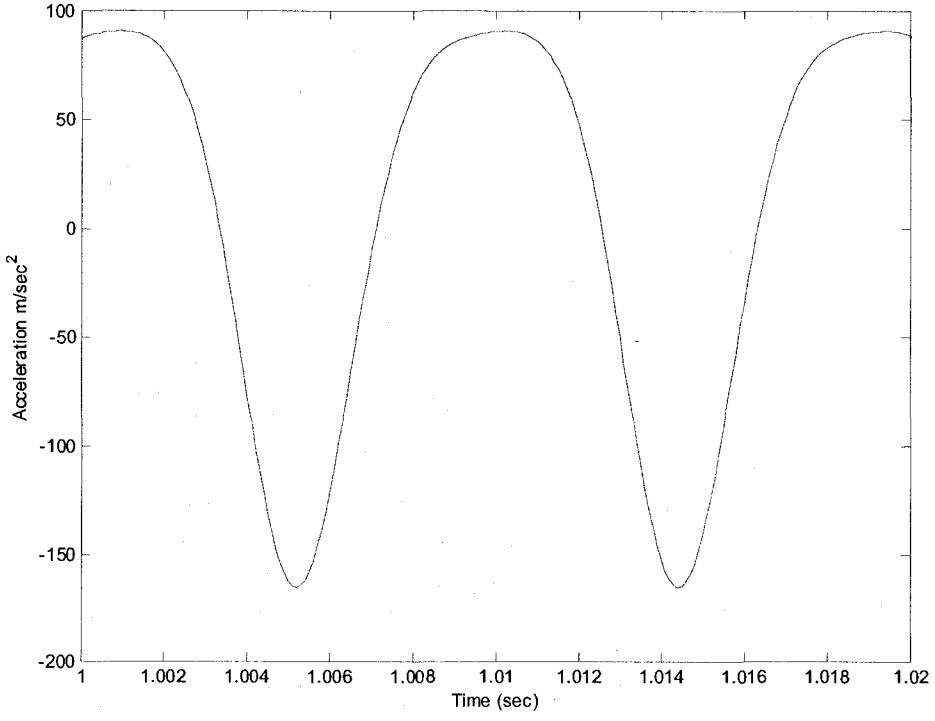

Figure 5-20 Rotor response with 0.005 m misalignment at 6500 rpm in time domain

5.4 Summary

The validated rotor system model was extended to include misalignment in this chapter to examine rotor responses. The inclusion of misalignment involved introduction of preload, resulting deflection and shape at the rotor location and introduction of nonlinear stiffness. K_n as a function of preload. It was first necessary to establish the methodology for selecting reasonable values for K_n and damping for the system.

To accomplish this, the first step was to study the effect of the non linear stiffness K_n and damping C on the shaft response. It was established that an increase of the nonlinear stiffness leads to an increase of the 2x response, but it also can slightly increase or decrease the 1x response in a nonlinear manner. The damping effect was also examined and the simulations showed that an increase of the damping will lead to a decrease in the 1x and 2x magnitude and slope. A methodology was established to select K_n based on misalignment magnitude. Using the selected K_n, the second step was to study the effect of misalignment on the shaft response, by running the simulation for different misalignment cases, which include parallel, angular and combined misalignment. The result showed that the 2x response increased with the increase of misalignment. Finally a case of severe misalignment was examined and it showed that the 1x response was altered significantly while 2x response also

increased. At the same time severe misalignment was found to introduce higher harmonics.

In the next chapter results from a rig test will be presented along with data obtained from a gas turbine engine that was misaligned on purpose to examine its response. In addition two case studies of engines that suffered from severe misalignment are presented to show the effect of misalignment on the 2x response. The analytical results obtained in this section can be readily compared with the experimental and field observed data prior to development of the proposed expert system.

Chapter 6

6 Experimental Rig and Field Engine Data

6.1 Introduction

A detail time and frequency domain analysis of a rotor system in the presence of misalignment was presented in chapter 5. The results in general show that regardeless of parallel or angular misalignment, it introduces a preload on the shaft and introduces additional nonlinear stiffness. Furthermore, the nonlinear stiffness parameter is a function of the magnitude of misalignment. The simulation results over a wide range of rotating speed show in general that the presence of misalignment introduces a rotor response at a frequency corresponding to two times the rotating speed referred to as 2x response. Furthermore there is always 1x response due to excitation generated from rotating unbalance. The 1x and 2x rotor responses, extensively investigated in the previous chapter, clearly show that misalignment has little influence on the 1x response which may reduce or increase slightly depending on the magnitude of misalignment. The 2x response on the other hand increases as the misalignment is increased.

In order to qualitatively confirm the trend in the response observed from simulations, this chapter is devoted to experiment with an available test rig. For this a Bentley-Nevada rig was used where misalignment could be realized by

introducing shims under one of the bearings. However the rotor response being difficult to measure, the rotor system response at one of the bearing was selected as a measure of response trend. Thus only a qualitative trend in the response could be compared with those obtained as rotor response in simulations.

Further to test rig responses to misalignment, data was also collected from field tests of full scale gas turbine engines with and without known misalignment. These results can also be readily compared with the trend observed from simulations and test of a simple rotor system. This chapter presents the details of the rig and field test results to confirm the trends observed in simulation. The confirmed simulation results are finally used in the next chapter for development of an expert system for identification of misalignment in rotor system such as gas turbine.

6.2 Rig layout

The geometrical specification of the Bentley Nevada test rig used for the experiment is shown in Figure 6-1. A photograph of the test rig is presented in Figure 6-2. The rig consists of an electric motor coupled to a rotor via a flexible shaft. The shaft is supported by two dry friction bearings made of brass. The rig is capable of a maximum speed of 10,000 rpm. The electric motor is controlled via an external controller and motor speeds can be pre-selected. The controller

can achieve a speed rate of 10,000 rpm/min, or can be selected to run at a fixed speed. Although a given unbalance can be easily introduced to the rotor, no intentional unbalance was introduced in consideration of the very high speed of operation. For the present investigation, the rig was modified to accommodate a given misalignment by shimming one of the bearings. Hence a parallel misalignment could be easily realized. Although simulated response of the rotor was considered a measure of misalignment effect it could not be done for test rig due to lack of instrumentation. As an alternative, response was measured at one of the bearings. For this an accelerometer was attached at bearing B as shown in Figure 6-1 and Figure 6-2. The accelerometer signal was passed through a charge amplifier and the signal was analyzed using a spectrum analyzer made by Hewlett Packard. The specifications of the electronics used for testing are detailed in Table 6-1.

6.3 Testing procedure

The accelerometer response at the bearing "B" was measured and recorded for selected rotor system speeds in the range of 0 to 10,000 rpm, using 500 rpm increments. Before each recording, time was allowed to stabilize the response of the system at each speed. The time response was then analyzed to establish the 1x and 2x response at each selected speed. Tests were carried out for aligned as well as misalignment of 0.2 and 0.4 mm. Each run was repeated for three times to ensure repeatability of the tests preformed.

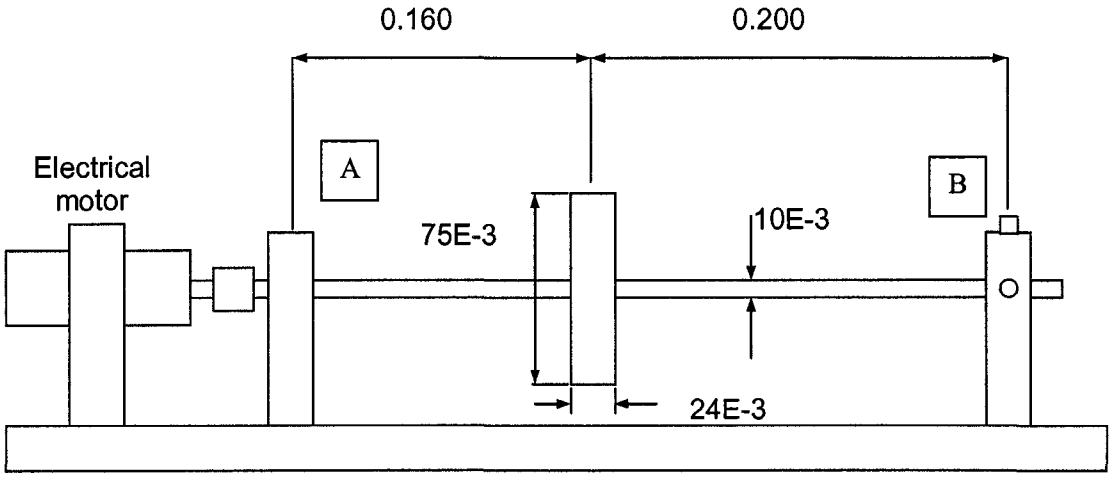

Figure 6-1 Rig layout all dimensions in meter

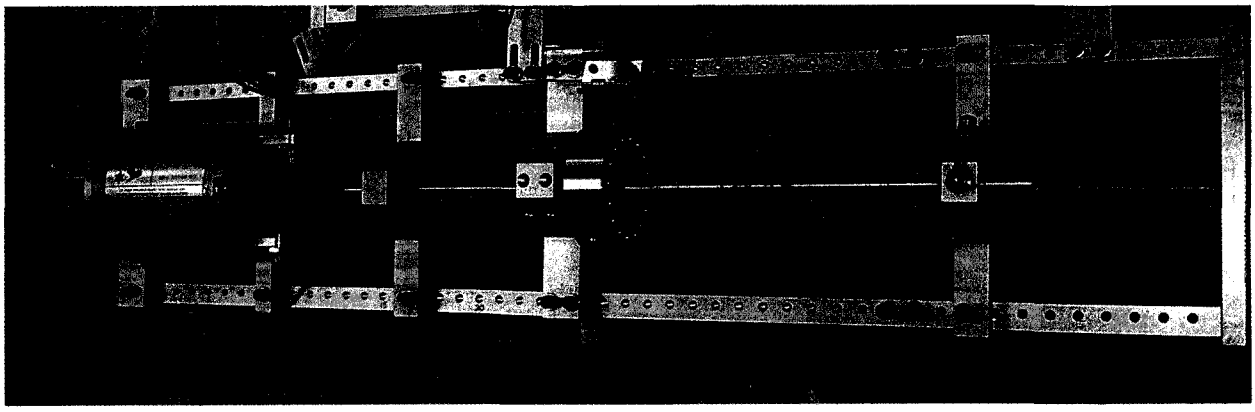

Figure 6-2 Picture of the Bentley Nevada rig

Table 6-1 Specification of the test components

Accelerometer type	Endevco Model 7240B
Sensitivity	2.59 pC/g
Charge amp	PCB
Specification of charge amp	9.96 mv/Pc

6.4 Test Results

The test results in terms of acceleration response for zero and 0.2mm misalignments are shown in Figures 6-3 and 6-4. Figure 6-3 shows the measured acceleration at bearing "B" at the frequency corresponding to the shaft rotation speed (1x). The 1x response for aligned system shows 4 distinct peaks. When this is compared with the simulated rotor response for zero misalignment in Figure 5-9 it clearly shows that the test produces 2 additional peaks at 3000 rpm and 4500 rpm in addition to the peaks expected at around 6000 rpm and 7000 rpm. The peaks are due to rig characteristics and associated with rig natural frequencies. As shown in Figure 6-3, when the 0.2 mm misalignment is introduced, it is found that the peaks corresponding to the rig natural frequencies are reduced. However the peak at 6000 rpm increased by the presence of misalignment. Similar trend was observed in simulation for moderate levels of misalignment. It should be pointed that no attempt is made here to compare the magnitude of the response from experiment to those of simulations, since the

experimental response is at the bearing while simulated results are for the rotor response.

Figure 6-4 shows the measured acceleration at bearing B at the frequency corresponding to twice the shaft rotation speed (2x). Similar to 1x response the rotor system 2x response at the bearing also show peaks at speeds other than 6000 rpm due to rig resonances. It is however clear that there is very little response at 6000 rpm when there is no misalignment. When misalignment of 0.2 mm is introduced, the results in Figure 6-4 show that peaks corresponding to the rig resonance decreases slightly while the response around 6000 rpm is significantly increased. This effect of misalignment on the 2x response of the rotor was clearly identified from the simulation results.

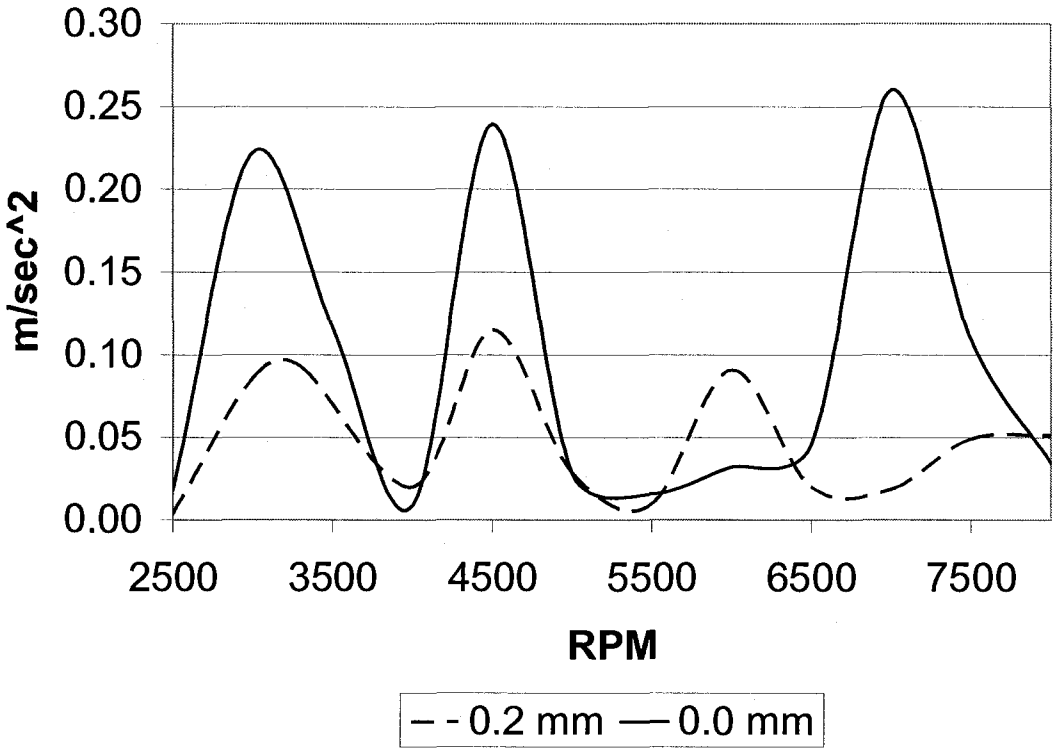

Figure 6-3 Support acceleration response 1 x component

Similar results for a more severe misalignment of 0.4 mm is shown in Figure 6-5 and 6-6. The 1x response shown in Figure 6-5 shows a slight reduction of the 1x component due to misalignment over the speed range except at around 7500 rpm where the response increases slightly. The 2x response shown in Figure 6-6 shows a behavior similar to the one obtained from the simulation in Figure 5-18 where the 2x response increases drastically due to the introduction of misalignment. In the simulation the increase in the 2x response occurs close to critical speed and is accompanied with a shift of the critical speed of the rotor system as it is clearly seen in Figure 5-17.

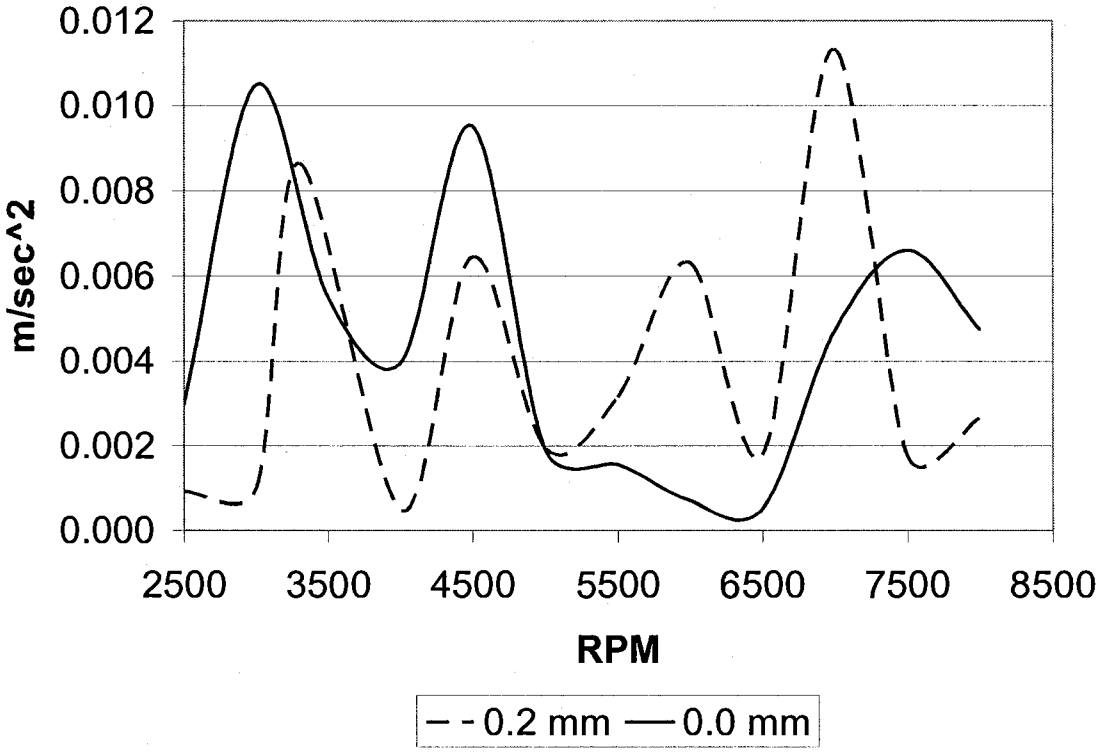

Figure 6-4 Support acceleration 2x component

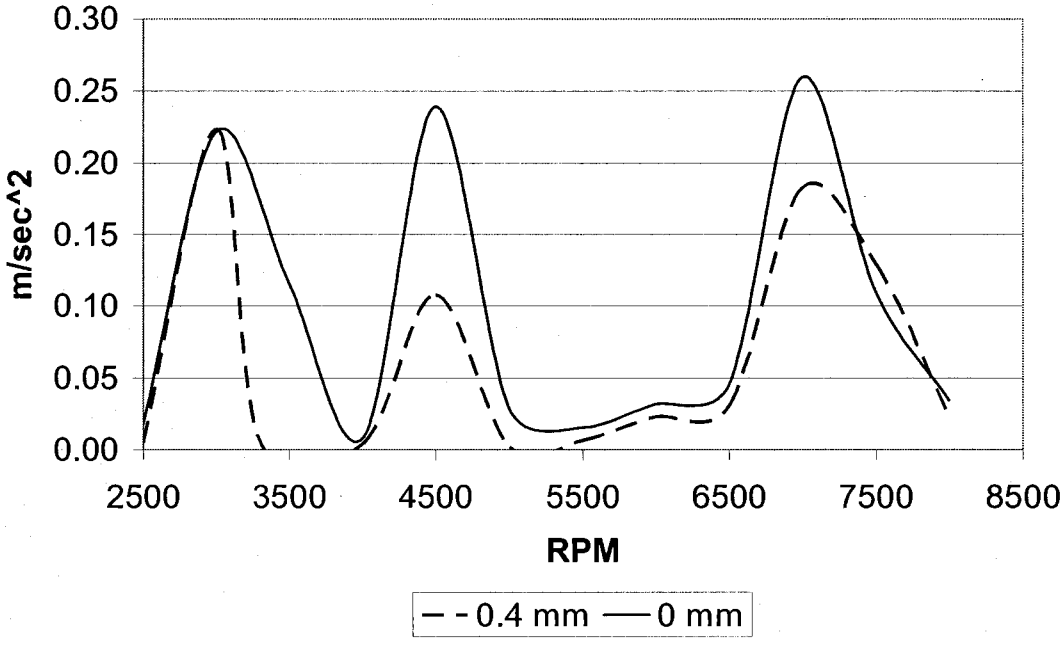

Figure 6-5 Support acceleration response 1x component

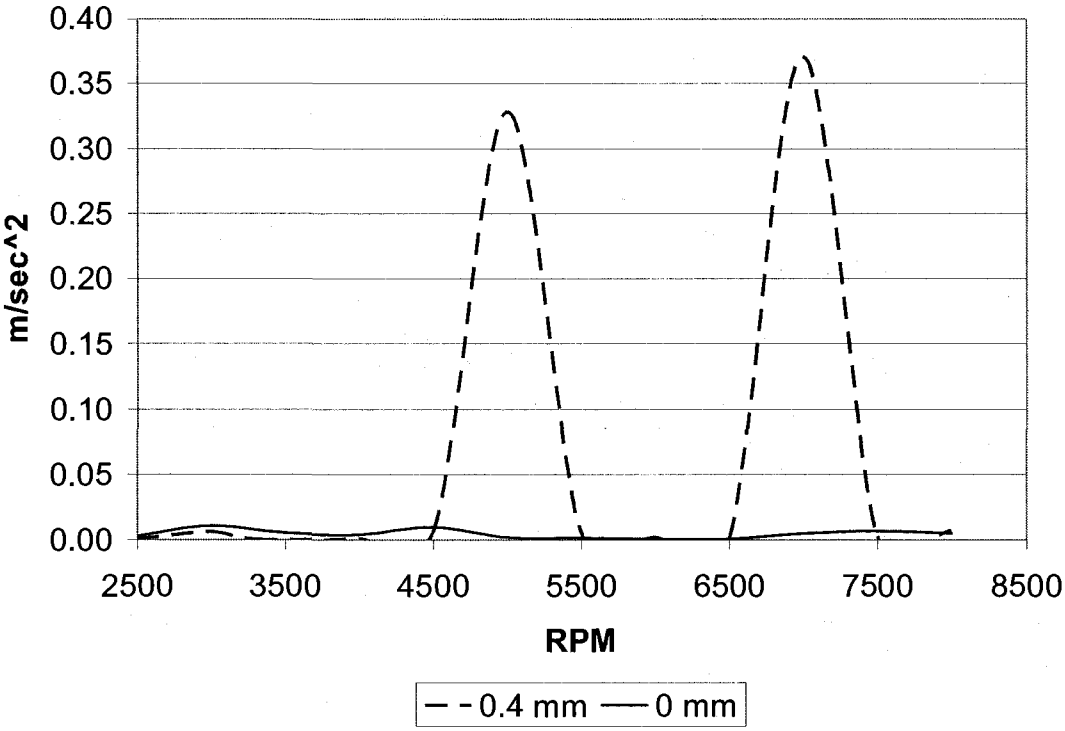

Figure 6-6 Support acceleration response 2x component

It must be admitted that there were several difficulties in performing the experiment due to limitations of the rig. Further increase in the misalignment beyond 0.4 mm was not possible due to locking of the bearings. Speeds beyond 8000 rpm were not possible due to excessive rig vibrations. Interpretation of results was also difficult due to various responses of the rig and its components.

In general, however, when the response of the rotor system which is expected around the rotor system natural frequency is examined closely it yielded reasonably good results that are in agreement with the simulation. It is important to note that comparing the 2x response of the rig at 0.4 mm misalignment with the 2x response of the rig at 0.2 mm misalignment we clearly notice a drastic

change in the response that suggests that nonlinear stiffness variation with misalignment does not seem to be linear. The change of the nonlinear stiffness with the severity of misalignment will need to be further investigated.

6.5 Data Collected from Engines

The researcher having access to real gas turbines engines was able to acquire data from field test. Data from two different types of engine were examined, the first engine is connected directly to the generator as shown in Figure 6-7 and the second type of engine drives the generator via a power turbine and is not directly coupled to the generator as shown in Figure 6-8. Both engines are equipped with accelerometers at the front close to the LPC, at the center close to the combustor and at the rear close to the LPT. The accelerometers are mounted on top of the bearing support as close as possible to the load path.

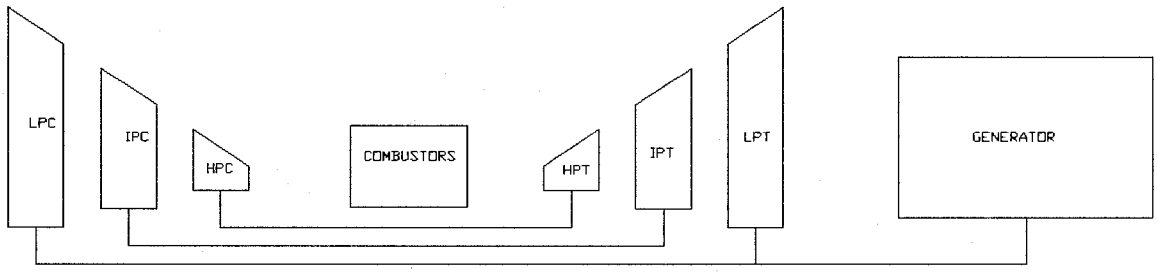

Figure 6-7 Three spool gas turbine connected to a generator

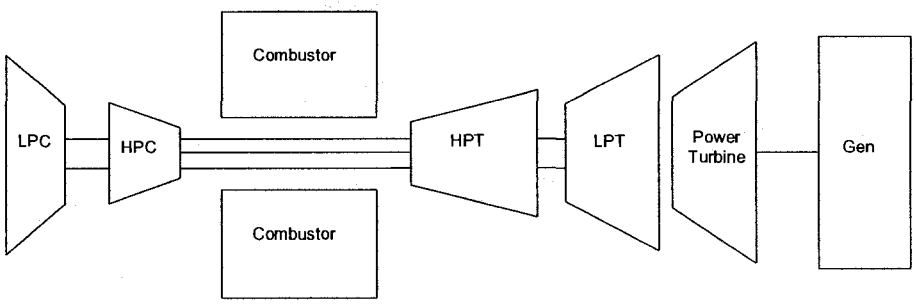

Figure 6-8 Two spool engine layout

6.5.1 Misalignment test

The first engine is a gas turbine that is connected to a generator using a flexible coupling as shown in Figure 6-7. The data presented here was generated from a test conducted to evaluate the sensitivity of a gas turbine to misalignment when connected to a generator using a flexible coupling. The engine is equipped with three accelerometers as standard equipment. These accelerometers are CE132 front, CE132 center and CE132 rear, in addition to these accelerometers and for the purpose of the test four more accelerometer were added to the engine center axial, center radial, rear axial and rear radial. The engine was at first aligned with the generator to ensure that the maximum misalignment is less than 0.3 mrad. The engine was run to maximum power and data from the different accelerometers was collected and stored. The engine was then the misaligned. The maximum misalignment achieved during the second test was 0.87 mrad. It is important to note that in both tests the misalignment were within the limits of the flexible coupling. At no time during this experiment the engine was aligned

beyond the limits of the coupling because such a test could damage the engine. Figure 6-9 and Figure 6-10 show respectively the engine response at baseload for a 0.3 mrad and 0.87 mrad misalignment. The engine shafts that is connected to the generator rotates at a speed of 3000 rpm, the 1x correspond to 50 Hz and the 2x correspond to 100 Hz. Both figures show the data collected from different accelerometers that are positioned at different location on the engine as explained.

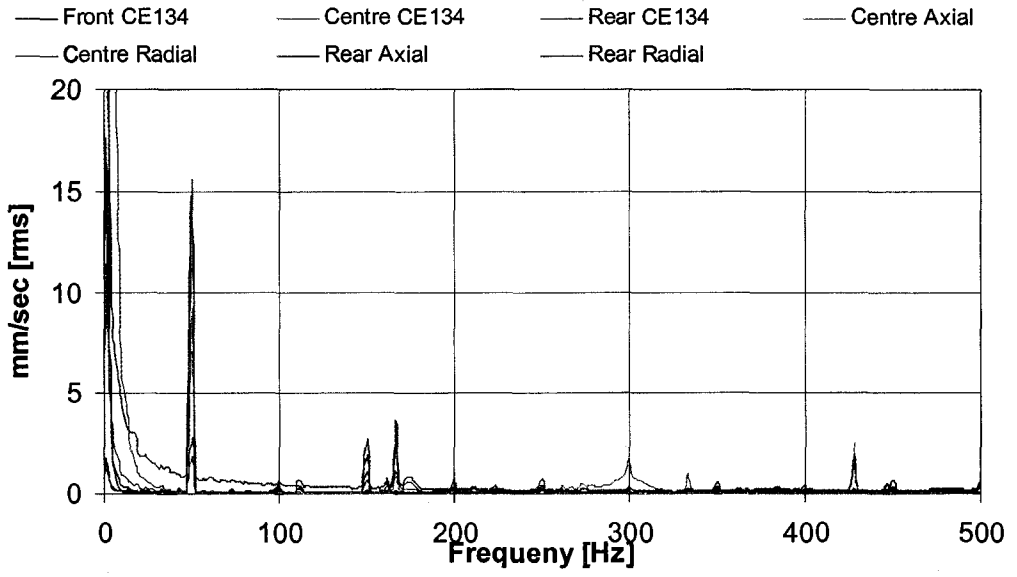

Figure 6-9 Engine accelerometer response for a misalignment of 0.3 mrad

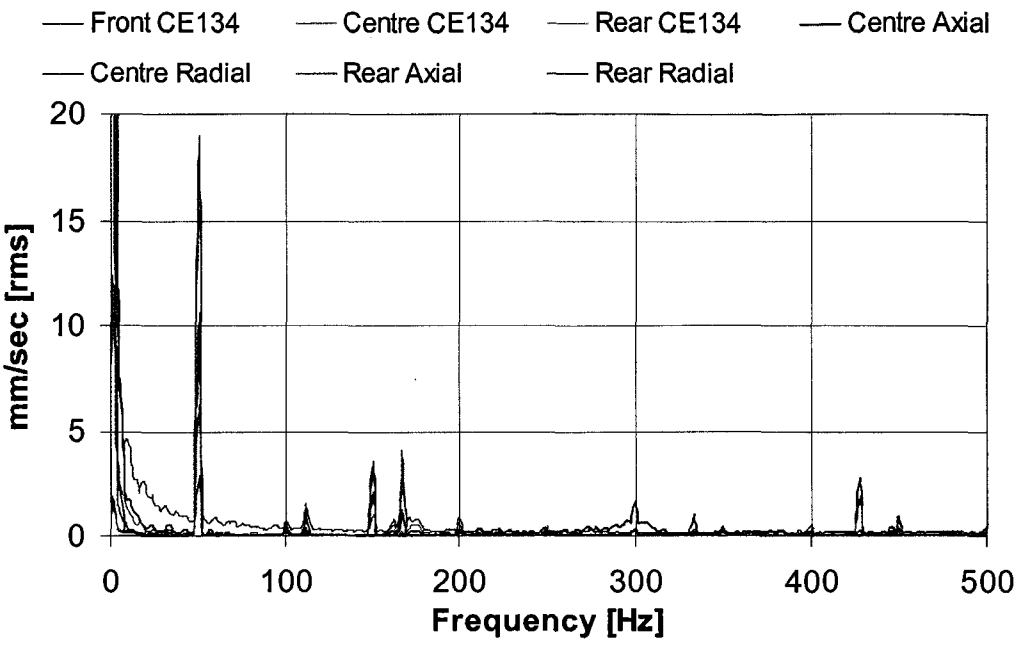

Figure 6-10 Engine accelerometer response for a misalignment of 0.87 mrad

Examining both graphs there is no noticeable change into the engine vibration response due to the misalignment. Data was also collected during engine startup to baseload. Figure 6-11 and Figure 6-12 show the data collected from the CE134 rear production accelerometer. Similarly to the data collected at baseload, the data presented in Figure 6-11 and Figure 6-12 did not show any noticeable change to the engine response.

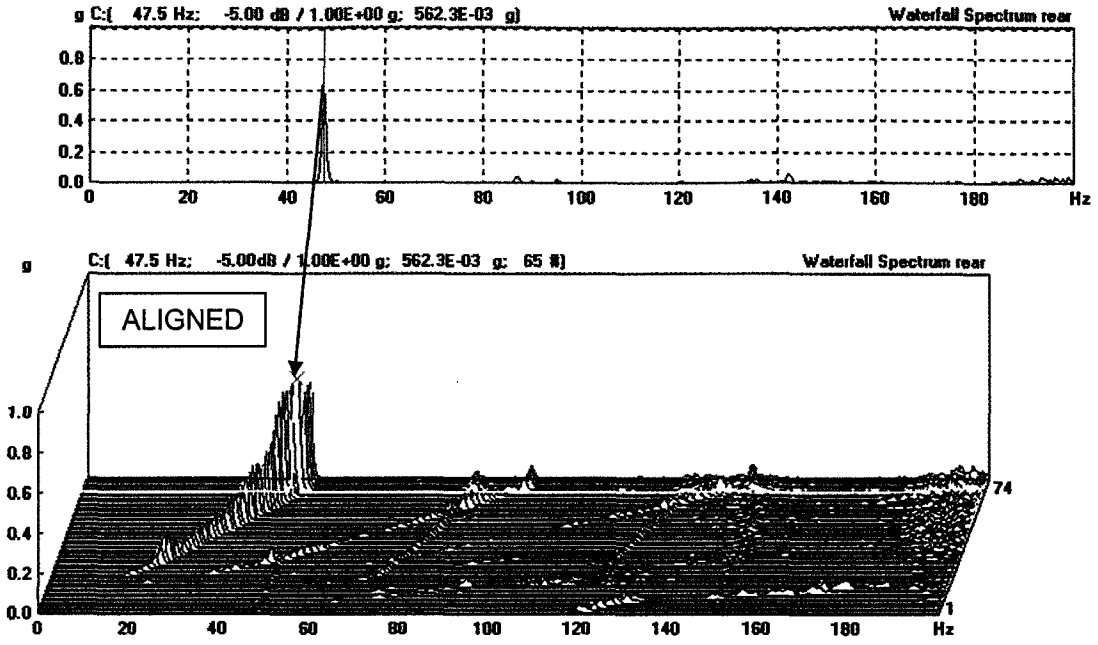

Figure 6-11 Data collected from Rear CE134 accelerometer at 0.3 mrad

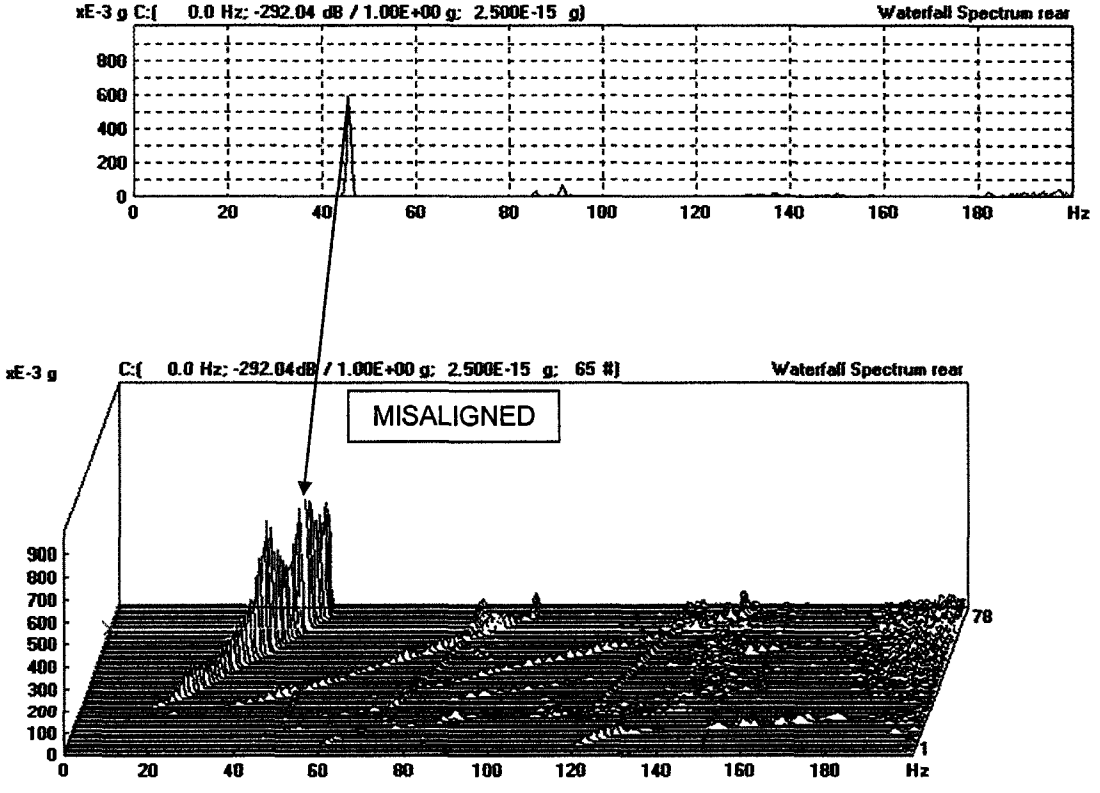

Figure 6-12 Data collected from Rear CE134 accelerometer at 0.87 mrad

One can only notice a very slight change into the 2x component and a very small component of 3x appearing in the misaligned condition, but because the engine and the generator were not misaligned beyond the flexible coupling limits the preload generated in the coupling is so small that it does not affect the nonlinear stiffness of the rotor significantly and hence the vibration response does not change significantly. These results can therefore be considered as those for no misalignment in the rotor system.

6.5.2 Data from Severely Misaligned shafts

Data was collected from two engines that have suffered from severe misalignment. The type of engine in question is a gas turbine that has 2 spools. Figure 6-8 shows the layout of a two spool engine. The low pressure compressor (LPC) is connected to the low pressure turbine (LPT). The high pressure compressor is connected to the high pressure turbine. The combustor takes the compressor air and mixes it with fuel that ignites. The combustion energy is transferred in useful work to rotate the compressors and the turbine. The excess energy is then sent to the power turbine that is connected to a generator. The engine drives a free turbine or a compressor, in the presented data the engine was driving a compressor.

The first engine had suffered an internal fire and was rebuilt and repaired by the owner according to the manufacturer recommendation. The engine was then

recommissioned. The vibration monitoring system on the engine monitors the broad band vibration. During the recommissioning the engine exhibited high vibration above the recommended limits of the manufacturer.

An investigation was launched and more data was collected from the engine. The engine was accelerated to power and stabilized for about 15 minutes. The vibration data was collected from the accelerometer and then integrated and transformed into velocity.

Figure 6-13 shows a plot of the frequency content, the x axis is the frequency in kHz and the y-axis is the vibration data in m/sec zero to peak. The vertical lines numbered 1 to 12 are the rotation orders also known as the engine orders (nX). The rotation of the high speed shaft was 9272 rpm. This corresponds to a 1x of 154.5 Hz. The figure shows clearly the existence of 1x and 2x components. It also shows the harmonics at 3x, 4x, 5x etc. Table 6-2 shows the summary of the engine vibration, the first column of the table shows the engine order, the orders correspond to 1x, 2x up to 12x, the second column present the frequency in Hertz, the third column present the vibration amplitude in m/sec zero to peak, and finally the fourth column present the presentation of the amplitude compared to the 1x amplitude. The table shows that the 2x and 4 x components are larger than 1x components, with the 2x component being 6.3 times larger.

In order to reconfirm the results, the engine was operated again with a different accelerometer and support bracket. Similar results were observed confirming that vibration signal is real. Figure 6-14 shows the vibration signal obtained with a different bracket and accelerometer at a rotation speed of 9335 rpm this corresponds to a 1x of 155.8 Hz.

Table 6-3 shows the summary of the engine vibration and it confirms the existence of 2x and harmonics. The engine was returned for more repairs and the misalignment problem was corrected upon which the engine went back to service and the vibration signal was normal.

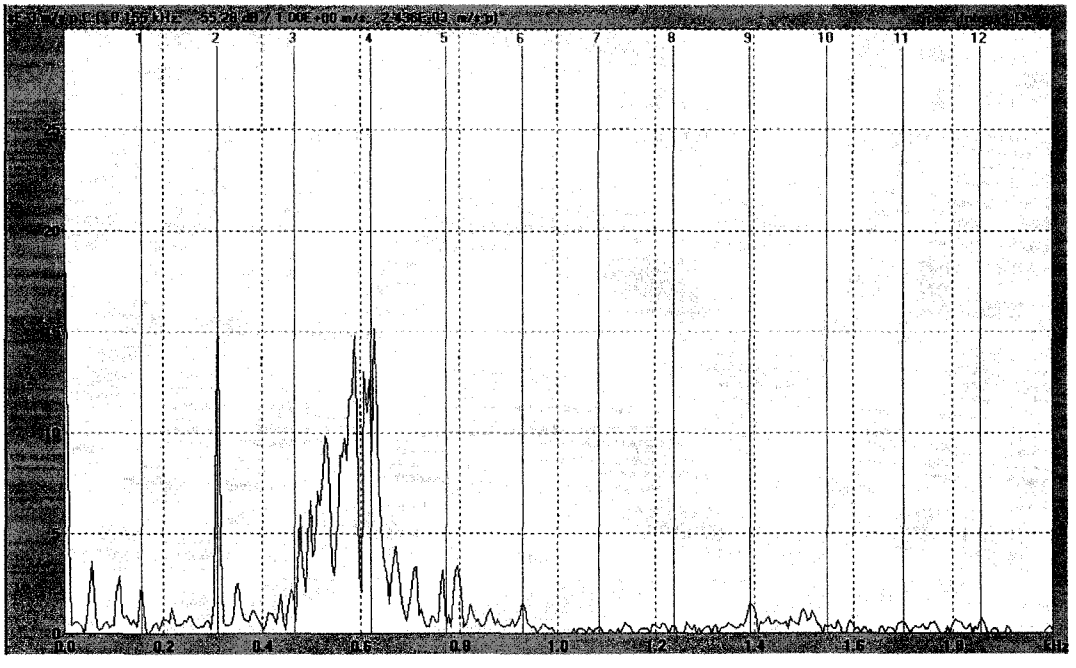

Figure 6-13 Engine vibration at a rotation speed of 9272 rpm

Table 6-2 Summary of engine vibration data

Engine orders	Frequency (Hz)	Vib. (m/sec) 0-Pk	% of 1 EO
1	154.5	2.447E-3	100
2	309.1	15.50E-3	633.43
3	463.6	646.7E-6	26.43
4	618.1	9.051E-3	369.88
5	772.7	896.8E-6	36.65
6	927.2	1.651E-3	67.47
7	1081.7	304.6E-6	12.45
8	1236.2	316.4E-6	12.93
9	1390.8	1.483E-3	60.60
10	1545.3	295.3E-6	12.07
11	1699.8	536.1E-6	21.91
12	1854.4	787.4E-6	32.18

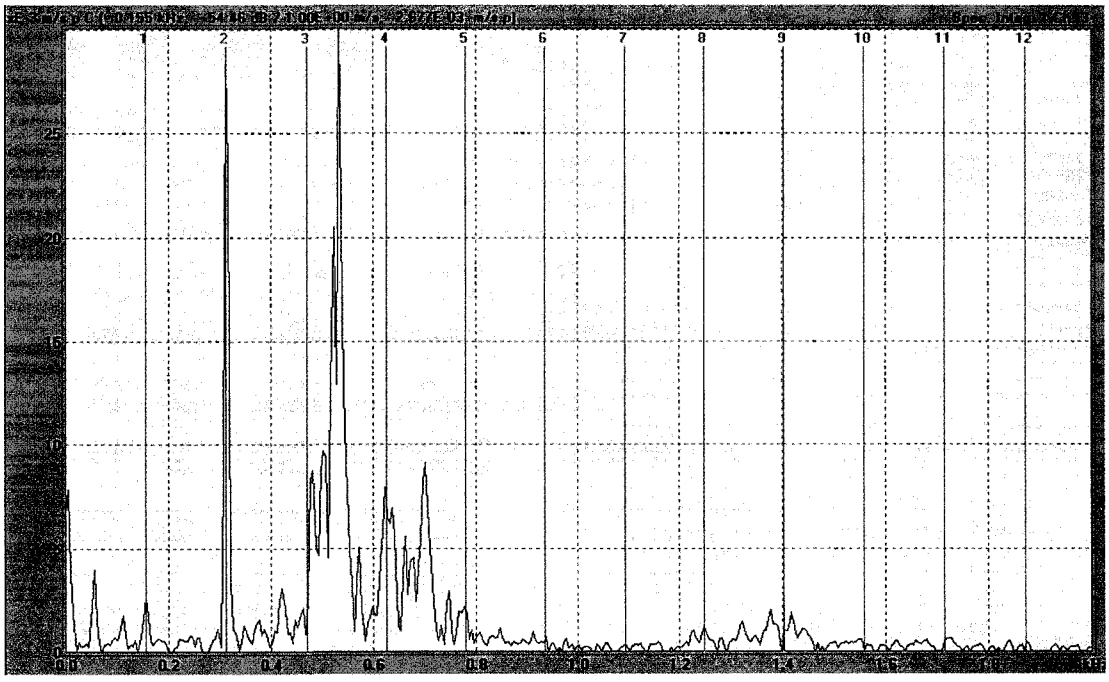

Figure 6-14 Engine vibration at a rotation speed of 9353 rpm.

Table 6-3 Summary of engine vibration data with new accelerometer

Engine orders	Frequency (Hz)	Vib. (m/sec) 0-Pk	% of 1 EO
1	155.8	2.718E-3	100
2	311.6	30.74E-3	999.99
3	467.3	847.6E-6	31.18
4	623.1	6.512E-3	239.59
5	778.9	1.819E-3	66.92
6	934.7	674.9E-6	24.83
7	1090.5	353.8E-6	13.02
8	1246.2	1.241E-3	45.66
9	1402.0	1.092E-3	40.18
10	1557.8	316.7E-6	11.65
11	1713.6	620.5E-6	22.83
12	1869.4	458.9E-6	16.88

The second engine had suffered gradual misalignment over its life period. This engine has undergone several overhauls over the span of its life and stored for a period of time without operation. When the engine was put back into service, it exhibited higher than normal vibration mainly harmonics with high first and second order, with smaller vibration at higher harmonics. Figure 6-15 shows a snapshot of the vibration after 10 minutes stabilization. The shaft was rotating at 9600 rpm. The first order frequency is hence 160 Hz. The snapshot shows clearly the first and second order. It also shows the existence of harmonics. Table 6-4 shows a summary of the vibration shown in figure above. It shows that the second engine order (2x) has a value that is 65.24% of the first engine order. This is clearly an indication of misalignment. Because the monitored vibration did

not exceed the manufacturer recommendation, this engine was accepted as is and the customer continued running the engine.

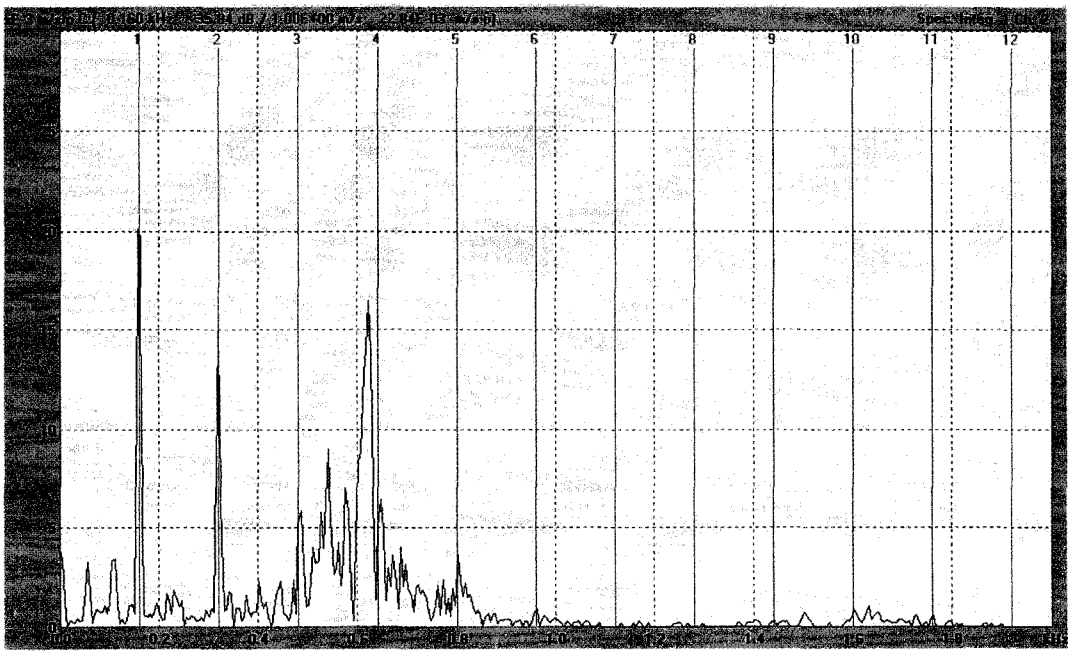

Figure 6-15 Engine vibration at a rotation speed of 9600 rpm.

In the presence of misalignment a consistency is identified from simulation, simple rig test and field test of highly complex rotor system. In brief it can be summarized as having significant influence on the 2x response of the rotor system while some effect on the 1x response. It is found that the 2x component of response invariably increases with misalignment and the increase is a function of the magnitude of misalignment.

Table 6-4 Summary of vibration from engine data

Engine orders	Frequency (Hz)	Vib. (m/sec) 0-Pk	% of 1 EO
1	159.8	22.84E-3	100
2	319.7	14.9E-3	65.24
3	479.5	5.22E-3	22.89
4	639.4	4.98E-3	21.80
5	799.2	3.713E-3	16.26
6	959.1	1.027E-3	4.50
7	1118.9	38.74E-6	0.17
8	1278.7	144.0E-6	0.63
9	1438.6	303.5E-6	1.33
10	1598.4	927.3E-6	4.06
11	1758.3	605.6E-6	2.65
12	1918.1	46.85E-6	0.21

6.6 Summary

In this chapter a comparison between the results of the simulation and the rig was presented. The simulation predicted a change in the 1 x component and an increase of the 2 x component. The rig produced similar results where the 1x response over the rig test changed in value either by increasing or decreasing due to misalignment and the 2 x component increased. In general the simulation and the rig show that:

1) Misalignment alters the 1x response,
2) Misalignment in general increases in the 2x response,

3) The existence of higher harmonics.

Data from real engines was also presented showing that misalignment produces higher harmonics and a significant increase in the 2x component. The increase in the 2x component was closely linked to the severity of misalignment. It is therefore concluded that the response predicted by simulation of simple rotor system with misalignment developed for this investigation could be effectively used to develop and train an expert system for identification of misalignment in a complex rotor system such as a gas turbine engine.

Chapter 7

7 Neurocomputing and Neural Network

7.1 Introduction

As discussed in chapter 1, Neurocomputing and Neural Network (N.N.) is an attempt in emulation of the human brain at a very basic level. Like the human brain, N.N. is formed of a number of interconnected artificial neurons, where each neuron has an input, processing and output areas. The technology for N.N. has been around for some time, but its application is being explored only over the last few years. This is made possible with the advancement of computers with fast and parallel processing capabilities. Neurocomputing and N.N. has been defined by experts as follows:

Neurocomputing: "is the technological discipline concerned with information processing systems that autonomously develop operational capabilities in adaptive response to an information environment" [41]

Neural Network: "is a parallel, distributed information processing structure consisting of processing elements interconnected via unidirectional signal channels called connections." [41]

Neurocomputing by itself is a subject of research extensively investigated by computer scientists, and is not within the scope of the present investigation. Several version of the N.N. technology has been developed as a tool, and applied

to a wide range of applications including pattern recognition, control classification, diagnostics, automation, system dynamics, etc.

The application of N.N. in the development of an expert system has been carried out by few researchers only in the very recent years as discussed in the literature review. The objective here is to apply an appropriate N.N. to develop an expert system to differentiate between unbalance and misalignment. As discussed in the literature review, there are many types of N.N. that are suitable for specific types of applications. In selecting a N.N. various aspects that must be considered include:

- Types of N.N. and their possible applications.
- Types of learning rules for the N.N.
- Transfer functions that can be used in the network.
- Various N.N. parameters and their selection.
- The procedure and steps used in building a N.N.

Each of these aspects are discussed in the following subsections in relation to the present application of N.N.

7.2 Types of N.N. and their Application

As discussed in the literature review, different types of N.N. have been developed over the years. Some books [40, 41, 42] have been published in the recent years with detailed introduction to various types of N.N. and their possible applications. Some of the well known N.N. includes:

Adaline and Madaline: has gained application in adaptive signal processing. It is a N.N. that can be implemented as filters to perform noise removal from information-bearing signals.

Adaptive Resonance Theory (ART): Has application in problems requiring clustering and pattern recognition.

Back-propagation: has application in problems requiring recognition of complex patterns and performing non-trivial mapping. It is a network that adapts itself to "learn" the relationship between a set of examples patterns, and able to apply the same relationship to a new input pattern. Back-propagation network, therefore, has potential application in pattern recognition, and expert systems.

General regression network: is a general purpose network. It gained applications in system modelling and prediction.

Modular neural network: is a generalization of back-propagation neural network. It is applied to system modelling, prediction, classification and filtering.

Among various N.N. developed to date, back-propagation network (BPN) has been used in a wide range of applications. It can be used in addressing problems requiring recognition of complex patterns and performing non-trivial mapping function, dynamic system modelling, control and optimization. This network has been demonstrated to be most successful in system modelling, control, and pattern recognition [41]. In basic terms a BPN can be trained through a set of input-output relationship to develop artificial intelligence. An adequately trained BPN can then be used to make prediction of the network output by providing the network input.

For the application of N.N. to the development of an expert system in this investigation BPN and a modified Logicon Projection, a network that combines the

advantages of an open boundary network such as ART and closed boundary network such as BPN, are selected. The rest of this chapter is devoted to description of BPN; selection of learning rule, transfer function and parameters for its use; and a flow chart for the BPN algorithm as well as a description of logicon projection is presented.

7.3 Back Propagation Network (BPN)

Back-propagation network (BPN), formalized by Werbos [76], and later by Parker [77], Rumelhart and McClelland [78], operate as a multi layer feed forward network using supervised learning. A detailed discussion of BPN and its architecture is not discussed here and is available in references [40, 41, 42].

The network architecture is formed of a number of layers the first one is the input layer, the last one is the output layer and the ones between them are called intermediate layers. Figure 7-1 shows a BPN formed of an input layer, two intermediate layers and an output layer. Each node of the network has a variable weight, and there is a predefined transfer function between nodes. In general terms, after an input pattern with known output is applied to the first layer of the network, it is then propagated through each upper layer until the network output is generated.

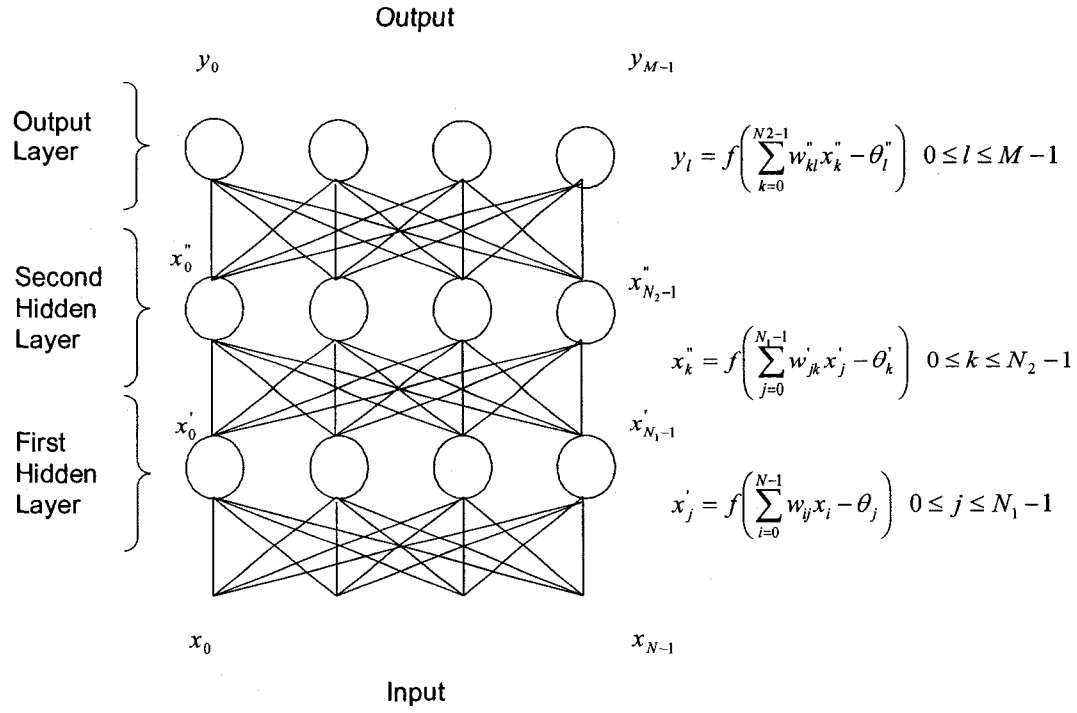

Figure 7-1 A Four layer BPN

The process of propagation through each layer is also shown in figure 7-1, where x is the input to the network, x' and x'' are the outputs of the first and second layers, and y is the network output. Here f represents the transfer function, where w is the weight and θ represents noise. The network output is compared to the desired known output and the mean square error is calculated for each output unit. The error is then transmitted backward to each node of intermediate layers that contribute directly to the output. The process is repeated and the internal values (weights) of the network are updated until a reasonable error is achieved.

After training, when presented with an arbitrary input pattern the network should be able to calculate the correct output. It must be noted, that trained network can not work properly if the relation between the arbitrary input and the required output is not similar to what it learned. Also sometimes a N.N. would not learn and minimize the error without any apparent reason [41].

In the implementation of the BPN, one should choose two major specification of the network. These specifications are the learning rule and the transfer function. The following subsections discuss each one of them briefly.

7.3.1 N.N. Learning Rules

The N.N. learning rules are used to adjust the weights and biases of the N.N. that minimizes the error between the network output and the desired output during training. There are several learning rules available [40, 79] that can be applied. Some of them include:

1. delta rule,
2. normal cumulative,
3. extended delta-bar-delta,
4. delta-bar-delta,

One of the difficulties in using a N.N. is that their behaviour is not very well understood. In practice, the learning rule is selected based on trial, where the

rule that leads to lowest error is used. For the present application, delta rule and normal cumulative were found to be most efficient.

7.3.1.1 Delta Learning Rule

The BPN error in the output layer is calculated as the difference between the desired output and the network output. This error, transformed by the derivative of the transfer function is back-propagated to prior layers where it is accumulated. This back-propagated and transformed error becomes the error term for that prior layer. The process of back-propagating the errors continues until the first layer is reached. The Delta learning rule changes the weights of the network by multiplying the error at each weight by the learning coefficient. The difference between the current weight and the previous weight is multiplied by a momentum to accelerate the minimization of the error. The following equation illustrates how the delta rule updates the weights of the BPN:

$$w(t+1) = w(t) + \alpha\,\delta\,x_i' + \gamma(w(t) - w(t-1)) \qquad 7\text{-}1$$

where $w(t+1)$ is the updated weight, $w(t)$ is the current weight, $w(t-1)$ is the previous weight, α is the learning coefficient, δ is the error, x_i' is the input to that connection and γ is the momentum.

7.3.1.2 Normal Cumulative Learning Rule

The normal cumulative learning rule is similar to the delta rule, the only difference is that instead of updating the weight for every set of data presented, the user specifies a number of presentation (Epoch) after which the weights are updated. The weights are updated in two phases:

1) at each data presentation:

$$m(t+1) = m(t) + \alpha\, \delta\, x_i' \qquad 7\text{-}2$$

where $m(t+1)$ is the updated dummy weight, $m(t)$ is the current weight, α is the learning coefficient, δ is the error and x_i' is the input to that connection.

2) after a certain number of presentation when the epoch number is reached,

$$\begin{aligned} w(t+1) &= w(t) + m(t) + \gamma\, a(t) \\ a(t) &= m(t) \\ m(t+1) &= 0 \end{aligned} \qquad 7\text{-}3$$

Where γ is the momentum and $a(t)$ is the dummy load at the beginning of the cycle.

7.3.2 Types of Transfer Functions

The transfer function is the function that relates the neuron output to the net output. Figure 7-2 shows the location of a transfer function in a N.N., from the figure, the neuron output x is defined as [79]:

$$x = \sum_{i=0}^{N-1} w_i x_i - \theta \qquad 7\text{-}4$$

Where w_i is the weight, x_i is the input, and θ is an offset or a noise function. The transfer function is applied to the neuron output and the network output is:

$$y = transf(x) = transf\left(\sum_{i=0}^{N-1} w_i x_i - \theta\right) \qquad 7\text{-}5$$

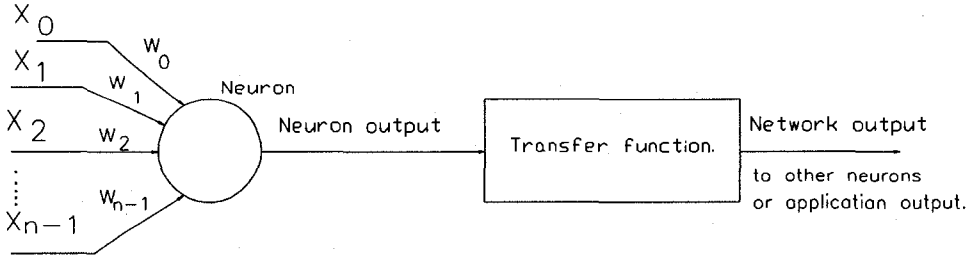

Figure 7-2 Transfer function location in a NN.

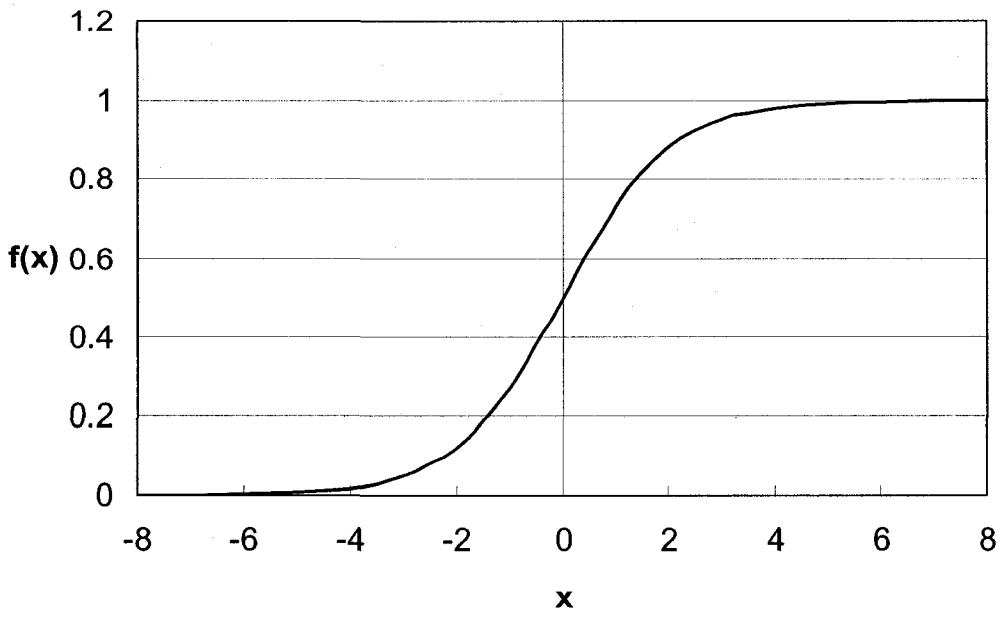

Figure 7-3 Sigmoid function

BPN is based on continuous change of the biases and weights of the network in the direction of steepest descent with respect to the error. It therefore requires a function with continuous differentiable non-linearity.

Different transfer functions can be used [40, 41], some of which include: linear transfer function, Sigmoid transfer function, step transfer function, tanh transfer function, etc. Although any continuous differentiable non-linear function can be used, Sigmoid transfer function is found to give, the best results in the present application. The sigmoid transfer function is a 'S' shaped continuous differentiable function shown in Figure 7-3, which can be expressed as:

$$f(x) = \frac{1}{1+e^{-x}} \qquad 7\text{-}6$$

The step transfer function shown in Figure 7-4, yields an output from the neuron that is equal to 0 or to 1 depending on the neuron input. It can be expressed as:

$$f(x) = 0 \text{ for } x < 0$$
$$f(x) = 1 \text{ for } x \geq 0 \qquad 7\text{-}7$$

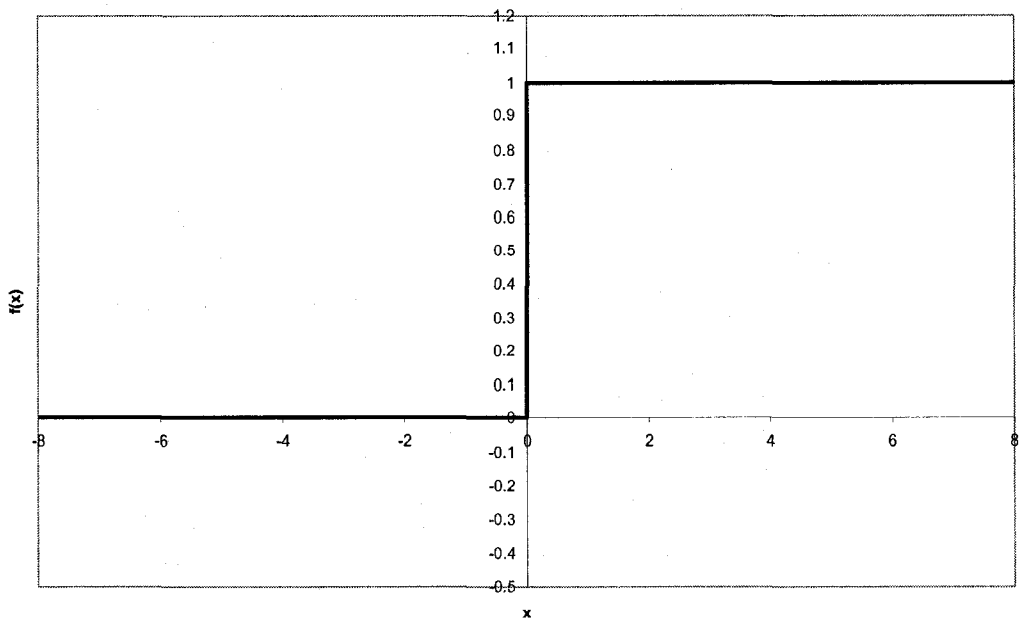

Figure 7-4 Step transfer function

7.4 The BPN Parameters

As expressed in equation 7-1, there are two main parameters required to operate the N.N., they are the learning coefficient α, and the momentum γ.

The learning coefficient α, controls the rate at which the error modifies the weights. If the value of the learning rate is too high, the network can become unstable. On the other hand, if the rate is too low, an extremely long training

period is required. The value of the learning coefficient between 0 and 1 is best selected by trial to achieve fast learning of stable network [40].

The other parameter, momentum γ, is a factor that dictates the speed of error minimization. This allows the network to respond not only to the local gradient but also to recent trend in error minimization. The momentum parameter is also selected by trial to achieve satisfying performance of the network [40].

7.5 BPN Algorithm and Flow Chart

The back-propagation N.N. learns by propagating the error between the N.N. output and the desired output. The propagated error is used to modify the weights; the rate by which the weights are modified depends on the learning coefficient and the momentum.

The method by which the back-propagation N.N. works is shown in the flow chart Figure 7-5 and the following steps. (The learning rule and the transfer function in the following steps are respectively the delta rule and Sigmoid).

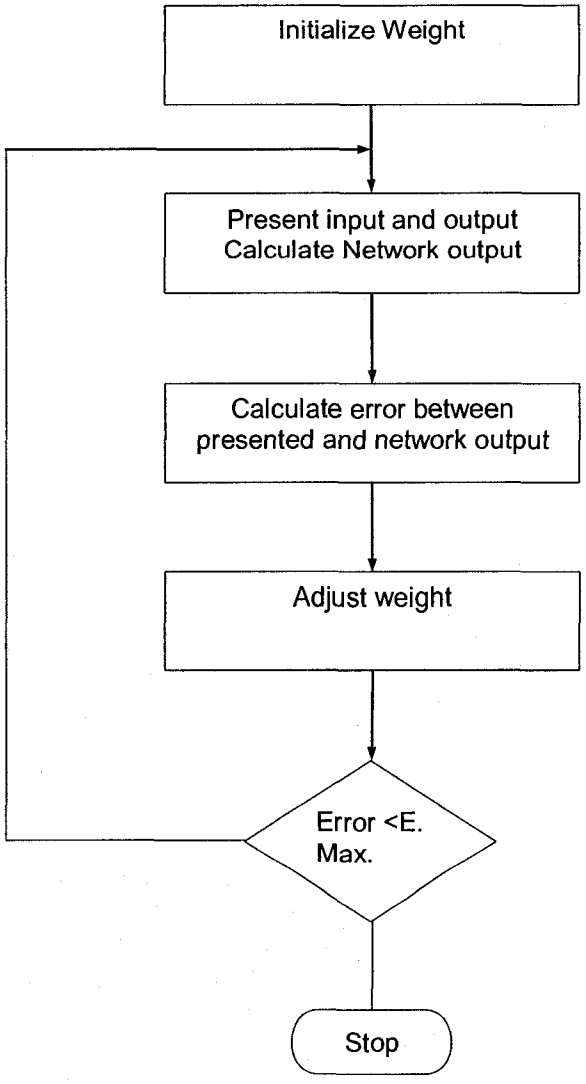

Figure 7-5 BPN Flow Chart

STEP 1: Specify the number of inputs, outputs, nodes (layers) and number of neuron per layer, Figure 7-1.

STEP 2: Initialize the weights and offsets,

STEP 3: Present inputs $x_0, x_1, ...x_{N-1}$ and desired outputs $d_0, d_1, ...d_{N-1}$ to the N.N.,

STEP 4: Calculate the error between the N.N. output $y_0, y_1, ...y_{N-1}$ and the desired output. The N.N. output is calculated by summing the weights at each

node then the transfer function is used to transfer the summation to the next node if there is any, or to get the N.N. output.

STEP 5: Back-propagate the error to all the nodes and neurons. The weights are updated using the calculated error, the learning coefficient and the momentum,

$$w(t+1) = w(t) + \alpha\, \delta_j\, x_i' \qquad 7\text{-}8$$

where $w(t+1)$ is the updated weight, $w(t)$ is the initial weight from hidden node i or from an input to node j, α is the learning rate, δ_j is an error term of node j and x_i' is either the output of node i or is an input. If node j is an output node, then

$$\delta_j = y_j(1-y_j)(d_j - y_j) \qquad 7\text{-}9$$

where d_j is the desired output of node j and y_j is the actual output. (N.N. output)

If node j is an internal hidden node, then

$$\delta_j = x_j'(1-x_j')\sum_k \delta_k w_{jk} \qquad 7\text{-}10$$

where k is over all nodes in the layer above node j. Convergence is sometimes faster if a momentum γ term is added and weights are smoothened by:

$$w(t+1) = w(t) + \alpha\, \delta_j\, x_i + \gamma(w(t) - w(t-1)) \qquad 7\text{-}11$$

where

$$0 < \gamma < 1$$

and $w(t-1)$ is the previous weight.

STEP 6: Repeat the steps from 3 to 5 until the error calculated is acceptable.

7.6 Logicon Projection Algorithm

The logicon projection algorithm was developed by Wilensky and Manukian [80] to improve the performance of the back propagation network. The logicon projection algorithm combines the advantages of a closed boundary network such as ART and the advantages of an open boundary network like BPN. The network has many advantages, it is faster than BPN, it initializes the weights and thresholds to prototype of the input set, it partitions the input space which allows easy separation of inputs into different classes.

The logicon projection projects the N dimensional input vector $\mathbf{x}$ into an $N+1$ dimensional input vector $\mathbf{x}'$. The projected inputs $\mathbf{x}'$ serve as the input to a feedforward neural network. The projection of the N dimensional vector into the $N+1$ dimensional vector can be expressed as [80]:

$$x_k' = R\left(\frac{2x_k / R_0}{1+\left(|\mathbf{x}|/R_0\right)^2}\right) \qquad 7\text{-}12$$

and the extra term is expressed as:

$$x_{extra}' = -\left(\frac{1-\left(|\mathbf{x}|/R_0\right)^2}{1+\left(|\mathbf{x}|/R_0\right)^2}\right) \qquad 7\text{-}13$$

where R_0 is the radius of the inner sphere onto which the original input vectors are projected form the north pole as shown in Figure 7-6.

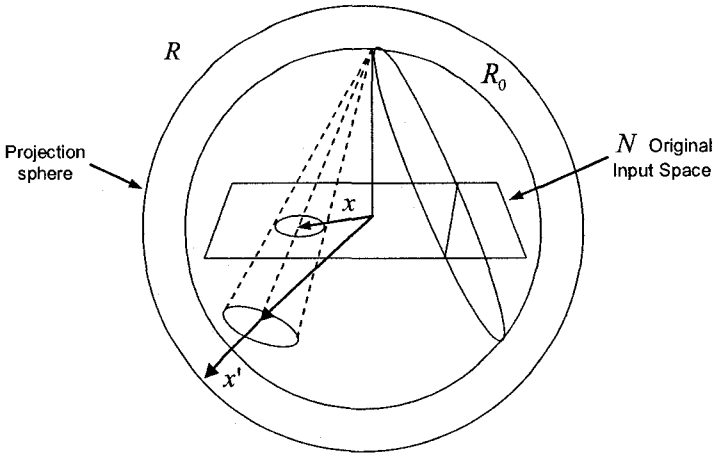

Figure 7-6 Logicon projection transformation

R is the overall scaling of the input vector and is the radius of the outer sphere and the projected vector x' is subjected to the following constraint:

$$|x'| = R \qquad 7\text{-}14$$

Since x' is an $N+1$ dimensional vector, the weight vector w' that connects it to any node to the first hidden layer must also be an $N+1$ dimensional vector and it is also forced to lie on the $N+1$-dimensional hypersphere so that its magnitude is always equal to the radius R:

$$|w'| = |x'| = R \qquad 7\text{-}15$$

The x' vector and the weight w' are then used as an input to feedforward network.

7.7 The Logicon Projection Parameters

Logicon projection as described in section 7.6 projects the input from a N dimensional vector to a $N+1$ dimensional vector. The projected vector is then passed to a feedforward network like BPN. Hence all the parameters that are used in BPN are still used for a Logicon projection network; in addition the projection sphere radius R and the inner sphere radius R_0 are required for a Logicon projection network to be built.

The sphere radius R is an overall multiplicative constant of the inputs. A large R may be useful for constructing tight sharp prototypes with small regions of influence in an area where the output varies rapidly and requires many prototypes. It was found that [81]:

$$R = 7.0 \qquad \text{7-16}$$

would yield good results. If a larger value of R is required it can be scaled with the typical prototype radius:

$$R = \frac{1}{a_p} \qquad \text{7-17}$$

where a_p, is the typical prototype radius in the original scaled but not projected input space. Equation 7-17 can yield a large value for R. Since R is used to set up the initial weights as defined in equation 7-15, the result could be large weights and the network might not achieve proper learning. It is therefore advisable to trade the sharpness of the prototypes for learning speed. In such case R can be scaled as the square root of the radius:

$$R = \frac{1}{\sqrt{a_p}} \qquad 7\text{-}18$$

The inner radius R_0 must be set so that the input vector can be projected onto a reasonable portion of the hypersphere in one higher dimension and separation of the input classes can be performed. It was found that the following equation yielded good results [81]:

$$R_0 = \sqrt{N} \qquad 7\text{-}19$$

where N is the input dimension. Generally it is best to set R_0 to be greater than each component of every input point:

$$R_0 > x_i \qquad 7\text{-}20$$

For all i and all $\mathbf{x}$.

7.8 Steps in Building a N.N.

The way to build a N.N. could be stated in the following steps:

1. Determine the problem type the inputs and the outputs that will be given to the N.N. to learn. It is important that the inputs and outputs be related.
2. Construct a data training file and a testing file, the training file could be used as a testing file. Be sure not to have similar inputs with different outputs or vice versa.
3. Determine the purpose of building the N.N. For this research the N.N. was needed for creating a network that can identify between three different

patterns, no fault, unbalance, and misalignment i.e. perform pattern recognition, this helped to determine that back-propagation N.N. and logicon projection are the most suitable for this problem.

4. Determine the number of neuron needed, the input and output neurons are equal to the number of inputs and outputs of the problem. The number of neuron and the number of layers are chosen by trial and error.
5. Determine a learning rule that will update the weights of the N.N., and achieve learning. For the N.N. the choice of the learning rule is done by trial.
6. Determine the most suitable transfer function.
7. Determine the N.N. parameters by trial.
8. Start the learning process and test the N.N. if error is acceptable the training is over if not change parameters and restart training until reaching the minimum error.
9. The trained N.N. can now be used for the needed application.

7.9 Summary

This chapter primarily presented the N.N., specially the BPN and Logicon projection. The chapter gave a general idea about the N.N. and the parameters which are essential in building a BPN and a Logicon projection network. The learning rules used in the research were explained. The transfer functions were explained and the Sigmoid and step transfer functions were formulated. The

BPN algorithm and Logicon projection were explained in detail. The steps to build a N.N. application were explained in a simple manner. The N.N. will be applied to create an expert system and evaluate the performance of the expert system using data from simulation and real engine date.

Chapter 8

8 Development of a N.N. to Identify Unbalance and Misalignment

8.1 Introduction

Typical rotating machinery will exhibit problems that result in excessive vibration. If left unaddressed the result is often very expensive repair. Most of the vibration problems in a rotating machine results from unbalance and misalignment as shown in Table 8-1. The instrumentation, used in most rotating machinery, is used to detect a sudden and excessive change in the vibration signature and shutdown the machine safely. The main problem with this type of protection is that it does not identify the problem that causes the vibration and often results in days of investigation to identify the reason for the vibration.

In this chapter an expert system is developed using N.N. to identify unbalance and misalignment. Both those defects represent 70% of defects seen in the field [82]. The methodology developed in this chapter can be extended to the detection of other failures.

Two tools are considered in the developing of the N.N. The first is Matlab and the second is Neural Ware. The tool of choice for the development of the N.N. is Neural Ware because of its flexibility and capabilities. Then, two types of N.N. were considered. The first is Back Propagation Network (BPN) and the second is

a Logicon Projection Network (LPN). The Networks developed are tested using simulation data and the engine data.

Table 8-1 Typical vibration problems and their approximate percentage of occurrence [82].

Typical Vibration problems	**Approximate percentage of occurrence**
Unbalance	40
Misalignment (on Coupled Machines)	30
Resonance	20
Belts and pulleys	30
Bearings	10
Motor vibrations	8
Cavitation in pumps	2
Fan and duct turbulence	5
Oil whirl	2
Sympathetic vibrations	3
Gears	2
False brinnelling	3
Piping	3
Bent shaft/bowed rotor	3
Looseness	5
Soft foot	5
Beats	2
Torsional vibrations	2
Vane passing	3

8.2 Detection Logic

From the simulation carried on chapter 4 and the data presented in chapter 5 it was shown that:

1. Unbalance will result in an increase in the 1x vibration component.
2. Misalignment will result in an increase in the 2x vibration component and the existence of harmonics.

Since all rotating machinery will have an inherent unbalance and misalignment due to machining imperfection, errors in the balancing, and accuracy of machining, it is expected that all rotating machinery will have a certain level of 1x and a 2x vibration. If this vibration is above a certain level it can cause damage to the mechanical equipment and it mainly results in shorter bearing life or under extreme condition it can cause component premature failure.

The following parameters are defined:

1. A_{Th_ω} is the threshold amplitude at 1x determined based on machine type and specs (Each machine will have a pre-determined amplitude that is an acceptable limit of operation) at the frequency that corresponds to the engine rotating speed.
2. $A_{Th_{2\omega}}$ is the threshold amplitude at 2x determined based on machinery type and specs.

3. A_{ω} is the measured amplitude at the frequency that corresponds to the engine rotating speed.
4. $A_{2\omega}$ is the measured amplitude at the frequency that corresponds to 2 times the rotating speed.

An unbalance fault exists if the first dimensionless amplitude ratio at 1x is:

$$\frac{A_{\omega}}{A_{Th\omega}} > 1 \qquad 8\text{-}1$$

And a misalignment fault exists if the second dimensionless amplitude ratio at 2x is:

$$\frac{A_{2\omega}}{A_{Th_{2\omega}}} > 1 \qquad 8\text{-}2$$

In case the above 2 conditions are not met there is no fault.

8.3 Neural Network Development

There are different methods to create N.N., for example, a code in C++, FORTRAN or any other language can be used. There are also tools that can create N.N. like Matlab or Neural Works. In this thesis two tools are considered, the first is Matlab and the second is Neural Works.

An attempt was made to use NN in Matlab. The NN in Matlab was not user friendly and did not have the flexibility found in Neural Works. For example, the data files in Neural Works are simple ASCII files and each row contains

consecutively the input followed by the output in a vector form. NN in Matlab requires a matrix for the input and a matrix for the output.

It is preferable to have a learning coefficient that will change over the training process to allow for quick adaptation of weights at the beginning of the learning process. As the learning process progresses and the error between the N.N. output and the given output reduces, it is desirable that the learning coefficient reduces so that the N.N. does not overshoot to a local minima. The learning rate in Matlab is fixed during the learning process, this could be changed but requires special functions, while in Neural Works the learning rate will change based on a gradient coefficient and the number of training iterations. The learning rate will change so that it reduces after a certain number of training sets. This is done through the graphical user interface. In Neural Works the connection between neurons can be altered and modified, different learning rules can be used between layers, in general it was found that Neural Ware offers more flexibility compared to Matlab, it was therefore chosen for this application.

8.3.1 Neural Network Development

Two types of N.N are studied and developed using Neural Ware, the first is a back propagation N.N., and the second is a Logicon projection N.N. Both N.N. are trained using the same training data set and evaluated with the same data. The data is created using the simulation presented in chapter 4.

The data used for training the NN is created using the following step:

1) Establish a threshold value: A threshold value for 1x and 2x was chosen. The curves defining the 1x threshold and 2x threshold are shown in Figure 8-1 and Figure 8-2 consecutively. The two figures represent a shaft response with a misalignment of 0.8E-3 m, a mass offset of 0.09E-3 m and a dynamic unbalance of 0.3 radian.
2) The simulation is run at different conditions for unbalance and misalignment.
3) An FFT is performed on the time domain data, the rotation speed is known from the simulation. If real data is used the rotation speed will be known from the rotation speed sensor.
4) A filtering code is created to extract from the FFT 3 amplitudes close to the 1x rotation speed and 3 amplitudes close to the 2x rotation speed.
5) The extracted data is then compared to the threshold value as defined in equations 8-1 and 8-2.
6) Knowing for each simulation the condition at which the shaft is running (perfectly aligned, unbalance, and/or misalignment) the output 3x1 vector is created as follows:

$$\text{No Fault} = \begin{bmatrix} 1 \\ 0 \\ 0 \end{bmatrix} \qquad 8\text{-}3$$

$$\text{Unblanace} = \begin{bmatrix} 0 \\ 1 \\ 0 \end{bmatrix} \quad \text{8-4}$$

$$\text{Misalignment} = \begin{bmatrix} 0 \\ 0 \\ 1 \end{bmatrix} \quad \text{8-5}$$

7) The created data is then presented to different NN for training.

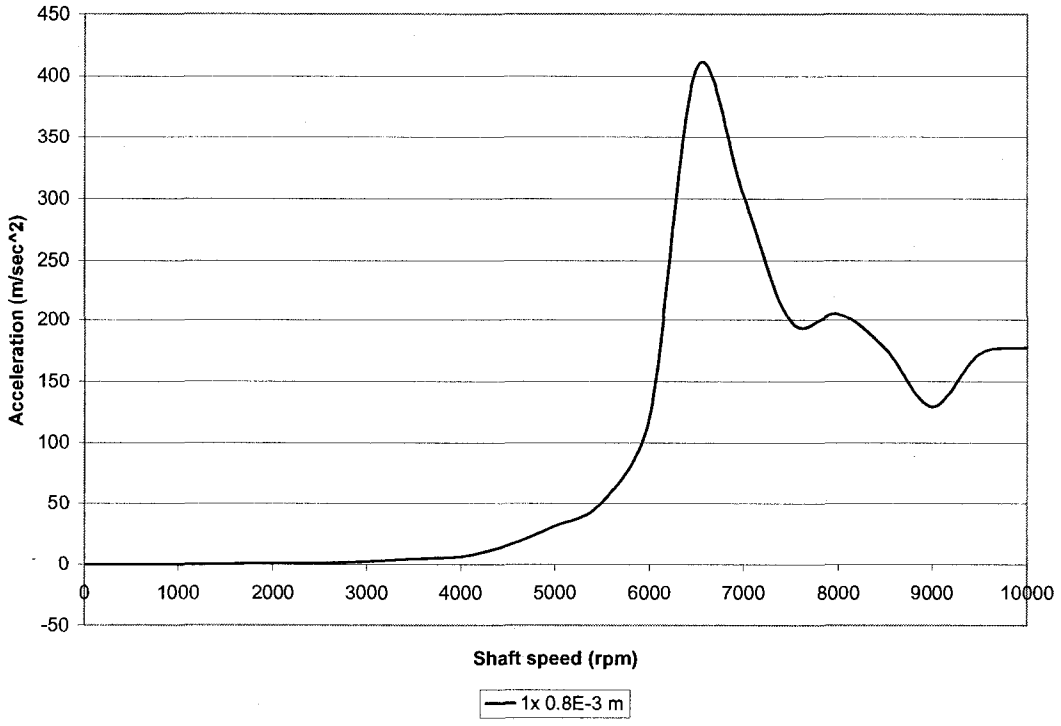

Figure 8-1 Threshold amplitude for creation of NN Data at 1x

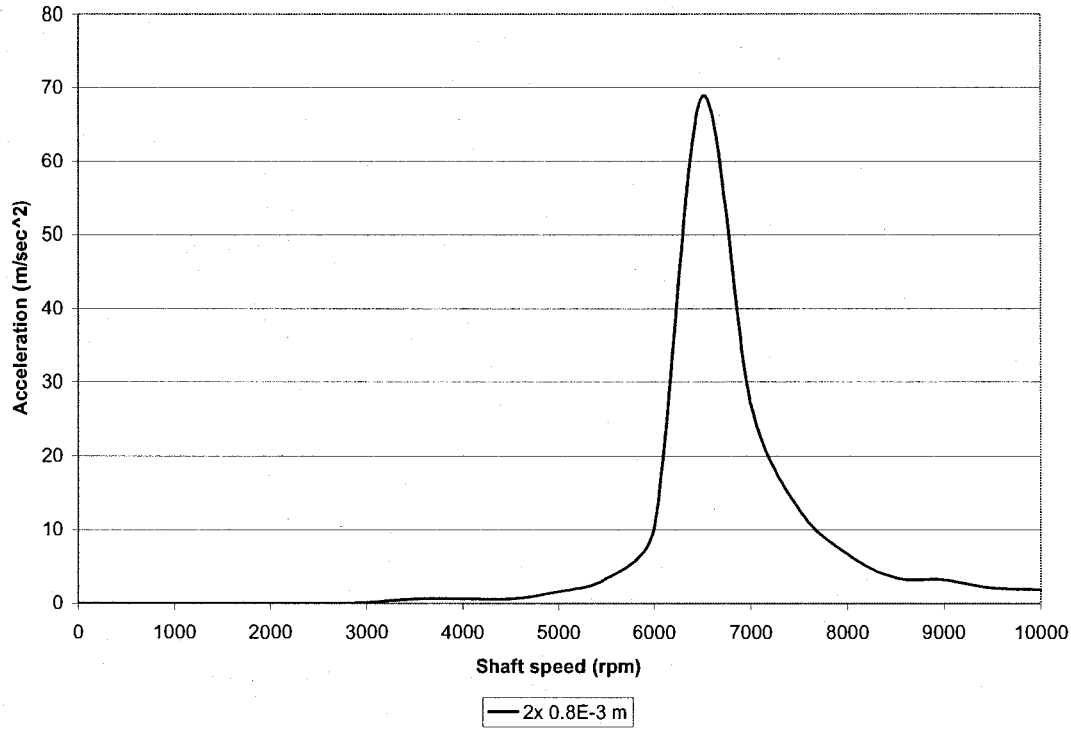

Figure 8-2 Threshold amplitude for creation of NN Data at 2x

During training the NN output is monitored and the network output is compared to the training output data set. When the root mean square of the error between the NN output and the training set output is very small (usually close to zero) the network has then completed its training, and is ready for testing.

Table 8-2 shows the training data set that is generated using the simulation. The output of the simulation is filtered and 3 values close to 1x and 3 values close to 2x are extracted. These values are then divided by the threshold value shown in Figure 8-1 and Figure 8-2 at the same rotation value to create the N.N. input vector. The N.N. output is created from the known condition.

Table 8-2 Training set

	Simulation condition and output in m/sec^2			NN Input			NN output		
1	e=0.06E-3 m, thau=0.3 deg, mis-axial=0.4E-3 m								
	rpm	3000							
	1x	0.43	1.51	0.09	0.194	0.680	0.041	1.000	0.000	0.000
	2x	0.01	0.03	0.01	0.083	0.249	0.083	1.000	0.000	0.000
2	e=0.08E-3 m, thau=0.3 deg, mis-axial=2.00E-3 m								
	rpm	3000							
	1x	0.562623	1.983056	0.119804	0.253	0.893	0.054	0.000	0.000	1.000
	2x	0.122054	0.235572	0.046237	1.014	1.958	0.384	0.000	0.000	1.000
3	e=0.1E-3 m, thau=0.3 deg, mis-axial=0.4E-3 m								
	rpm	3000							
	1x	0.696814	2.456819	0.148455	0.314	1.107	0.067	0.000	1.000	0.000
	2x	0.0331	0.07589	0.017264	0.275	0.631	0.143	0.000	1.000	0.000
4	e=0.06E-3 m, thau=0.3 deg, mis-axial=0.4E-3 m								
	rpm	4000							
	1x	1.261591	4.519979	3.879391	0.189	0.679	0.583	1.000	0.000	0.000
	2x	0.025056	0.132991	3.02E-04	0.044	0.233	0.001	1.000	0.000	0.000
5	e=0.08E-3 m, thau=0.3 deg, mis-axial=2.00E-3								
	rpm	4000							
	1x	1.660556	5.946251	5.100798	0.249	0.893	0.766	0.000	0.000	1.000
	2x	0.222797	1.137417	0.001032	0.390	1.993	0.002	0.000	0.000	1.000
6	e=0.1E-3 m, thau=0.3 deg, mis-axial=0.4E-3 m								
	rpm	4000							
	1x	2.057691	7.371789	6.326658	0.309	1.107	0.950	0.000	1.000	0.000
	2x	0.066943	0.349864	5.02E-04	0.117	0.613	0.001	0.000	1.000	0.000
7	e=0.06E-3 m, thau=0.3 deg, mis-axial=0.4E-3 m								
	rpm	5000							
	1x	0.512505	21.2889	3.519473	0.016	0.678	0.112	1.000	0.000	0.000
	2x	0.012274	0.361668	0.096378	0.008	0.230	0.061	1.000	0.000	0.000
8	e=0.08E-3 m, thau=0.3 deg, mis-axial=2.00E-3 m								
	rpm	5000							
	1x	0.678862	28.18797	4.658691	0.022	0.898	0.148	0.000	0.000	1.000
	2x	0.11607	3.171921	0.794977	0.074	2.015	0.505	0.000	0.000	1.000
9	e=0.1E-3 m, thau=0.3 deg, mis-axial=0.4 E-3 m,									
	rpm	5000							
	1x	0.836262	34.73581	5.742321	0.027	1.106	0.183	0.000	1.000	0.000
	2x	0.033714	0.960398	0.248546	0.021	0.610	0.158	0.000	1.000	0.000
10	e=0.06E-3 m, thau=0.3 deg, mis-axial=0.4E-3 m									
	rpm	6000							
	1x	43.39403	79.27275	14.73081	0.362	0.661	0.123	1.000	0.000	0.000
	2x	0.533558	2.267886	1.286961	0.053	0.225	0.128	1.000	0.000	0.000
11	e=0.08E-3 m, thau=0.3 deg, mis-axial=1.00E-3 m									
	rpm	6000							
	1x	59.09754	1.08E+02	20.0662	0.493	0.900	0.167	0.000	0.000	1.000
	2x	2.246325	10.192	6.233068	0.223	1.011	0.618	0.000	0.000	1.000
12	e=0.1E-3 m, thau=0.3 deg, mis-axial=0.4E-3 m									
	rpm	6000							
	1x	71.19294	1.30E+02	24.16933	0.593	1.084	0.201	0.000	1.000	0.000
	2x	1.363098	6.001707	3.549185	0.135	0.595	0.352	0.000	1.000	0.000

To test the N.N. a new set of data is prepared in the same way the training set of data is created. It is important that the testing data be different than the training set as much as possible. If the N.N. is properly trained the output generated from the N.N. will match the output expected. I.e. the N.N. will identify the fault.

It is possible that the NN output does not identify all the failures this is normal if the testing data differs significantly form the training set.

8.3.2 Back-propagation N.N. as an expert system

8.3.2.1 Development of the back-propagation N.N.

A back propagation N.N. is used to create a neural network. To create the back propagation N.N. the quick network setup option is used. The N.N. has six inputs and three outputs. The inputs correspond to the number of extracted data from the simulation. The outputs correspond to the output vector that is established in equations 8-3 to 8-5. Two hidden layers are used to create the N.N. All transfer functions are sigmoid except for the output layer transfer function which is a step function because the output of the N.N. is binary. The neurons from each layer are connected to the layers from all the prior layers. Table 8-3 shows the optimum parameters for the back propagation network that are obtained after numerous trials of different parameters.

The network is trained using the data presented in Table 8-2. During the training the roots mean square of the error is monitored until it reaches a value close to zero, at that point the network is fully trained.

Table 8-3 Neural Network Parameters

Input	6
First Hidden Layer	4
Second Hidden Layer	3
Output	3
Learning coefficient for input	0.9
Learning coefficient for second hidden layer	0.25
Learning coefficient for output	0.15
Momentum	0.4
Transfer point	10,000
Learning coefficient ration	0.5
Offset	0.1
Learning rule	Delta Rule
Transfer function for all layers except output	Sigmoid
Transfer function for output	Step function

8.3.2.2 Testing the back-propagation N.N.

The network is then tested in using the training set shown in Table 8-2 and with the testing set shown in Table 8-4. The data is presented to the trained N.N. and

the data input, the output of the N.N. and the expected output are stored and analyzed for both training sets.

Table 8-5 presents the testing results of the N.N. when tested using the training set data. The N.N. managed to predict the required output of the data vectors. Table 8-6 presents the testing result of the N.N. when tested with a set of data that is not used to train the network. The results show good performance of the N.N. considering that only 12 data sets are used to train the network. The N.N. predicted the fault presented to it accurately. Back-propagation network can be used as shown to identify different faults presented to it.

Table 8-4 Data used for testing the N.N. and its expected output

	Simulation condition and output in m/sec^2				NN Input			NN output		
1	e=0.03E-3 m, thau=0.2 deg, mis-parallel=0.2E-3 m									
	rpm	9000								
	1x	41.93424	44.78001	1.33E+01	0.324	0.346	0.103	1	0	0
	2x	0.012319	0.097818	0.026819	0.004	0.030	0.008			
2	e=0.07E-3 m, thau=0.1 deg, mis-parallel=0.2E-3 m									
	rpm	8500								
	1x	14.16806	1.36E+02	49.26809	0.080	0.766	0.278	1	0	0
	2x	0.18391	0.555444	0.369973	0.053	0.159	0.106			
3	e=0.07E-3 m, thau=0.25 deg, mis-parallel=1.5E-3 m									
	rpm	5500								
	1x	8.922258	39.82725	26.2288	0.176	0.785	0.517	0	0	1
	2x	1.672039	3.927243	0.53434	0.491	1.153	0.157			
4	e=0.08E-3 m, thau=0.08 deg, mis-parallel=2.0E-3 m									
	rpm	5500								
	1x	10.31343	46.03347	30.31343	0.203	0.907	0.597	0	0	1
	2x	2.966593	6.961579	0.946388	0.871	2.043	0.278			
5	e=0.1E-3 m, thau=0.6 deg, mis-parallel=0.5E-3 m									
	rpm	4500								
	1x	7.178746	17.76568	2.2326	0.462	1.143	0.144	0	1	0
	2x	0.510162	0.471135	0.117359	0.875	0.808	0.201			
6	e=0.2E-3 m, thau=0.6 deg, mis-parallel=0.5E-3 m									
	rpm	6500								
	1x	6.63E+01	6.28E+02	4.84E+01	0.553	5.233	0.404	0	1	1
	2x	21.25308	1.77E+02	11.28716	0.309	2.581	0.164			
7	e=0.2E-3 m, thau=0.3 deg, mis-parallel=0.2E-3 m									
	rpm	7500								
	1x	3.22E+02	4.46E+02	1.08E+02	1.621	2.249	0.545	0	1	0
	2x	0.666227	7.983178	3.145781	0.052	0.623	0.245			

Table 8-5 Testing results using training data.

N.N. Input						Expected Output			N.N. Output		
0.194	0.68	0.041	0.083	0.249	0.083	1	0	0	1	0	0
0.253	0.893	0.054	1.014	1.958	0.384	0	0	1	0	0	1
0.314	1.107	0.067	0.275	0.631	0.143	0	1	0	0	1	0
0.189	0.679	0.583	0.044	0.233	0.001	1	0	0	1	0	0
0.249	0.893	0.766	0.39	1.993	0.002	0	0	1	0	0	1
0.309	1.107	0.95	0.117	0.613	0.001	0	1	0	0	1	0
0.016	0.678	0.112	0.008	0.23	0.061	1	0	0	1	0	0
0.022	0.898	0.148	0.074	2.015	0.505	0	0	1	0	0	1
0.027	1.106	0.183	0.021	0.61	0.158	0	1	0	0	1	0
0.362	0.661	0.123	0.053	0.225	0.128	1	0	0	1	0	0
0.493	0.9	0.167	0.223	1.011	0.618	0	0	1	0	0	1
0.593	1.084	0.201	0.135	0.595	0.352	0	1	0	0	1	0

Table 8-6 Testing results using unseen data by the network

N.N. Input						Expected Output			N.N. Output		
0.324	0.346	0.103	0.004	0.003	0.008	1	0	0	1	0	0
0.08	0.766	0.278	0.053	0.159	0.106	1	0	0	1	0	0
0.176	0.785	0.517	0.491	1.153	0.157	0	0	1	0	0	1
0.203	0.907	0.597	0.871	2.043	0.278	0	0	1	0	0	1
0.462	1.143	0.144	0.875	0.808	0.201	0	1	0	0	1	0
0.553	5.233	0.404	0.309	2.581	0.164	0	1	1	0	1	1
1.621	2.249	0.545	0.052	0.623	0.245	0	1	0	0	1	0

8.3.3 Logicon Projection N.N. as an Expert System

8.3.3.1 Development of the Logicon Projection Network.

The Logicon projection network is chosen for its robustness, ability to learn with minimum data and quick convergence. The network is created using the quick setup menu. The number of input neurons is six and the number of output neuron is three. The network has two hidden layers, the first is the Logicon projection layer and it has seven neurons (input + one) and three neurons in the hidden layer. The connect prior option is used. The network is trained using the same data used to train the back-propagation network and is presented in Table 8-2.

During the training process numerous parameters are used and it is found that the parameters presented in Table 8-7 resulted in the network converging and achieving good results.

8.3.3.2 Testing the Logicon Projection N.N.

The exact same method used to test the back-propagation N.N. is used to test the Logicon projection N.N. First the Logicon projection N.N. is tested using the data that is used to train it.

Table 8-7 Neural Network Parameters

Input	6
Logicon projection	7 (Input +1)
Hidden Layer	4
Output	3
Learning coefficient for input	0.9
Learning coefficient for output	0.15
Learning rule	Delta Rule
Transfer function for input	Sigmoid
Transfer function for output	Step function
Projection Radius	6
Inner projection Radius	2.4495
Default prototype radius	0.1

The results of the test are presented in Table 8-8. The output of the Logicon projection N.N. is identical to the output expected. This shows that the N.N can identify the fault presented to it.

The Logicon projection N.N. is then tested using the data presented in Table 8-9. This Logicon projection N.N. has not been trained with this set of data. The results of testing the N.N. are presented in Table 8-9.

Comparing the Logicon projection and the back-propagation N.N. performance by comparing the data in Table 8-9 and the data set in Table 8-6 it is clear that

the Logicon projection N.N. has achieved the same performance compared to the back-propagation N.N. During training the Logicon projection outperformed the back-propagation network in learning speed. From the literature surveyed logicon projection is more robust and less likely to get stuck at a local minima because its weight are pre-initialized using the training set.

Table 8-8 Logicon projection testing results using training data.

N.N. Input						Expected Output			N.N. Output		
0.194	0.68	0.041	0.083	0.249	0.083	1	0	0	1	0	0
0.253	0.893	0.054	1.014	1.958	0.384	0	0	1	0	0	1
0.314	1.107	0.067	0.275	0.631	0.143	0	1	0	0	1	0
0.189	0.679	0.583	0.044	0.233	0.001	1	0	0	1	0	0
0.249	0.893	0.766	0.39	1.993	0.002	0	0	1	0	0	1
0.309	1.107	0.95	0.117	0.613	0.001	0	1	0	0	1	0
0.016	0.678	0.112	0.008	0.23	0.061	1	0	0	1	0	0
0.022	0.898	0.148	0.074	2.015	0.505	0	0	1	0	0	1
0.027	1.106	0.183	0.021	0.61	0.158	0	1	0	0	1	0
0.362	0.661	0.123	0.053	0.225	0.128	1	0	0	1	0	0
0.493	0.9	0.167	0.223	1.011	0.618	0	0	1	0	0	1
0.593	1.084	0.201	0.135	0.595	0.352	0	1	0	0	1	0

Table 8-9 Testing results using unseen data by the network

N.N. Input						Expected Output			N.N. Output		
0.324	0.346	0.103	0.004	0.003	0.008	1	0	0	1	0	0
0.08	0.766	0.278	0.053	0.159	0.106	1	0	0	1	0	0
0.176	0.785	0.517	0.491	1.153	0.157	0	0	1	0	0	1
0.203	0.907	0.597	0.871	2.043	0.278	0	0	1	0	0	1
0.462	1.143	0.144	0.875	0.808	0.201	0	1	0	0	1	0
0.553	5.233	0.404	0.309	2.581	0.164	0	1	1	0	1	1
1.621	2.249	0.545	0.052	0.623	0.245	0	1	0	0	1	0

8.4 Testing the N.N. with engine Data

The N.N. of choice to be tested with real engine data is the Logicon projection network. The Logicon projection N.N. has demonstrated quicker learning. The data that will be used to test the Logicon projection was presented in chapter 5 and it is for two engines that are diagnosed with misalignment.

To be able to test the N.N. the vibration threshold value must be established. The following steps are followed to establish the vibration threshold:

1) Vibration amplitude from engines that are known to be healthy are examined and recorded in the time domain and the data is then transferred into the frequency domain using FFT. This will give an idea on what typical engine vibration amplitude is,

2) The maximum value of the vibration amplitude that the engine can tolerate without any damage is established from safety criteria, design limitation,
3) The threshold value is established to be somewhere in between these two maximum value and the typical value.

Figure 8-3 and Figure 8-4 shows the vibration response for a typical engine and the very low 2x component. The engine is known to be in good condition and the data shows very low vibration amplitude for 1x, 2x compared to the values reported in chapter 5 (shown in figures 5-12 to 5-14).

For the engine presented in chapter 5 the threshold value for the vibration 0-Peak for the 2x and 1x is established to be:

$$A_{Th_{\omega}} = 7 \text{ mm/sec} \qquad 8\text{-}6$$

$$A_{Th_{2\omega}} = 7 \text{ mm/sec} \qquad 8\text{-}7$$

From the data presented in Figure 6-13 and Figure 6-15 the data to test the N.N. is extracted and divided by the threshold value established above. Table 8-10 shows the data extracted and the input data for the N.N.

The data extracted show two cases the first one of an engine with misalignment where the 2x components is above 7 mm/sec and the second case of an engine with high 1x and 2x. It is expected that the N.N. output will be [0, 0, 1] and [0, 1, 1].

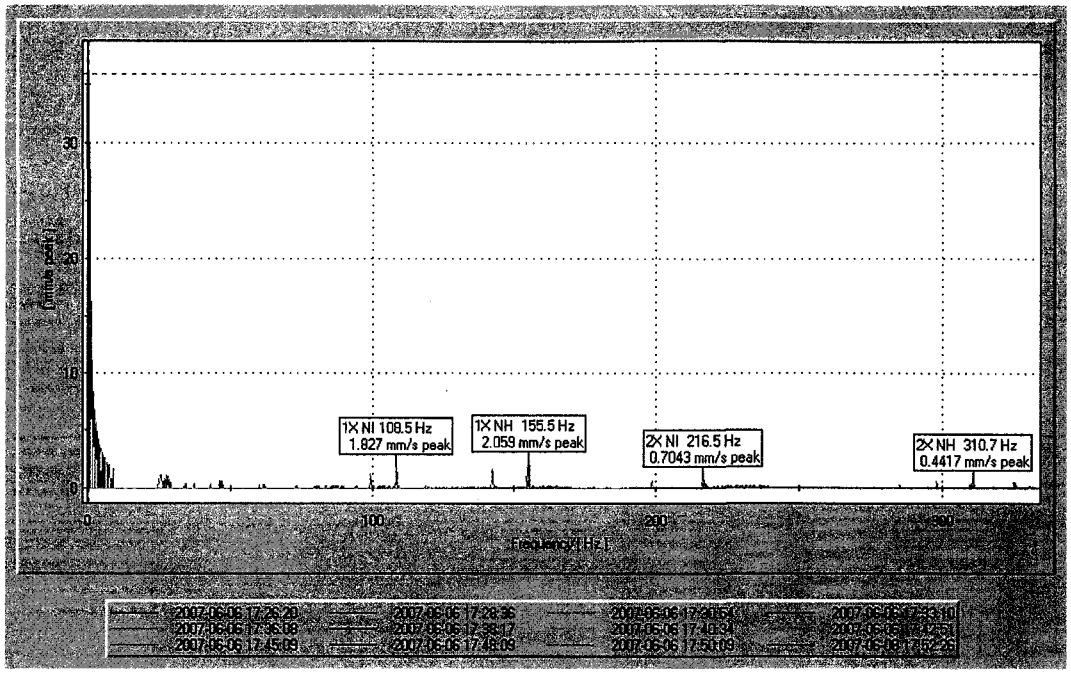

Figure 8-3 Vibration response of a normal engine at 9330 rpm

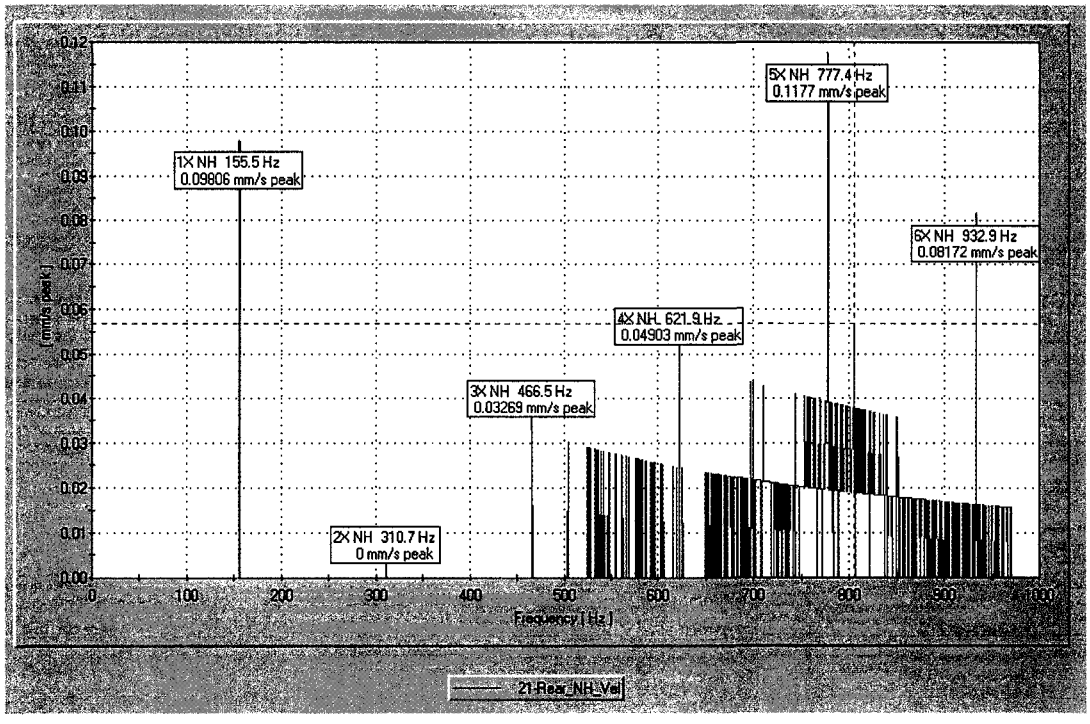

Figure 8-4 Vibration response of a normal engine no 2x components

Table 8-10 Data used to test the Logicon projection N.N.

	1x			2x		
First engine data (m/sec)	2.10E-3	2.45E-3	2.00E-3	1.45E-2	1.55E-2	1.30E-2
N.N. Input first engine	0.30	0.35	0.29	2.07	2.21	1.86
Second engine (m/sec)	2.10E-2	2.28E-2	2.30E-2	1.40E-2	1.49E-2	1.37E-2
N.N. Input second engine	3.00	3.26	3.29	2.00	2.13	1.96

Table 8-11 N.N. input and output.

	1x			2x			N.N. output		
N.N. Input first engine	0.30	0.35	0.29	2.07	2.21	1.86	0	0	1
N.N. Input second engine	3.00	3.26	3.29	2.00	2.13	1.96	0	1	1

Table 8-11 shows the data input to the N.N. and the output from the N.N. It is clear from the table that the developed N.N. is able to diagnose the engine problem. The N.N. that is developed for predicting engine problems was developed using a simple rotor and simulation to train the N.N. yet it managed to predict the engine fault when real life data is presented from a multi rotor engine. The logic used to create the N.N. can also be expanded to add more fault detection like, bearing and gear defect.

8.5 Summary

In this chapter two N.N. were developed the first using a back-propagation and the second using Logicon projection. Both N.N. were developed using a simple rotor simulation data. The data was normalized and used to train the N.N. A very limited number of samples was used.

Both N.N. were tested using the data from the training set and a testing data set that was not used to train the N.N. The Logicon projection learned faster than the back-propagation network.

The logicon projection N.N. was then tested using data from two real engines in the field. The first engine was diagnosed with misalignment and the second was diagnosed with misalignment and excessive unbalance. The Logicon projection managed to diagnose both engines correctly. The work presented in the chapters shows that:

1) N.N. can be trained off line to diagnose engine problems as long as the data presented to the N.N. is dimensionless
2) N.N. managed to predict engine problems and combination of problems

3) Few data sets are required to achieve adequate learning as long as the data presented to the N.N. is representative of the problem being diagnosed.

Chapter 9

9 Conclusions and Recommendations for Future Work

9.1 General

Unbalance and misalignment create majority of vibration problems seen in the field [82]. They result in excessive repair cost. In addition, to diagnose these problems seen in the field it is very time consuming and results in excessive down time and cost. There is very limited research conducted on misalignment with sometimes contradicting results. Most research shows the existence of 2x components, and harmonics [24, 25, 26, 27, 28]. Hussein and Redmond [29] could not show the existence of harmonics in their model. Research from the field reported the effect of misalignment on the 2x component [30].

In this study a rotor model was developed using the energy method to show:

- The effect of neglecting the higher order terms in developing the equation of motion,
- The effect of nonlinear stiffness caused by misalignment on the shaft response.

An experimental rig was used to confirm the results obtained from the simulation and showed that misalignment results in an increase in the 2x component and a

change of the 1x component. Real engine responses were presented showing the effect of misalignment and unbalance.

The rotor was modeled using finite element and the response of the shaft due to unbalance was confirmed.

The developed rotor model was then used to train and test two different type of N.N. The developed N.N. that showed the best performance was then tested using real engine data and predicted both presented cases accurately.

9.2 Major Highlights and Conclusions

The study presented in this thesis is an investigation of the effect of unbalance and misalignment on the response of a rotor and the development of an expert system using N.N. to detect these two defects on real gas turbine engines. The thesis presents the method to develop a shaft rotor dynamic model and evaluate the effect of ignoring the higher order terms, in the formulation of the equations of motion, on the shaft response. The success of the N.N. and its ability to detect these two defects, which represent the majority of engine problems in the field, show that the developed method can be successfully extended to detect other problems in the field thus shortening the diagnostic time and cost of operating gas turbine engines. The major highlights of the thesis are summarized as follows:

1) The different energy terms required to formulate the rotor model are presented in detail. Shaft stiffness matrix was formulated for a shaft under different support configuration,
2) Three sets of equations of motion for the rotor were developed the first ignoring all the higher order terms, the second taking into account the higher order terms for the dynamic unbalance, and the third for a misaligned rotor. The third set of equation of motion introduces damping and nonlinear stiffness caused by misalignment,
3) Validation of the developed equations was carried out using analytical solution, and finite element,
4) The effect of the higher order terms on the rotor response was examined and it was established from this study that the higher order terms did not affect the 1x and 2x response of the rotor significantly,
5) The use of finite element to predict the effect of misalignment on rotor response was presented. It was shown in this research that the finite element model does not predict the effect of misalignment on the rotor response because of the lack of the nonlinear stiffness,
6) Simulation for the third sets of the equation of motion was carried out and the results showed that:
    a. Misalignment of the shaft results in an increase or decrease of the 1x components,
    b. Misalignment of the rotor leads to an increase of the 2x response. The increase is a function of the severity of misalignment.

7) Limited testing was performed on a rig with results confirming the trend seen from the simulation. In addition data from the field was presented showing the effect of misalignment on the rotor response,
8) Neural networks theory is then presented showing different types of neural networks and their applications. Special attention is given to back-propagation and Logicon projection. Details of how to create these two N.N. are presented as well as the method to specify their parameters to achieve good performance and quick learning,
9) The development of N.N. is then carried out using back-propagation and Logicon projection. The logic to detect both failures was developed. The N.N. are trained and tested showing good results with the Logicon projection and back-propagation detecting all the failure cases presented to it. The Logicon projection N.N. is then tested using engine data and managed to detect the failure case correctly.

9.3 Recommendations for Future Studies

This research has presented a model of a rotor where the dynamics of the bearings are not considered to emphasize the effect of the nonlinear stiffness on the shaft response due to misalignment. The rotor dynamics in the future can be expanded to study:

1) The effect of the nonlinear stiffness coupled with bearing non linear properties,

2) A shaft supported on multiple bearings,
3) Multiple shafts can be modeled to study the effect of misalignment,
4) In this study a nonlinear stiffness was introduced as a result of misalignment. It is recommended to further study the characteristic of the non linear stiffness and perform a sensitivity analysis on the factors that affect the nonlinear stiffness,
5) The rig testing used in the study can also be expanded to add multiple shafts and bearings.

In view of the N.N. potential to be used as a diagnostic tool in rotor dynamics a list of future work recommended are as follows:

1) Create a N.N. to diagnose bearing and gear problems
2) Evaluate the use of N.N. to diagnose the existence of oil in rotating drums
3) Evaluate the use of N.N. to identify other problems on gas turbine engines, like surge, combustion issues, rubs, etc.
4) Use the N.N. created in this research and add to it other networks to create an integrated expert tool that can identify a wide range of vibration problems as shown in Figure 9-1.

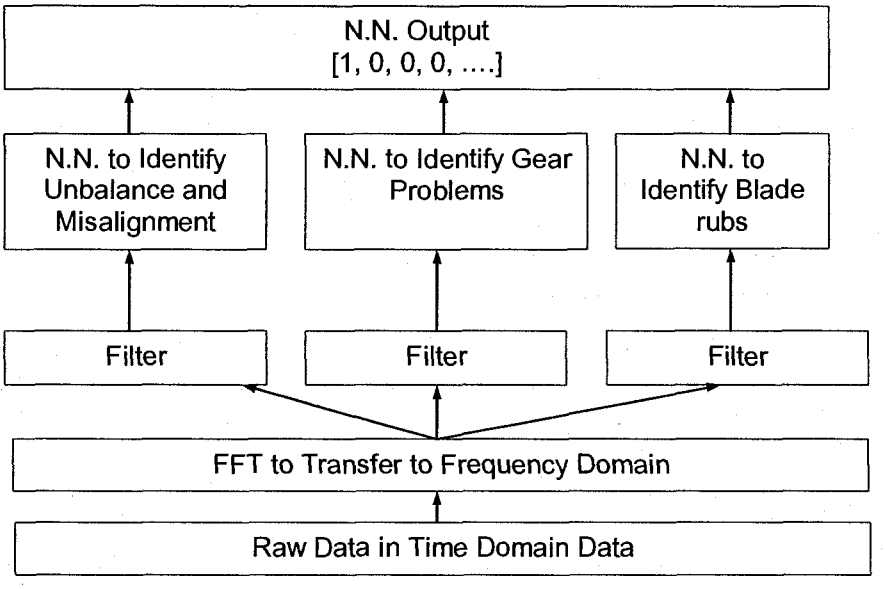

Figure 9-1 Layout of N.N. to identify multiple faults

References

1. William Carnegie, *"Vibrations of Rotating Cantilever Blading: Theoretical Approaches to the Frequency Problem Based on Energy Methods"*, Journal of Mechanical Engineering Science, Vol #3, 1959, P235 – 240.
2. M.M. Bhat, V. Ramamurti and C. Sujatha, *"Studies in the Determination of Natural Frequencies of Industrial Turbine Blades"*, Journal of Sound and Vibration (1996) 196(5), 681-703,
3. R.B. Bhat, *"Natural Frequencies of Rectangular Plates Using Characteristic Orthogonal Polynomials in Rayleigh-Ritz Method"*, Journal of Sound and Vibration (1985) 102, 493-499,
4. N.S. Vyas and J.S. Rao, *"Equations of Motion of a Blade Rotating with Variable Angular Velocity"*, Journal of Sound and Vibration (1992) 156(2) 327-336.
5. G. Hernried, *"Forced Vibration Response of a Twisted Non-Uniform Rotating Blade"*, Computers and Structures Vol. 41 No. 2 P 207-212, 1991.
6. S. V. Hoa, *"Vibration of A Rotating Beam With Tip Mass"*, Journal of Structure and Vibration (1979) 67(3) P 369-381.
7. R. B. Bhat, *"Transverse Vibrations of a Rotating Uniform Cantilever Beam with Tip Mass as Predicted By Using Beam Characteristic Orthogonal Polynomials in the Rayleigh-Ritz Method"*, Journal of Sound and Vibration (1986) 105(2), P. 199-210.

8. Sinha, Sunil K, *"Determination of Natural Frequencies of a Thick Spinning Annular Disk Using a Numerical Rayleigh-Ritz's Trial Function"*, Journal of Acoustic Soc. Vol. 81 February 1987, P357-369.
9. Z. Celep, "*Axially Symmetric Stability of a Completely Free Circular Plate Subjected to a Non-Conservative Edge Load*", Journal of Sound and Vibration, 1979, 65(4), 549-556.
10. W. D. Iwan and T. L. Moeller, *"The stability of a spinning Elastic Disk with a Transverse Load System"*, Journal of Applied Mechanics, September 1976, P 485-490.
11. Adams, George G., *"Critical Speed for a Flexible Spinning Disk"*, J. Mech. Sci Vol. 29, No 8 P525-531, 1987.
12. S. Chonan, *"Vibration and Stability of Annular Plates Under Conservative and Non-Conservative Loads"*, Journal Sound and Vibration (1982) 80(3), P 413 – 420.
13. B. F. Lehman and S. G. Hutton, *"Self-Excitation in Guided Circular Saws"*, Journal of Vibration and Acoustics, Stress, and Reliability in Design, July 1998, Vol. 110 page 338-344.
14. H. K. Tönshoff and J. Jendryschik, *"Dynamical Behavior of Disklike Rotating Tools"*, Computers and Structures Vol. 21 No. ½ pp 203-211, 1985.
15. J. T. Wagner, *"Coupling of Turbomachine Blade Vibrations Through the Rotor"*, Transaction of the ASME October 1967 P502, 512.
16. D. J. Ewins, *"Vibration Characteristics of Bladed Disc Assemblies"*, Journal Mechanical Engineering Science, Vol 15 No 3 1973 P 165-185

17. S. J. Wildheim, *"Natural Frequencies of Rotating Bladed Disks Using Clamped – Free Blade Modes",* Transaction of the ASME Journal of Vibration, Acoustics, Stress and Reliability in Design, October 1983, Vol. 105, P 416-424,

18. V. Omprakash and V. Ramamurti, *"Natural Frequencies of Bladed Disks by a Combined Cyclic Symmetry and Rayleigh Ritz Method",* Journal of Sound a Vibration (1988, 125(2), P. 357-366),

19. C. Rajalingham, G.D. Xistris and R.B. Bhat, *"Stability of Rotors Under the Combined Influence of Fluid Film Bearing Characteristics and Shaft Material Damping"*, Tribology Transactions Volume 35(1992), 3, 566 570,

20. José A. Vázquez, Lloyd E. Barrett and Ronald D. Flack, *"A Flexible Rotor on Flexible Bearing Supports: Stability and Unbalance Response",* Journal of Vibration and Acoustics, April 2001 Vol 123 pp 137 144

21. A.W. Lees and M.I. Friswell, *"The Evaluation of Rotor Imbalance in Flexibly Mounted Machines",* Journal of Sound and Vibration (1997) 208(5), 671-683

22. P. N. Bansal, R.G. Kirk, *"Stability and Damped Critical Speeds of Rotor-Bearing Systems",* Transactions of the ASME Journal of Engineering for Industry, Nov 1975 pp1325-1332

23. K.M. Al-Hussain, *"Dynamic Stability of Two Rigid Rotors Connected by a Flexible Coupling with Angular Misalignment",* Journal of Sound and Vibration 266 (2003) 217-234

24. M. Xu, and R.D. Marangoni, *"Vibration Analysis of a Motor-Flexible Coupling-Rotor System Subject to Misalignment and Unbalance Part I: Theoretical*

Model and Analysis" Journal of Sound and Vibration (1994) 176(5), 663 – 679.

25. M. Xu, and R.D. Marangoni, *"Vibration Analysis of a Motor-Flexible Coupling-Rotor System Subject to Misalignment and Unbalance Part II: Experimental Validation"* Journal of Sound and Vibration (1994) 176(5), 681 – 691.
26. A.S. Sekhar, and B.S. Prabhu, *"Effects of coupling Misalignment on Vibrations of Rotating Machinery"*, Journal of Sound and Vibration (1995) 185(4), 655 – 671.
27. Y.-S. Lee, and C.-W. Lee, *"Modelling and Vibration Analysis of Misaligned Rotor-Ball Bearing Systems"*, Journal of Sound and Vibration (1999) 224(1), 17 - 32.
28. J.S. Rao, *"Vibratory Condition Monitoring of Machines",* CRC Press, 2000.
29. K. M. Al-Hussain, and I Redmond, *"Dynamic Response of Two Rotors Connected by Rigid Mechanical Coupling with Parallel Misalignment"* Journal of Sound and Vibration (2002) 249(3), 483-498.
30. A. El-Shafei, *"Diagnosis of Installation Problems of Turbomachinery"*, Proceedings of ASME Turbo Expo 3-5 June 2002, Amsterdam, The Netherlands.
31. P.N. Saavedra, and D.E. Ramirez *"Vibration analysis of rotors for the identification of shaft misalignment. Part 1: Theoretical Analysis",* Proc. Instn Mech Engrs vol 218 Part C: J. Mechanical Engineering Science, P. 971 – 985. IMechE 2004

32. P.N. Saavedra, and D.E. Ramirez *"Vibration analysis of rotors for the identification of shaft misalignment. Part 2: Experimental validation"*, Proc. Instn Mech Engrs vol 218 Part C: J. Mechanical Engineering Science, P. 987 – 999. IMechE 2004

33. Agnieszka (Agnes) Muszynska, *"Rotordynamics"*, CRC Press, 2005

34. A.W. Less, *"Misalignment in Rigidly Coupled Rotors"*, Journal of Sound and Vibration, 305 (2007) 262-271

35. McCulloch, W.S., and Pitts, *"A Logical Calculus of the Ideas Immanent in Nervous Activity"*, Bulletin of Math. Bio., 5, 115-133, 1943

36. Von Neumann, J, *"Probabilistic Logics and the Synthesis of Reliable Organisms from Unreliable Components"*, in Shannon, C. E., and McCarthy, J.[Eds.], Automata Studies, 43-98, Princeton University Press, Princeton NJ. 1956.

37. Von Neumann, J, *"The General and Logical Theory of Automata"*, in Jeffress, L. A. [Ed.], Cerebral mechanisms in behavior, 1-41, Wiley, New York, 1956.

38. Hebb, D., *"The organization of Behavior"*, wiley, New York 1949.

39. Rosenblatt, F., *"The perceptron: A probalistic model for information storage and organization of the brain"*, Psychol. Rev., 65, 386-408, 1958.

40. Zurada Jacek M., *"Introduction to Artificial Neural Systems"*, West publishing company.

41. Hecht-Nielsen Robert, *"Neurocomputing"*, Addison-Wesley publishing company.

42. Freeman James A. and Skapura David M., *"Neural Networks"*, Computation and neural systems series.

43. Domany E., van Hemmen J.L. and Schulten K., *"Models of Neural Networks"*, Springer-Verlag.

44. C-G. Taraboulsi, *"Neural Network Application to Vehicle System Dynamics"*, Master Thesis, Concordia University, 1995

45. Hunt K.J. and Sbarbaro D., *"Studies in Neural Network Based Control"*, Neural networks for control and systems. (94-122)

46. S. Edwards, A.W. Lees, M.I. Friswell, *"Fault Diagnosis of Rotating Machinery"*, Shock and Vibration Digest, Vol. 30, No. 1, pages 4-13, 1998

47. H. R. DePold, F. D. Gass, *"The application of Expert Systems and Neural Networks to Gas Turbine Prognostics and Diagnostics"*, Journal of Engineering for Gas Turbines and Power, October 1999, Vol 121, 607-612

48. P.-J Lu, M.-C Zhang, T.-C Hsu, J. Zhang, *"An Evaluation of Engine Faults Diagnostics Using Artificial Neural Network"*, Transaction of the ASME vol. 123, April 2001, p 340-346.

49. K. K. Botros, G. Kibrya, A. Gtover, *"A Demonstration of Artificial Neural-Networks-Based Data Mining for Gas-Turbine-Driven Compressor Stations"*, Transaction of the ASME, vol. 124, April 2002, P 284-297.

50. A. J. Volponi, H. Depold, R. Ganguli, and C. Daguang, *"The use of Kalman Filter and Neural Network Methodologies in Gas Turbine Performance Diagnostics: A Comparative Study"*, Journal of Engineering for Gas Turbines and Power, October 2003, Vol 125 p. 917-924.

51. H. S. Tan, *"Fourier Neural Networks and Generalized Single Hidden Layer Networks in Aircraft Engine Fault Diagnostics"*, Journal of Engineering for Gas Turbines and Power, October 2006, Vol 128 p. 773-782.

52. Rajeev Verma, Niranjan Roy, Ranjan Ganguli, *"Gas Turbine Diagnostics using a Soft Computing Approach"*, Applied Mathematics and Computations 172(2006) 1342-1363.

53. Q. Wang, F. Chu, *"Experimental Determination of the Rubbing Location by Means of Acoustic Emission and Wavelet Transform"*, Journal of Sound and Vibration (2001) 248(1), 91 103

54. S. Seibold, K. Weinert, *"A Time Domain Method for the Localization of Cracks in Rotors"*, Journal of Sound and Vibration (1996) 195(1), 57 73

55. B.S. Yang, T. Han, J.L. An, *"ART-Kohonen Neural Network for Fault Diagnosis of Rotating Machinery"*, Mechanical Systems and Signal Processing 18 (2004) P 645-657,

56. B.S Yang, T. Han, Y.S. Kim, *"Integration of ART-Kohonen Neural Network and Case-Based Reasoning for Intelligent Fault Diagnosis"*, Expert System with Applications 26(2004) 387-395,

57. R.B.W. Heng, M.J.M. Nor, *"Statistical Analysis of Sound and Vibration Signals for Monitoring Rolling Element Bearing Condition"*, Applied Acoustics, Vol. 53, No 1-3, pp 211-226, 1998

58. J.M. Krodkiewski, J. Ding and N. Zhang, *"Identification of Unbalance Change Using a Non-Linear Mathematical Model for Multi-Bearing Rotor Systems"*, Journal of Sound and Vibration (1994) 169(5), 685-698

59. C.H. Oppenheimer and S. Dubowsky, *"A Methodology for Predicting Impact-Induced Acoustic Noise in Machine Systems"*, Journal of Sound and Vibration 266(2003) 1025-1051

60. A.J. Hoffman and N.T. van der Merwe, *"The application of neural networks to vibrational diagnostics for multiple fault conditions"*, Computer Standards and Interfaces 24(2002) 139-149

61. X. Hu, J Vian, J. Chois, D. Carlson, D.C. Wunsch II, *"Propulsion Vibration Analysis Using Neural Network Inverse Modeling"*, Proc. International Joint Conference on Neural Networks 02, World Congress on Computational Intelligence, paper #2351,May 12-17, 2002.

62. F. Fileppetti, G. Franceschini, and C. Tassoni, *"Neural Networks Approach to Electric Machine On-line Diagnostics"*, Power Electronics and Applications, 1993. Fifth European Conference on 13 Sep 1993 Pages 213 – 218 vol. 4

63. Peter Tse and D.D. Wang, *"A Hybrid Neural Networks Base Machine Condition Forecaster and Classifier by using Multiple Vibration Parameters"*, IEEE International Conference on Neural Networks - Conference Proceedings, v 4, 1996, p 2096-2100

64. Crupi, V. Guglielmino, E.; Milazzo, G. *"Neural-network-based system for novel fault detection in rotating machinery"* Journal of Vibration and Control, v 10, n 8, August, 2004, p 1137-1150

65. McCormick, Andrew C. Nandi, Asoke K. *"Neural network autoregressive modeling of vibrations for condition monitoring of rotating shafts"*, IEEE

International Conference on Neural Networks - Conference Proceedings, v 4, 1997, p 2214-2218

66. W. Li, Y.P. Tsai, C.L. Chiu, *"The Experimental Study of the Expert System for Diagnosing Unbalances by ANN and Acoustic Signals"*, Journal of Sound and Vibration 272 (2004) 69-83

67. Serhat Şeker, Emine Ayaz, Erdinç Türkcan, *"Elman's Recurrent Neural Network Applications to Condition Monitoring in Nuclear Power Plant and Rotating Machinery"*, Engineering Application of Artificial Intelligence 16(2003) 647-656

68. J.E. Shigley, *"Mechanical Engineering Design"*, First Metric Edition Mc Graw Hill

69. M.L. James, G.M. Smith, J.C. Wolford, P.W. Whaley, *"Vibration of Mechanical and Structural Systems"*, 1989 Harper and Row Publishers Inc.

70. H. Goldstein, *"Classical Mechanics"*, 1965 Addison-Wesley Publishing Company, Inc.

71. L.D. Landau, E.M. Lifshitz, *"Mechanics"*, 1960 Addison-Wesley Publishing Company, Inc.

72. John M. Vance, *"Rotordynamics of Trubomachinary"*, John Wiley & Sons, Inc 1988.

73. Michel Lalanne and Guy Ferraris, *"Rotordynamics Prediction in Engineering"*, John Wiley & Sons, Inc 1988.

74. MSC. Nastran, *"Quick Reference Guide"*, 2001

75. K.H. Huebner, E.A. Thoornton, T.G. Byrom, *"The Finite Element Method for Engineers"*, Third edition, A. Wiley-Interscience Publication, 1995.

76. P. Werbos, *"Beyond Regression: New Tools for Prediction and Analysis on the Behavioral Sciences"*, PhD thesis Harvard, Cambridge, MA, August 1974

77. D.B. Parker, *"Learning Logic. Technical report TR-47"*, Center for Computational Research in Economics and Computational Science, MIT Cambridge, MA, April 1985.

78. James McClelland and David Rumelhart, *"Parallel Distributed Processing"*, volumes 1 and 2, MIT Press, Cambridge, MA, 1986.

79. Lippman Richard P., *"An Introduction to Computing with Neural Nets"*, IEEE Transaction on neural networks Vol. 1, No. 1 March 1990 (4-27).

80. Gregg D. Wilensky, Narbik Manukian, *"The Projection Neural Netwrok"*, IEEE, International Joint Conference on Neural Networks, 1992, Volume II pp. 358-367, 1992

81. Neural Computing, a Technology Handbook for NeuralWorks Professional II/Plus

82. Victor Wonk, *"Machinery Vibration Measurement and Analysis"*, McGraw-Hill, Inc 1991